

T H E U N I V E R S I T Y O F M A N I T O B A

CURRENT INJECTION, ELECTROLUMINESCENCE

AND

PHOTOVOLTAIC EFFECT IN ORGANIC SEMICONDUCTORS

by

WEI HWANG

A THESIS

SUBMITTED TO THE FACULTY OF GRADUATE STUDIES

IN PARTIAL FULFILLMENT OF THE REQUIREMENTS FOR THE DEGREE

OF DOCTOR OF PHILOSOPHY

DEPARTMENT OF ELECTRICAL ENGINEERING

WINNIPEG, MANITOBA

MAY, 1974

CURRENT INJECTION, ELECTROLUMINESCENCE
AND
PHOTOVOLTAIC EFFECT IN ORGANIC SEMICONDUCTORS

by
WEI HWANG

A dissertation submitted to the Faculty of Graduate Studies of
the University of Manitoba in partial fulfillment of the requirements
of the degree of

DOCTOR OF PHILOSOPHY

© 1974

Permission has been granted to the LIBRARY OF THE UNIVERSITY OF MANITOBA to lend or sell copies of this dissertation, to the NATIONAL LIBRARY OF CANADA to microfilm this dissertation and to lend or sell copies of the film, and UNIVERSITY MICROFILMS to publish an abstract of this dissertation.

The author reserves other publication rights, and neither the dissertation nor extensive extracts from it may be printed or otherwise reproduced without the author's written permission.

ACKNOWLEDGEMENTS

The author wishes to express his grateful appreciation to Professor K.C. Kao for suggesting this thesis subject and for his constant encouragement, advice and supervision throughout the entire work.

Sincere thanks are given to the graduate students of the Material Research Laboratory and the staff of the Electrical Engineering Department of The University of Manitoba for their assistance and co-operation, and to Mrs. Constance LeBlanc for typing this thesis.

Finally, this research was supported by the National Research Council of Canada through the research grant (Grant Number A3339) awarded to Professor Kao.

A B S T R A C T

The effects of traps due to either chemical impurities or lattice imperfections on the steady state current-voltage characteristics of a solid crystal have been theoretically investigated in a unified manner for the single injection of charge carriers of one type (holes), and for the double injection of charge carriers of two types (electrons and holes) into the crystal from metallic contacts. Various forms of trap distributions in energy and in space have been considered. The computed results based on the theoretical expressions for both single injection and double injection cases under various conditions are in good agreement with presently available experimental results in anthracene corresponding to the same conditions.

In anthracene slices cleaved along the a-b plane with vacuum-deposited-Ag electrodes, electroluminescence appears first at the electrode edges. The threshold voltage for the onset of electroluminescence is strongly dependent on temperature. Generally, the voltage for self-sustaining electroluminescence is smaller than the threshold voltage. It is proposed that the minority carriers (electrons) required for the formation of singlet exciton following electron-hole recombination are emitted from the cathode by tunneling.

For electroluminescence in the specimen with double injection, a theoretical model for the formation of filamentary currents is presented. The expressions for the intensity of electroluminescence as a function of applied average electric field, current density and temperature have been derived on the basis of this model. The computed

results are in good agreement with presently available experimental results for undoped anthracene and anthracene doped with tetracene.

A general formulation is also presented for the photovoltaic effect in a solid with traps. Analytical expressions for the photovoltage for two cases, (1) local charge neutrality with traps and (2) local charge non-neutrality without traps, have been derived, and the computed results for two extreme conditions (i) strong absorption and (ii) weak absorption are in good agreement with the experimental results for naphthalene, anthracene and tetracene crystals. These expressions can be used not only for the determination of the photovoltage under various conditions, but can also be used as a tool to determine the absorption coefficient, carrier diffusion length, surface recombination velocity and other bulk properties by measuring the photovoltage as a function of wavelength of the illuminated light, temperature and the thickness of the crystal specimen.

TABLE OF CONTENTS

CHAPTER I - INTRODUCTION	1
CHAPTER II - REVIEW OF PREVIOUS WORK ON ORGANIC SEMICONDUCTORS . . .	7
2.1 CARRIER INJECTION FROM CONTACTS	9
2.2 ELECTROLUMINESCENCE IN ORGANIC SEMICONDUCTORS	17
2.2.1 The recombination mechanisms	19
(i) Carrier recombination	19
(ii) Exciton recombination	21
2.2.2 The efficiency of electroluminescence.	25
(i) The theory of radiative and non-radiative transition processes.	25
(ii) The efficiency of radiative transition.	30
(a) Exciton-exciton interactions	30
(b) Exciton-carrier interactions	31
(c) Exciton-surface interactions	32
2.2.3 Experimental results in anthracene	33
(i) Effects of doping impurities.	33
(ii) Field dependence of electroluminescence	35
(a) D.C. electroluminescence	35
(b) A.C. electroluminescence	37
(c) Pulsed electroluminescence	40
(iii) Temperature dependence of electroluminescence.	40
2.3 PHOTOELECTRIC EFFECT.	41
2.3.1 Photoconduction processes.	41
(i) One-quantum processes	41
(ii) Two-quantum processes	44
(iii) Multi-quantum processes	46
2.3.2 Photovoltaic phenomena	47
(i) General theory of photovoltaic effect in solids.	48
(ii) Experimental results of photovoltaic phenomena in organic semiconductors	50
(a) Light wavelength dependence.	50
(b) Surface condition dependence	54

CHAPTER III - UNIFIED APPROACHES TO THE THEORY OF CURRENT INJECTION IN SOLIDS	57
3.1 THEORY OF SINGLE INJECTION	57
3.1.1 The traps confined in a single discrete energy level	60
3.1.2 The traps distributed exponentially within the forbidden energy gap.	61
3.1.3 The traps distributed uniformly within the forbidden energy gap.	63
3.2 EXPERIMENTAL AND COMPUTED RESULTS FOR SINGLE INJECTION .	64
3.2.1 Uniform spatial distribution.	66
3.2.2 Exponential spatial distribution with the max- imum density at the injecting electrode (at $x = 0$).	66
3.2.3 Exponential spatial distribution with the max- imum density at both electrodes (at $x = 0$ and $x = d$)	67
3.3 CONCLUDING REMARKS FOR SINGLE INJECTION.	70
3.4 THEORY OF DOUBLE INJECTION	71
3.4.1 The traps confined in a single discrete energy level	73
3.4.2 The traps distributed exponentially within the forbidden energy gap.	76
3.4.3 The traps distributed uniformly within the forbidden energy gap.	79
3.5 COMPUTED RESULTS FOR DOUBLE INJECTION.	83
3.5.1 The traps confined in a single discrete energy level	84
3.5.2 The traps distributed exponentially within the forbidden energy gap.	86
3.6 CONCLUDING REMARKS FOR DOUBLE INJECTION.	88
CHAPTER IV - FILAMENTARY DOUBLE INJECTION AND ELECTROLUMINESCENT PHENOMENA	89
4.1 THEORY OF FILAMENTARY DOUBLE INJECTION	89
4.1.1 The traps confined in a single discrete energy level	92
4.1.2 The traps distributed exponentially within the forbidden energy gap.	97

4.2	ELECTROLUMINESCENCE IN MOLECULAR CRYSTALS DUE TO DOUBLE INJECTION	101
4.2.1	Current dependence of electroluminescent intensity.	105
4.2.2	Voltage dependence of electroluminescent intensity.	116
4.2.3	Temperature dependence of electroluminescent intensity.	120
4.3	ELECTROLUMINESCENCE IN ANTHRACENE CRYSTALS DUE TO FIELD ENHANCED INJECTION	125
4.4	CONCLUDING REMARKS.	129
CHAPTER V - PHOTOVOLTAIC EFFECT IN ORGANIC SEMICONDUCTORS.		130
5.1	THEORY OF THE PHOTOVOLTAIC EFFECT	130
5.1.1	Local charge neutrality with traps	136
5.1.2	Local charge non-neutrality without traps.	138
5.2	COMPUTED RESULTS AND DISCUSSIONS.	140
5.2.1	The photovoltage created in the bulk of the crystal.	140
	(i) Strong absorption	140
	(ii) Weak absorption	143
5.2.2	The photovoltage created at the front and back surface.	147
5.2.3	Computed results	148
5.3	CONCLUDING REMARKS.	156
CHAPTER VI - CONCLUSIONS		158
APPENDIX		160
REFERENCES		162

LIST OF FIGURES

FIGURE 2.1 - ELECTROLUMINESCENT PROCESSES IN ORGANIC CRYSTALS.	
(a) Prompt Electroluminescence	
(b) Delayed Electroluminescence.	24
FIGURE 2.2 - THE POTENTIAL ENERGY DIAGRAM OF A DIATOMIC MOLECULE.	
The total energy (electronic and vibrational energy)	
of the molecules as a function of the nuclear	
separation, r .	
$(E_{Fc})_a$, Franck-Condon maximum in absorption;	
$(E_{Fc})_e$, Franck-Condon minimum in emission	28
FIGURE 2.3 - THE SPECTRA OF FLUORESCENCE AND ELECTROLUMINESCENCE	
FOR UNDOPED ANTHRACENE AND DOPED WITH TETRACENE.	
(after Zschokke-Gränacher [175]).	36
FIGURE 2.4 - PHOTOCARRIER GENERATION PROCESSES.	
(a) One-quantum process; (b) Two-quantum process;	
(c) Three-quantum process; (d) Four-quantum process.	45
FIGURE 2.5 - SPECTRAL DEPENDENCE OF THE PHOTOVOLTAGE OF ANTHRACENE	
CRYSTALS AND SPECTRAL DEPENDENCE OF ABSORPTION	
COEFFICIENTS. (after Vertsimaka [157])	51
FIGURE 2.6 - THE ENHANCEMENT OF PHOTOVOLTAGE DUE TO LOCAL CHARGE	
NON-NEUTRALITY IN NAPHTHALENE CRYSTALS.	
(a) Red light produced by previously illuminating	
the specimen with violet light;	
(b) Red light produced by previously illuminating	
the specimen with green light.	
(after Tavares [149]).	53
FIGURE 2.7 - THE CHANGE OF THE PHOTOVOLTAGE IN ANTHRACENE CRYSTAL	
DUE TO CHANGE IN THE AMBIENTS. (after Nakada et al	
[102])	55

- FIGURE 3.1 - THE CURRENT-VOLTAGE CHARACTERISTICS OF ANTHRACENE FILMS OF THICKNESS
 (a) 1.62μ ; (b) 2.49μ ; (c) 3.90μ ; (d) 8.80μ ;
 and (e) 11.50μ 65
- FIGURE 3.2 - d_{eff}/d AS A FUNCTION OF d/x_0 FOR
 (a) $S(x) = 1$
 (b) $S(x) = 1 + 0.5 \exp(-x/x_0)$
 (c) $S(x) = 1 + 0.5\{\exp(-x/x_0) + \exp[-(d-x)/x_0]\}$
 (d) $S(x) = 1 + \exp(-x/x_0)$
 (e) $S(x) = 1 + \{\exp(-x/x_0) + \exp[-(d-x)/x_0]\}$
 (f) $S(x) = 1 + 2 \exp(-x/x_0)$
 (g) $S(x) = 1 + 2\{\exp(-x/x_0) + \exp[-(d-x)/x_0]\}$ 68
- FIGURE 3.3 - I AND d_{eff}/d AS FUNCTIONS OF FILM THICKNESS FOR
 (a) $V = 20V$; and (b) $V = 10V$ 69
- FIGURE 3.4 - μ_{eff}/μ_0 AS A FUNCTION OF $(E_c - E_{\text{tn}})/kT$ FOR TRAPS
 CONFINED IN A SINGLE DISCRETE ENERGY LEVEL 85
- FIGURE 3.5 - μ'_{eff}/μ_0 AS A FUNCTION OF V/d FOR TRAPS DISTRIBUTED
 EXPONENTIALLY WITHIN THE FORBIDDEN ENERGY GAP. 87
- FIGURE 4.1 - ELECTROLUMINESCENT BRIGHTNESS AS A FUNCTION OF
 CURRENT FOR (a) UNDOPED ANTHRACENE CRYSTALS, and
 (b) ANTHRACENE CRYSTALS DOPED WITH TETRACENE. 115
- FIGURE 4.2 - ELECTROLUMINESCENT BRIGHTNESS AS A FUNCTION OF
 APPLIED VOLTAGE FOR UNDOPED ANTHRACENE CRYSTALS
 AT 20°C 118
- FIGURE 4.3 - ELECTROLUMINESCENT BRIGHTNESS AS A FUNCTION OF
 TEMPERATURE FOR UNDOPED ANTHRACENE CRYSTALS FOR
 (a) APPLIED VOLTAGE: 1.2 kV , and (b) APPLIED
 VOLTAGE: 1.0 kV 121
- FIGURE 4.4 - ELECTROLUMINESCENT BRIGHTNESS (A, B AND C CURVES)
 AND d.c. THRESHOLD VOLTAGE FOR THE ONSET OF ELECTRO-
 LUMINESCENCE (D CURVE) AS FUNCTIONS OF TEMPERATURE . . . 127

FIGURE 4.5 - THE d.c. CURRENT-VOLTAGE CHARACTERISTICS.	128
FIGURE 5.1 - THE VARIATION OF V_{bI}/V_{bo} WITH d/L FOR THE CASE OF LOCAL-CHARGE NEUTRALITY WITH TRAPS UNDER STRONG ABSORPTION CONDITIONS	150
FIGURE 5.2 - THE VARIATION OF V_{bII}/V_{bo} WITH d/L FOR THE CASE OF LOCAL-CHARGE NEUTRALITY WITH TRAPS UNDER WEAK ABSORPTION CONDITION.	152
FIGURE 5.3 - THE VARIATION OF V_{bI}/V_{bo} WITH d/L FOR THE CASE OF LOCAL-CHARGE NON-NEUTRALITY WITHOUT TRAPS UNDER STRONG ABSORPTION CONDITIONS.	154
FIGURE 5.4 - THE VARIATION OF V'_{bII}/V_{bo} WITH d/L FOR THE CASE OF LOCAL-CHARGE NON-NEUTRALITY WITHOUT TRAPS UNDER WEAK ABSORPTION CONDITIONS.	155

LIST OF TABLES

TABLE 2.1 - THE CHEMICAL STRUCTURE, MELTING POINT AND DRIFT MOBILITIES OF NAPHTHALENE, ANTHRACENE AND TETRACENE.	8
TABLE 2.2 - THE EXPRESSIONS FOR THE CURRENT-VOLTAGE CHARACTERISTICS FOR SINGLE AND DOUBLE INJECTION WITH AND WITHOUT TRAPS	10
TABLE 2.3 - SUMMARY OF PREVIOUS EXPERIMENTAL RESULTS OF CARRIER TRAPS IN ANTHRACENE CRYSTALS.	14
TABLE 2.4 - SUMMARY OF PREVIOUS EXPERIMENTAL DATA FOR SINGLET AND TRIPLET EXCITONS IN ANTHRACENE CRYSTALS	23
TABLE 2.5 - THE ABSORPTION AND EMISSION SPECTRUM RANGES OF NAPHTHALENE, ANTHRACENE AND TETRACENE CRYSTALS.	34
TABLE 2.6 - MATERIALS USED AS CARRIER INJECTING CONTACTS TO ANTHRACENE CRYSTALS	38
TABLE 2.7 - SUMMARY OF PREVIOUS EXPERIMENTAL RESULTS OF ELECTROLUMINESCENCE IN ANTHRACENE CRYSTALS	39
TABLE 2.8 - SUMMARY OF PREVIOUS EXPERIMENTAL RESULTS OF PHOTOVOLTAIC EFFECT IN ANTHRACENE CRYSTALS	56

LIST OF MOST USED SYMBOLS

B, B^d	brightness of electroluminescence for undoped and doped crystal, respectively.
C_G	dopant (guest molecule) concentration.
d	specimen thickness.
D_n, D_p	electron and hole diffusion coefficients, respectively.
E	energy level.
E_c, E_v	energy levels at conduction band and valence band edges, respectively.
E_{Fn}, E_{Fp}	quasi-Fermi levels for electrons and holes, respectively.
E_g	energy band gap.
E_u, E_l	upper and lower limits of the trapping energy levels, respectively.
E_{tn}, E_{tp}	electron and hole trapping energy levels, respectively.
f_n, f_p	Fermi-Dirac distribution functions for trapped electrons and holes, respectively.
f, f'	fractions of triplet-triplet and triplet-trapped triplet annihilations, respectively, which create singlet excitons.
F	electric field.
g_b	bulk photo-carrier generation rate.
g_n, g_p	degeneracy factors of trap states for electrons and holes, respectively.
g_s, g_T	fraction of electron-hole pairs that produces the singlet excitons and triplet excitons, respectively, after recombination.

h_n, h_p	trap density distribution functions for electrons and holes, respectively.
H_{an}, H_{ap}	trap densities for electrons and holes, respectively, for the traps confined in a single discrete energy level.
H_{bn}, H_{bp}	trap densities per unit energy interval for electrons and holes, respectively, for the traps distributed exponentially within the forbidden energy gap.
H_{dn}, H_{dp}	trap densities per unit energy interval for electrons and holes, respectively, for the traps distributed uniformly within the forbidden energy gap.
I	total current
J, J_n, J_p	total, electron, and hole current densities, respectively.
k	Boltzmann constant.
K_{es}, K_{et}	energy transfer constant for singlet excitons and triplet excitons, respectively.
K_s, K_t	carrier-singlet exciton and carrier-triplet exciton reaction rates, respectively.
ℓ	$= T_c/T$
L	effective carrier diffusion length.
n, n_f, n_t	total, free, and trapped electron densities, respectively.
n_{fo}, n_{to}	free and trapped electron densities in thermal equilibrium without light illumination.
n_{at}	trapped electron density for the traps confined in a single discrete energy level.
n_{bt}	trapped electron density for the traps distributed exponentially within the forbidden energy gap.

n_{dt}	trapped electron density for the traps distributed uniformly within the forbidden energy gap.
$\Delta n, \Delta n_f, \Delta n_t$	total, free and trapped excess electron densities, respectively.
N_c, N_v	effective densities of states in the conduction and the valence bands, respectively.
p, p_f, p_t	total, free and trapped hole densities, respectively.
p_{fo}, p_{to}	free and trapped hole densities in thermal equilibrium without light illumination.
p_{at}	trapped hole density for the traps confined in a single discrete energy level.
p_{bt}	trapped hole density for the traps distributed exponentially within the forbidden energy gap.
p_{dt}	trapped hole density for the traps distributed uniformly within the forbidden energy gap.
$\Delta p, \Delta p_f, \Delta p_t$	total, free and trapped excess hole densities, respectively, after light illumination.
q	electronic charge.
Q	quantum yield for carriers generation.
R	electron-hole recombination rate.
$[s], [s_G]$	free and trapped singlet excitons, respectively.
T	absolute temperature.
t_{hs}, t_{hp}	hopping time for singlet excitons and triplet excitons, respectively.
T_b	brightness characteristics temperature.
T_c	characteristic constant of the trap distribution.

$[T], [T_G]$	free and trapped triplet excitons, respectively.
v	thermal velocity of carriers.
V	applied voltage.
V_{ph}	photo-voltage.
x_s	surface path length of singlet excitons.
α_1, α_2	rate constants for the radiative and nonradiative transition with emission of photons for singlet excitons, respectively.
α_{G1}, α_{G2}	rate constants for the radiative and nonradiative transition with emission of photons for trapped singlet excitons, respectively.
α_{HG}	transfer rate constant between free and trapped singlet excitons.
β_1, β_2	rate constants for the radiative and nonradiative transition with emission of photons for triplet excitons, respectively.
β_{1G}, β_{2G}	rate constants for the radiative and nonradiative transition with emission of photons for trapped triplet excitons, respectively.
β_{HG}	transfer rate constant between free and trapped triplet excitons.
γ, γ_G	the effective rate constants for triplet-triplet annihilation and triplet-trapped triplet annihilation, respectively.
ϵ	dielectric constant.
ϵ_a	absorption coefficient.
η_e	light extraction efficiency.
η_g	light generation efficiency.
η_i	carrier injection efficiency.
η_{int}	internal quantum efficiency.

η_q	external quantum efficiency.
λ_S, λ_T	diffusion length of singlet excitons and triplet excitons, respectively.
μ_n, μ_p	electron and hole mobilities, respectively.
ρ	space charge density.
σ	conductivity.
σ_R	electron-hole recombination cross section.
τ_n, τ_p	lifetimes of excess electrons and holes inside the crystal, respectively.
$\langle v\sigma_R \rangle_o$	electron-hole recombination constant without traps.
$\langle v\sigma_R \rangle_a$	electron-hole recombination constant for the traps confined in a single discrete energy level.
$\langle v\sigma_R \rangle_b$	electron-hole recombination constant for the traps distributed exponentially within the forbidden energy gap.
$\langle v\sigma_R \rangle_d$	electron-hole recombination constant for the traps distributed uniformly within the forbidden energy gap.

CHAPTER I

INTRODUCTION

In the past ten years organic semiconductors have been extensively studied, both experimentally and theoretically, by many investigators [8,55,71,80]. Research in this field is rapidly growing, partly because of their potentialities for electronic devices, and partly because of their organic structures, and the study of these materials may throw some light on the understanding of the behaviour of biological systems.

Among the known organic semiconductors, anthracene possesses a relatively simple crystal structure and a reasonable carrier mobility ($\sim 1 \text{ cm}^2/\text{v-sec}$) and is relatively easy to purify and to grow. This is one of the reasons that it has been used as the model material by the majority of the investigators in their studies of organic semiconductors.

Since approximations have to be made in developing theoretical models, discrepancies occur between theoretical and experimental results reported by different investigators. The present state of art indicates that not only the theoretical models have to be improved, but also the significance of some physical factors which have been ignored must be re-examined. The main purpose of the investigation being reported in this thesis is to study all possible factors that may control injection, electroluminescence and photovoltaic phenomena and to determine the conditions for their occurrence and subsequent effects.

Current injection in a solid can be classified into (i) single

injection and (ii), double injection. In the case of single injection of one type of charge carriers (electrons or holes) from an ohmic contact electrode, the injected carrier will interact with the traps present in the solid, thus controlling the carrier flow and determining the current-voltage (J-V) characteristics, many investigators [77] have used the J-V characteristics to determine the possible distribution of traps in energy within the forbidden gap by comparing their experimental results with the theoretical expressions available for different forms of trap distribution. Muller [98] has reported a unified approach for obtaining the J-V characteristics in a solid having traps distributed non-uniformly in energy but homogeneously in space. However, it can be imagined that the spatial distribution of traps can never be homogeneous because there always exist discontinuities between the material and electrodes [103,146]. The thinner the material specimen used for experimental studies, the more is the influence of the form of spatial distribution of traps on the J-V characteristics. In the case of double injection, charge carriers of both types (electrons and holes) are present and the problem becomes much more complicated because in this case the recombination which controls the J-V characteristics may either be bimolecular - direct band to band recombination, or occur through one or more sets of localized traps - indirect recombination. In deriving the J-V characteristics many investigators [10,77] either neglected the effect of trapping centers or assumed that the quasineutrality approximation could be made. For partially or completely filled deep traps Lampert and Schilling [76] have derived the J-V characteristics using the regional approximation method that the specimen is

divided into regions which either satisfy the quasineutrality approximation or are dominated by trapped or free space charge. In Chapter III of this thesis we shall present our new approaches to the theory of current injection in solid for the cases of single injection and double injection, taking into account the effects of traps of different types of distribution in space and in energy, and some computed results to compare with experimental results.

Electroluminescence in undoped and doped anthracene crystals with a pair of double-injection electrodes has been observed by many investigators [51,54,124,125,167,168,170]. Earlier than this, Pope et al [109,119] have reported their observation of electroluminescence in undoped anthracene crystals and anthracene crystals doped with 0.1 mole % of tetracene using silver paste for electrodes, which has been known [12,61] to provide a contact which weakly injects holes and blocks electron injection at low fields. Recently, a similar electroluminescent phenomenon using silver single injection electrodes has also been reported by Williams et al [168], and some Russian investigators [17,176] in anthracene; and by Lohmann et al [83] in naphthalene.

For double injection the recombination of the injected holes with the injected electrons will yield singlet and triplet excitons and it is these singlet excitons that radiatively decay producing electroluminescence. For single injection (say, hole injection) the other type of charge carriers (say, electrons) is also supplied from the counter electrode (say, electrons from the cathode) but in this case the supply of minority carriers occurs only at relatively high fields. Thus, the so called single injection would become double injection at the threshold

voltage for the onset of electroluminescence. In fact, many materials have been used as electrodes [51,92,167,170,175] to produce electroluminescence in anthracene. The fact that different materials used for electrodes result in different values of threshold voltages indicates that there are no perfect ohmic contacts, and that different electrode materials in contact with a crystal surface will form different potential barriers for carrier injection.

It can also be imagined that the interface between an electrode and a crystal surface which is not microscopically identical from domain to domain is never homogeneous and uniform. Thus, there must be one or more microregions at which the potential barrier has a profile more favourable to carrier injection than at other regions of the interface. Furthermore, the crystal itself is never microscopically homogeneous and uniform. For all these unavoidable imperfections, the current passing through a crystal specimen is filamentary, at least from a microscopic point of view. For an electrical field applied to the specimen longitudinally, the field will not be uniform longitudinally due to the effect of space charge and the current density will not be uniform radially due to the formation of filamentary paths. The current filaments formed in Si, GaAs, ZnTe, $\text{GaAs}_x\text{P}_{1-x}$ and polycrystalline Si have been observed by Barnett et al [8,9]. Therefore, in Chapter IV of this thesis we shall present our new approach to the double injection filamentary theory and discuss some electroluminescent phenomena based on this filamentary theory.

The photovoltaic effect can be considered to be the inverse process of electroluminescence. In organic crystals, Kallmann and Pope [63] were the first to report that when an anthracene was illuminated with

a strong light of the fundamental absorption region of anthracene ($\lambda = 3650 \text{ \AA}$), a photovoltage of magnitude up to 0.2V was produced with negative polarity on the illuminated surface. This phenomena was attributed to the diffusion of more photo-generated holes from the illuminated to the non-illuminated surfaces since the hole mobility is larger than the electron mobility in anthracene crystals [69,80,100]. Since then, many investigators [44,48,87,102,149,157,159] have reported their observation of the photovoltaic effect in organic crystals. Piryatinskii et al [157,159] have reported that if the anthracene was illuminated with the light of the wavelengths unimportant to absorption (e.g. $\lambda \geq 4000 \text{ \AA}$) the polarity of the photovoltage produced was reversed to that observed by Kallmann et al. They have attributed this phenomenon to the photo-release of the electrons from the traps inside the crystal and to the formation of anti-barrier bending of the bands at the illuminated surface. It has also been reported [102,157,159] that the spectral distribution of the photovoltage amplitude correlates closely to the absorption spectrum, and the change of light intensity changes only the photovoltage amplitude but does not affect this correlation, and that the photovoltage is sensitive to the surface condition. Adsorption of oxygen atoms on the crystal surfaces reduces the amplitude of the photovoltage. However, this important phenomenon neither has been systematically studied experimentally nor has it been rigorously analyzed theoretically for organic crystals. Therefore, in Chapter V of this thesis, we shall present our theoretical analysis of this photovoltaic phenomenon taking into account the effects of traps.

As a great deal of work in this field has been available in the

literature, a brief review of available knowledge about current injection, electroluminescence and photovoltaic phenomena, particularly in anthracene crystals, would give a general outlook about the progress of this field. Such a brief review is therefore given in Chapter II. Conclusions arising from the present investigation are given in Chapter VI.

CHAPTER II

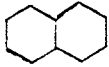
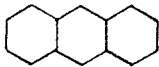
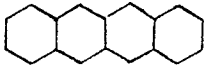
REVIEW OF PREVIOUS WORK ON ORGANIC SEMICONDUCTORS

In the past few years several extensive review articles in the field of organic semiconductors have been published [5,21,48,55,71,77,108,115,173]. In this Chapter, only a brief review on the work relevant to the present investigation is given, with particular emphasis on the work which has not been included in the aforementioned review articles.

In general, molecular crystals of simple organic structures have the characteristics of wide energy gap, high resistivity, low carrier mobility and low melting point; for example, anthracene crystal has an energy band gap of about 4 eV, resistivity of about 10^{16} to 10^{20} ohm-cm and mobility of about $1 \text{ cm}^2/\text{v-sec}$ at 20°C , and melting point of 216°C (see Table 2.1). Therefore, it is almost impossible to generate a great number of carriers by the thermal excitation process because of its large energy band gap. Generally, the generation of carriers in such materials, requires external sources. There are three important sources for carrier generation, and they are (i) carrier injection from chemically active ohmic contacts, (ii) carrier generation in the bulk by the photo-excitation and (iii) carrier emission from electrodes through photoemission process. We shall discuss the source (i) in Section 2.1 and source (ii) and source (iii) in Section 2.3. Source (i) provides the advantage that holes and electrons can be injected separately. The radiative recombination of electrons and holes injected

TABLE 2.1

THE CHEMICAL STRUCTURE, MELTING POINT AND DRIFT MOBILITIES OF NATHTHALENE, ANTHRACENE AND TETRACENE

Organic Semiconductors	Chemical Structure	Melting Point	Types of Charge Carriers	Crystal Axis	Mobilities (cm ² /v-sec) at 20°C	Temperature (T) Dependence	Reference
Naphthalene C ₁₀ H ₈		80.2°C	electrons	a b c'	0.51 0.63 0.68	T ^{-0.1} T ^{-0.0} T ^{-0.9}	[93]
			holes	a b c	0.88 1.41 0.99	T ^{-1.0} T ^{-0.8} T ^{-2.1}	[93]
Anthracene C ₁₄ H ₁₀		216°C	electrons	a b c'	1.7 1.0 0.4	T ^{-1.0} T ^{-1.5}	[69,80,100]
			holes	a b c'	1.0 2.0 0.8	T ^{-0.0} T ^{-2.0} T ^{-1.7}	[69,80,100]
Tetracene (Naphthacene) C ₁₈ H ₁₂		357°C	electrons	a b c'	0.5		[7,44,147]
			holes	a b c'	0.01		[7,44,147]

from opposite contacts produces electroluminescence and this will be discussed in Section 2.2. Finally, the photovoltaic effect is discussed in Section 2.3.

2.1 CARRIER INJECTION FROM CONTACTS

The book of Lampert and Mark [77], has given quite a comprehensive review on the current injection from contacting electrodes to inorganic crystals. In this Section, we shall review mainly the work in this field for organic crystals. Current injection into a solid is generally classified into (a) single injection and (b) double injection. Single injection means that the current flow is mainly due to one type of carriers (electrons or holes) injected from a contacting electrode into the solid. These injected carriers would gradually establish a space-charge leading to the well known single-carrier space-charge-limited current. Double injection means that the current flow involves two types of carriers, electrons injected from the cathode and holes from the anode. In double injection, recombination kinetics control all the electrical properties. The recombination process may either be bimolecular (i.e., band-to-band electron-hole recombination) or may occur through one or more sets of localized recombination centers. In the following, we shall limit ourselves to the steady state electrical properties. The general expressions for the current-voltage (J-V) characteristics for the most important cases are summarized in Table 2.2. The J-V characteristics are strongly dependent on the concentration and the distribution function of traps inside the specimen.

The diffusion term can be considered to be much smaller than the

TABLE 2.2

THE EXPRESSIONS FOR THE CURRENT-VOLTAGE CHARACTERISTICS FOR SINGLE AND DOUBLE INJECTIONS WITH AND WITHOUT TRAPS

	Single Injection in Solids	Reference	Double Injection in Solids	Reference
Trap-free	$J = 9/8 \epsilon \mu_p V^2/d^3$	[99]	$J = 9/8 \epsilon \mu_{eff} V^2/d^3$ $\mu_{eff} = \mu_{R0} \mu_n \mu_p \left(\frac{2}{3}\right)^2 \left[\frac{(\frac{3}{2}(\nu_n + \nu_p) - 1)!}{(\frac{3}{2}\nu_n - 1)! (\frac{3}{2}\nu_p - 1)!} \right]^2 \left[\frac{(\nu_n - 1)! (\nu_p - 1)!}{(\nu_n + \nu_p - 1)!} \right]^3$	[106]
Traps confined in a single discrete energy level.	$J = 9/8 \epsilon \mu_p \theta V^2/d^3$ $\theta = N_v/N_t \exp(-E_t/kT)$	[55,77,120]	See Chapter III	[59]
Traps distributed exponentially within the forbidden energy gap.	$J = N_v \mu_p q \left(\frac{\epsilon \ell}{\mu_b q \ell (\ell+1)} \right)^\ell \left(\frac{2\ell+1}{\ell+1} \right)^{\ell+1} \frac{V^{\ell+1}}{d^{2\ell+1}}$ $\ell = T_c/T$	[7,55,77,89]	See Chapter III	[59]
Traps distributed uniformly within the forbidden energy gap.	$J = \frac{q \mu_p N_v}{d} V \exp\left(-\frac{E_g}{kT}\right) \exp\left(\frac{2eV}{e h_c k T d^2}\right)$	[98,117,153]	See Chapter III	[59]

drift term if the applied field is large as to make the drift term predominant. In general, for the applied voltage larger than several kT/q [55,82] the diffusion term may be neglected without causing a serious error.

As there is no perfect crystals, there are always traps present in the crystals. In organic semiconductors two types of carrier trap distributions have been reported [48,55], and they are (i) the traps confined in discrete energy levels in the forbidden energy gap and (ii) the traps with a quasi-continuous distribution of energy level (normally following an exponential form), having a maximum trap density near the band edges [55,89]. Both types of traps have been extensively investigated in anthracene crystals [13,55,89,113,114,120,121,125,142,145,152,108]. Simultaneous presence of both types of carrier trap distributions have also been observed [120,152]. The energy levels and the distribution of carrier traps can be experimentally determined either by the space-charge-limited current (SCLC) method [55], by the thermo-stimulated current (TSC) method [151], or by the photoemission method [21]. Although these methods may provide some information about the energetic and kinetic parameters of traps, they do not give any hint as to the possible physical nature of traps. Some general considerations have been suggested to relate the discrete traps with chemical impurities introduced into the lattice (chemical traps) and to relate the quasi-continuous trap distribution with the imperfection of the crystal structure (structural trap).

We shall discuss the case of discrete traps. Hoesterey and Letson [57] have shown that tetracene molecules doped into an anthracene crystals form shallow discrete traps both for electrons and for holes. However,

anthraquinone molecules in anthracene do not form effective discrete traps for electrons. Several investigators [55,120] have derived the expression for the J-V characteristics for this case with traps confined in a single discrete energy level. This expression is given in Table 2.2. The only difference between this case and the case without traps is a multiplication factor θ , which is defined as the ratio of free carrier density to the total carrier density and its value is usually much smaller than unity. When the applied voltage increases or the injection level becomes so high that the traps are gradually filled up, then the expression of current-voltages with discrete traps will be superseded by the expression for the case without traps (see Table 2.2). The current for both cases is proportional to the square of the applied voltage. The transition from a small current (trap-controlled) to a higher current (trap free--after all traps are filled) occurs very sharply at a critical voltage V_{TFL} , where TFL stands for the trap-filled-limited region. By measuring the value of V_{TFL} , we can determine the trap density based on the relation [77,117]

$$N_t \sim \frac{3}{2} \frac{\epsilon}{q} \frac{V_{TFL}}{d^2} \quad (2.1)$$

Now we shall discuss the case with traps distributed exponentially within the forbidden energy gap. Measurements of the steady-state space-charge-limited current in single crystals and polycrystalline specimens of naphthalene [83], anthracene [89,113,114,120,145,152], tetracene [7], perylene [93], p-terphenyl [148], p-quarterphenyle [148] and phthalocyanines [49,143] as well as in inorganic semiconductors [117] have shown that the currents are controlled by the traps distributed

in the forbidden energy gap following the relation

$$h(E) = \frac{H_b}{kT_c} \exp \left(- \frac{E}{kT_c} \right) \quad (2.2)$$

where H_b is the total trap density and kT_c is the characteristic energy distribution. This indicates that the traps in those specimens may be due to the structural defects. On the assumptions that the diffusion term is neglected and $T_c > T$, the expression for the J-V characteristics has been derived by many investigators [7,83,89] and it is given in Table 2.2. Since $\ell > 1$, the dependence of J on V follows a power-law, and is stronger than that for the case without traps and for the case with discrete traps, in both of which $J \propto V^2$. On the basis of the experimental results for anthracene the total overall hole trap densities have been calculated to be of the order of $10^{14} - 10^{19} \text{ cm}^{-3}$ with the characteristic energies distributed between 0.035 and 0.25 eV (see Table 2.3) above the valence band edge [114].

The space-charge-limited current-voltage characteristics for the case with uniform continuous trap densities were first investigated by Rose [117]. The J-V characteristics depend on the bandwidth of the distribution, its position in the forbidden band gap. The trap distribution can be written as

$$h(E) = N_t / (E_{tu} - E_{t\ell}) = H_c \quad (2.3)$$

where H_c is the density of traps per unit energy interval, N_t is the total trap density, E_{tu} and $E_{t\ell}$ are, respectively, the upper and lower energy limits of the trap energy distribution. By assuming $E_{t\ell} = 0$ and $E_{tu} = E_g$ the expression for the J-V characteristics is given in Table 2.2.

TABLE 2.3

SUMMARY OF PREVIOUS EXPERIMENTAL RESULTS OF CARRIER TRAPS IN ANTHRACENE CRYSTALS

Specimen Preparation	Trap Density H_b (cm^{-3})	ℓ (from $j \propto V^{\ell+1}$)	kT_c (eV)	Trapping Level E_t (eV)	Trap Density N_t (cm^{-3})	Reference
Melt - grown	1.5×10^{19}	1.4	0.035			[114,152]
	2.73×10^{18}	1.5	0.0375			
	1.5×10^{18}	1.64	0.041			
	3.5×10^{13}	4.8	0.12			
	1.1×10^{17}	1.0	0.25			
Vapor - grown	1.2×10^{17}	2.28	0.057			[114,152]
	1.1×10^{13}	2.5	0.0625			
	3.6×10^{15}	2.6	0.065			
Solution - grown	5.75×10^{16}	1.9	0.0475			[114,152]
	1.75×10^{15}	4.2	0.13			
	4.2×10^{14}	5.6	0.14			
Melt--grown (zone refined)				0.53 ± 0.03 eV	1.5×10^{19}	[120,145, 152]
Doped with Tetracene				0.43 eV		[57]
Doped with Perylene				0.25 eV		[57,144]

Based on the analysis of experimental results, such uniform trap distribution has so far not been identified to exist in organic semiconductors. However, the experimental results on amorphous Se films [153] show that a uniform trap distribution in the forbidden energy gap does exist, and the dark conduction at high fields depends on this form of trap distribution. Touranine et al [153] have reported that for amorphous Se the band width of the distribution is 0.25 eV and $E_{t\ell}$ lies 0.74 eV above the valence band edge, that the trap density per unit energy is $5 \times 10^{14} \text{ cm}^{-3} \text{ eV}^{-1}$; and that these values are not affected by the change of temperature in the range from 233°K to 293°K.

In the above discussion, we have assumed that the diffusion term is neglected. If the diffusion term is taken into account, the mathematical treatment is very complicated even for the case without traps. However, if the crystal is very thin, then diffusion current may become large enough to produce various effects even at voltages greater than that usually used, because the "virtual cathode" (for electron injection) or "virtual anode" (for hole injection) is moving away from the geometric cathode or anode into the crystal, creating a maximum field in the region in which the concentration of free carriers is higher than that in the rest of the crystal. This is equivalent to saying that the effective thickness of the specimen is reduced, and thus the current flow is higher than the flow that would be expected when based on actual specimen thickness. From the current flow equation and the Poisson equation, we obtain

$$\frac{d^2 F}{dx^2} + \left(\frac{q^2}{2\epsilon kT} \right) \frac{dF^2}{dx} + \frac{qJ}{\epsilon \mu_p kT} = 0 \quad (2.4)$$

Several investigators [82,135,174] have attempted to solve equation (2.4).

Wright [174] was the first to obtain a general solution in terms of Bessel functions, and later Lindmayer et al [82] obtained one in terms of difference equations. Sinharay et al [135] has solved equation (2.4) in terms of Airy functions, and they give explicitly the position of the maximum field inside the crystal as a function of current density.

The number of different possible conditions for double injection to occur is certainly larger than that for one-carrier single injection, because a large number of independent physical processes may come into play for double injection. For this reason, the analytical difficulties are much greater for this case than for the case of single injection. Even if the diffusion currents are neglected, the combination of space-charge and recombination effects makes it difficult to analyze this case analytically. So far only the case in which the diffusion term and the effect of traps are neglected has been solved in analytic form by Parmenter and Ruppel [106], and this is given in Table 2.2. Since the cases taking into account the effect of arbitrary trap distribution have not yet been solved in analytic forms, part of our aim is therefore to present our unified approaches to this problem. This shall be discussed in more detail in Chapter III.

Lampert et al [76,77] have used the so called "the regional approximation method" to analyze the case for the traps confined in a single discrete energy level either fully occupied or partially occupied. Based on their analysis, there is a current-controlled negative differential resistance region caused by double injection. Using this regional approximation method, they have dealt with some special cases which we shall not discuss here. However, the details can be found in the literature

[76,77]. It should be noted that Lampert's model has been used to explain the experimental results of the negative differential resistance observed in anthracene crystals [121,122] with double injection.

By considering the double injection current to be filamentary rather than uniformly distributed, Barnett et al [8,9] have derived an expression for the J-V characteristics for the case without traps which is

$$I = \left(\frac{2\pi}{a}\right) [8 q \epsilon \mu_n \mu_p (\mu_n + \mu_p) / \langle v \sigma_R \rangle_0]^{\frac{1}{2}} (V^2/d^3) \\ \times [\ln(1+ar_d) + 1/(1+ar_d) - 1] \quad (2.5)$$

where r_d is the devices radius, or its equivalent radius, if the device is not circular in cross-sectional area; and

$$a = [2 \epsilon \mu_n \mu_R \langle v \sigma_R \rangle_0 / q(\mu_n + \mu_p)]^{\frac{1}{4}} (V/3D_a)^{\frac{1}{2}} (1/d) \quad (2.6)$$

Their model can explain well the experimental results for Si [8] and GaAs [9].

As the effect of the traps is very important. We devise a new unified approach to extend their work to the cases with traps. The details will be given in Chapter IV. It will be shown that our unified approach can explain quantitatively many electroluminescent phenomena in organic semiconductors.

2.2 ELECTROLUMINESCENCE IN ORGANIC SEMICONDUCTORS

Electroluminescence has been observed in undoped-anthracene crystals [51,54,167,168,170], tetracene-doped anthracene crystals [33,66,109,124,125,175] and naphthalene crystals [83], either with double injection or with single injection electrodes. It is well understood that the

electroluminescence is produced in the bulk of the crystal by direct recombination of electrons and holes simultaneously injected into the crystal from injecting electrodes. Electron-hole recombination may lead to both radiative and non-radiative transitions, and it is the radiative transition which produces electroluminescence. In general, there are five different processes [47] for radiative transitions in solids and they are: (i) band-to-band recombination, (ii) recombination via shallow donor or acceptance levels, (iii) donor-acceptor recombination, (iv) recombination via deep energy levels and (v) exciton transitions. In inorganic semiconductors, processes (i) - (iv) may be dominant. However, in organic semiconductors the last process (v) is the most important process. It is generally accepted [54] that the recombination of injected holes with injected electrons in organic semiconductors will yield singlet and triplet excitons and it is these singlet excitons that radiatively decay, producing electroluminescence. The quantum yield of electroluminescence depends on the probabilities of radiative and non-radiative transitions and on the relative efficiency of producing the radiative exciton. There are many possible processes for non-radiative transitions [78]. In inorganic semiconductors two possible processes, (i) multiphonon transition and (ii) Auger recombination, are dominant. However, in organic semiconductors, again the process of exciton transitions leading to non-radiative transitions of the exciton is the most important processes. The exciton transitions can be classified into (i) the non-radiative, such as intersystem crossing and internal-conversion and simple monomolecular decay; (ii) exciton-exciton interactions, (iii) exciton-carrier interactions; and (iv) exciton-surface interactions. In the following, we shall briefly

discuss the mechanisms responsible for electroluminescence and the effects on its intensity.

2.2.1 The recombination mechanisms

In general, most inorganic semiconductors have a large mobility and a small recombination rate constant, but most organic semiconductors have a much smaller mobility and a much larger recombination rate constant. In this subsection, we shall review briefly the carrier and exciton recombination mechanisms and their relation to the electroluminescence in organic semiconductors.

(i) Carrier recombination

Generally, carrier recombination involves two steps: (a) the electron and the hole have to get close enough to one another so that they can become trapped in each other's Coulomb field, and (b) they have to lose sufficient energy to become trapped. Classically, an electron becomes trapped in a Coulomb field if its kinetic energy is less than its potential energy in the field. Therefore, if an electron gets close to a hole with a distance less than a critical radius r_c defined by

$$\frac{3}{2} kT = \frac{q^2}{\epsilon r_c} \quad (2.7)$$

the probability for this electron to be trapped and eventually to recombine with the hole increases markedly. For anthracene crystals, $\epsilon = 3.14 \epsilon_0$ [54], which ϵ_0 is the permittivity of free space, and hence $r_c = 120 \text{ \AA}$ at room temperature.

The recombination rate constant for anthracene has been calculated [54,94,138] on the basis of the Langevin recombination model [94].

In Langevin's theory [54] the carrier recombination probability in gases is appropriate if $\lambda_o \ll r_c$, where λ_o is the mean free path of carriers. For anthracene $\lambda_o \approx 7 - 10 \text{ \AA}$ this condition can be fulfilled. The relative drift velocity v_d of a positive or a negative ion when they are at a distance r apart is [94]

$$v_d = (\mu_+ + \mu_-)(q/\epsilon_o r^2) \quad (2.8)$$

where μ_+ and μ_- are the drift mobilities of the positive and negative ions, respectively. The rate of influx of positive ions into a sphere of arbitrary radius r drawn around a negative ion, or the recombination rate constant is

$$4 \pi r^2 \epsilon_o v_d = 4 \pi q (\mu_+ + \mu_-) \quad (2.9)$$

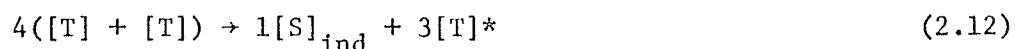
This theory for gases can be applied to electrons and holes in solids if the effect of dielectric constant is included. In anthracene the mean free path for carriers λ_o is less than r_c so that it is likely that the Langevin theory might apply. If we take $\mu_+ + \mu_- \approx 2 \text{ cm}^2 \text{ v}^{-1} \text{ sec}^{-1}$ and $\epsilon = 3.14 \epsilon_o$, the recombination rate constant according to Langevin's theory should be $1.2 \times 10^{-6} \text{ cm}^3 \text{ sec}^{-1}$ [94,138]. This value is in fact in very good agreement with that determined experimentally [54]. The recombination rate constant is large but finite and thus a certain charge overlap occurs. The width of recombination zone is given by [54,55]

$$W = 4q \mu_n \mu_p d / \langle v \sigma_R \rangle \epsilon (\mu_n + \mu_p) \quad (2.10)$$

It should be noted that [168] that if the hole and the electron mobilities differ considerably, e.g., $\mu_p \gg \mu_n$; then the recombination zone is confined in some particular portion of the crystal. This effect may become more apparent at lower temperatures owing to either the different temperature dependence of mobility or to the different trapping effects for the different types of carriers.

(ii) Exciton recombination:

Following the electron-hole recombination, the excited states finally formed may have either singlet or triplet character. Taking into account the different multiplicities of these states, and the formation of excited singlets indirectly from the triplet-triplet exciton recombination in pairs, then under steady state conditions the kinetic equation for electron-hole recombination may be formulated on the basis of the following assumptions: (a) the rates of production of singlet [5] and triplet [7] excitons by carrier recombination are proportional to the multiplicities of the respective states, this means that three times more triplets than singlets would be generated. (b) Two triplet excitons of lowest energy and with total spin of 1 (atomic units) can recombine to give one electronically or vibronically excited triplet exciton $[T]^*$, and (c) in the process $[T] + [T] \rightarrow [S]$ the two triplet excitons have total spin of 0. This means that three times more pairs of triplets with total spin 1 than with total spin 0 can be formed and that the triplet-triplet recombination also produces three times more triplets than singlets. Thus we may write



As monomolecular triplet decay is neglected, equation (2.10) is applicable only to the case with high triplet concentration. In general, the excited triplet excitons would decay into the lowest triplet state in a time much shorter than the lifetime of the latter. By adding the generated triplet excitons to triplet concentration, equation (2.12) may be rewritten as

$$5[T] \rightarrow 1[S]_{\text{dir}} \quad (2.13)$$

and by combining equations (2.9) and (2.11), we obtain

$$\begin{aligned} 20(e+h) &\rightarrow 5[S]_{\text{dir}} + 15[T] \\ &\rightarrow 5[S]_{\text{dir}} + 3[S]_{\text{ind}} \end{aligned} \quad (2.14)$$

where e and h represent, respectively, the electron and hole, $[S]_{\text{dir}}$ and $[S]_{\text{ind}}$ are, respectively, the singlet excitons produced by the direct and indirect processes. It is the population of $[S]_{\text{dir}}$ and $[S]_{\text{ind}}$ in the crystal, which governs the electroluminescent intensity. Since there is a great difference in lifetime between the singlet and triplet excitons (for example, they are 10^{-8} sec and 10^{-2} sec, respectively, in anthracene, see Table 2.4), the total electroluminescence consists of prompt electroluminescence due to $[S]_{\text{dir}}$ and delayed electroluminescence due to $[S]_{\text{ind}}$ (see Fig. 2.1) and exhibits time constants corresponding to both of these decays. In the steady state, the electroluminescence intensity is the combination of both prompt and delayed components.

TABLE 2.4

SUMMARY OF PREVIOUS EXPERIMENTAL DATA FOR SINGLET AND TRIPLET EXCITONS IN ANTHRACENE CRYSTALS

	Singlet Exciton	Reference	Triplet Exciton	Reference
Energy Level	3.14 eV	[48,115]	1.8 eV	[5,48,134]
Lifetime	10^{-8} sec	[48,115]	2.2×10^{-2} sec	[5,48,134]
Diffusion Coefficients	$2 \times 10^{-3} \text{ cm}^2 \text{ sec}^{-1}$	[48,115]	$2 \times 10^{-6} \text{ cm}^2 \text{ sec}^{-1}$ $1.6 \times 10^{-5} \text{ cm}^2 \text{ sec}^{-1}$ (in c' axis)	[5,48,164]
Diffusion Length	4.6×10^{-6} cm	[105]	$(2+1) \times 10^{-3}$ cm	[164]
Mono-molecular decay rate constant	$5 \times 10^7 \text{ sec}^{-1}$	[16,48]	40 sec^{-1}	[5,48,134]
Bi-molecular decay rate constant	$(4+2) \times 10^{-8} \text{ cm}^3 \text{ sec}^{-1}$	[16,48]	$2 \times 10^{-11} \text{ cm}^3 \text{ sec}^{-1}$	[5,48,134]
Exciton-carrier interaction constant	$5 \times 10^{-5} \text{ cm}^3 \text{ sec}^{-1}$	[160]	$6 \times 10^{-10} \text{ cm}^3 \text{ sec}^{-1}$ (for electrons) $1.1 \times 10^{-9} \text{ cm}^3 \text{ sec}^{-1}$ (for holes)	[161]

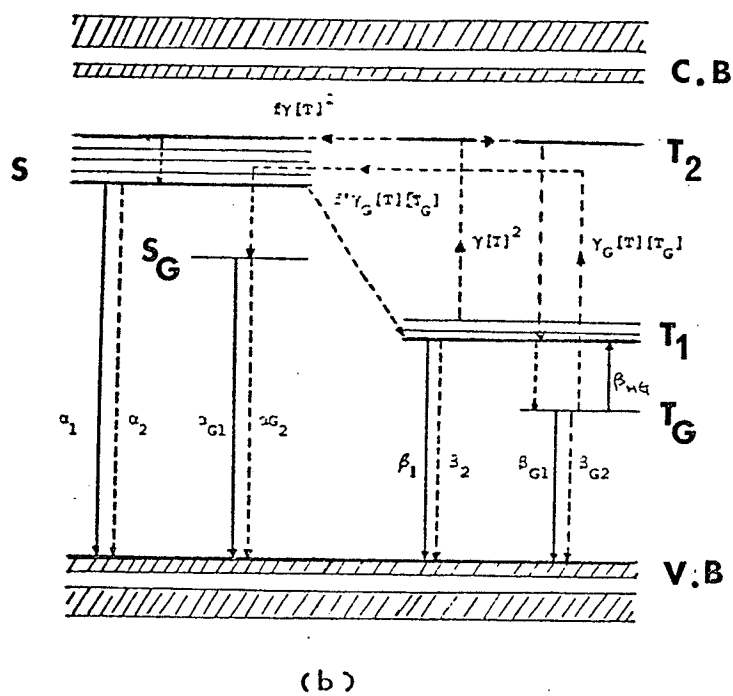
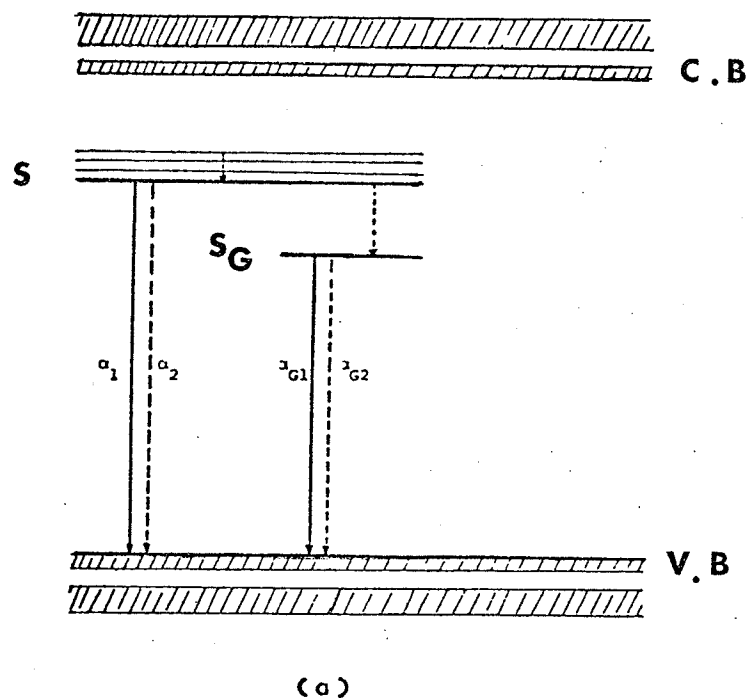


Fig. 2.1 - Electroluminescent processes in organic crystals.

Solid lines, radiative transition; dash lines, non-radiative transition.

(a) Prompt electroluminescence

(b) Delayed electroluminescence

2.2.2 The efficiency of electroluminescence

In this section we shall confine ourselves to the work related to the efficiency of quantum yield of electroluminescence. First of all, we shall review the general theory of radiative and non-radiative transition processes, and then the efficiency of radiative transition.

(i) The theory of radiative and non-radiative transition processes:

There are several important approximations or rules to form the basis for the quantum-mechanical theory of radiative and non-radiative transition processes in molecules. They are [17] the Born-Oppenheimer approximation, the Einstein Coefficients, the electric-dipole transition moments, the Franck-Condon principle and the selection rules, etc. In the Born-Oppenheimer approximation the total energy of the ground states (E_t) and that of the excited states (E'_t) in molecules are described as the sum of electronic (E_e , E'_e) and vibrational energies; and the wavefunction (ψ) of a vibronic state are expressed as the product of electronic (θ) and vibrational Φ wavefunctions. Thus we may write

$$\psi_{li} = \theta_l(x, Q) \Phi_{li}(Q) \quad (2.15)$$

as the wavefunction of the li vibronic state, where i indicates the i^{th} vibrational state of the lower electronic state l ; and

$$\psi_{mj} = \theta_m(x, Q) \Phi_{mj}(Q) \quad (2.16)$$

as the wavefunction of mj vibronic state, where j indicates the j^{th} vibrational state of the higher electronic state m ; and x and Q are the electronic and nuclear coordinates, respectively.

In the Einstein's radiation theory [17] there are two well known

coefficients: the Einstein A coefficient and the Einstein B coefficient. The Einstein A coefficient gives the probability of spontaneous emission, i.e., luminescence and its relation to the fluorescence spectrum and lifetime. The Einstein B coefficient gives the probability of absorption or induced emission. The relation between A and B coefficients for a molecule in a medium of refractive index η is [17]

$$A_{mj \rightarrow li} = (8 h^3 \nu_{mj \rightarrow li}^3 \eta^3 c^{-3}) B_{mj \rightarrow li} \quad (2.17)$$

where h is the Planck's constant, ν is the radiative frequency corresponding to the energy difference between the energy states m_j and l_i , and c is the light velocity.

The electric-dipole transition moment between any two states can be calculated with equations (2.15) and (2.16) as

$$\begin{aligned} M_{mj \rightarrow li} &= \langle \psi_{mj} | M' | \psi_{li} \rangle \\ &= \langle \theta_m | \bar{M}' | \theta_l \rangle \langle \phi_{mj} | \phi_{li} \rangle \\ &= |\bar{M}_{ml}| \cdot |S_{mj, li}| \end{aligned} \quad (2.18)$$

where M' is the electric dipole operator, \bar{M}_m is the mean electronic transition moment and $S_{mj, li}$ is the vibrational overlap integral. This integral represents the quantum-mechanical statement of the Franck-Condon principle. The Franck-Condon principle states that because the time required for an electronic transition is negligible compared with that of nuclear motion, the most probable vibronic transitions is one which involves no changes in the nuclear coordinates. This transition, which is referred to as the Franck-Condon maximum, represents a vertical

transition on the potential energy diagram (see Fig. 2.2). In quantum mechanical term, the Franck-Condon maximum corresponds to maximum overlap between the ground state vibrational wavefunction $\psi_{\ell i}$ and the excited state vibrational wavefunction ψ_{mj} ; i.e., when $S_{mj, \ell i}$ is a maximum.

On the basis of the above arguments, the probability for radiative transition ($k_{m\ell}^r$) from an initial vibronic state of wavefunction ψ_{mj} to a final vibronic state of wavefunction $\psi_{\ell i}$, is proportional to the square of the electronic transition moment. Thus, we can write

$$\begin{aligned} k_{m\ell}^r &\propto |M_{mj \rightarrow \ell i}|^2 \\ &= |\langle \theta_m | \bar{M}' | \theta_\ell \rangle|^2 |\langle \phi_{mj} | \phi_{\ell i} \rangle|^2 \\ &= |\bar{M}_{m\ell}|^2 |S_{mj, \ell i}|^2 \end{aligned} \quad (2.19)$$

For convenience, the radiative transition probability per unit time for vibronic transition is expressed in terms of Einstein coefficient as [17]

$$k_{m\ell}^r = A_{\ell m} F \quad (2.20)$$

where $A_{\ell m}$ is the Einstein A coefficient for the complete electronic transition which is equal to $|\bar{M}_{m\ell}|^2$ and F is the Franck-Condon factor which is equal to $|S_{mj, \ell i}|^2$.

The non-radiative transition probability per unit time $k_{m\ell}^{nr}$ is given by [17]

$$k_{m\ell}^{nr} = \frac{4\pi^2 \rho_E}{h^2} |H_{m\ell}|^2 = P C_{m\ell} F \quad (2.21)$$

in which

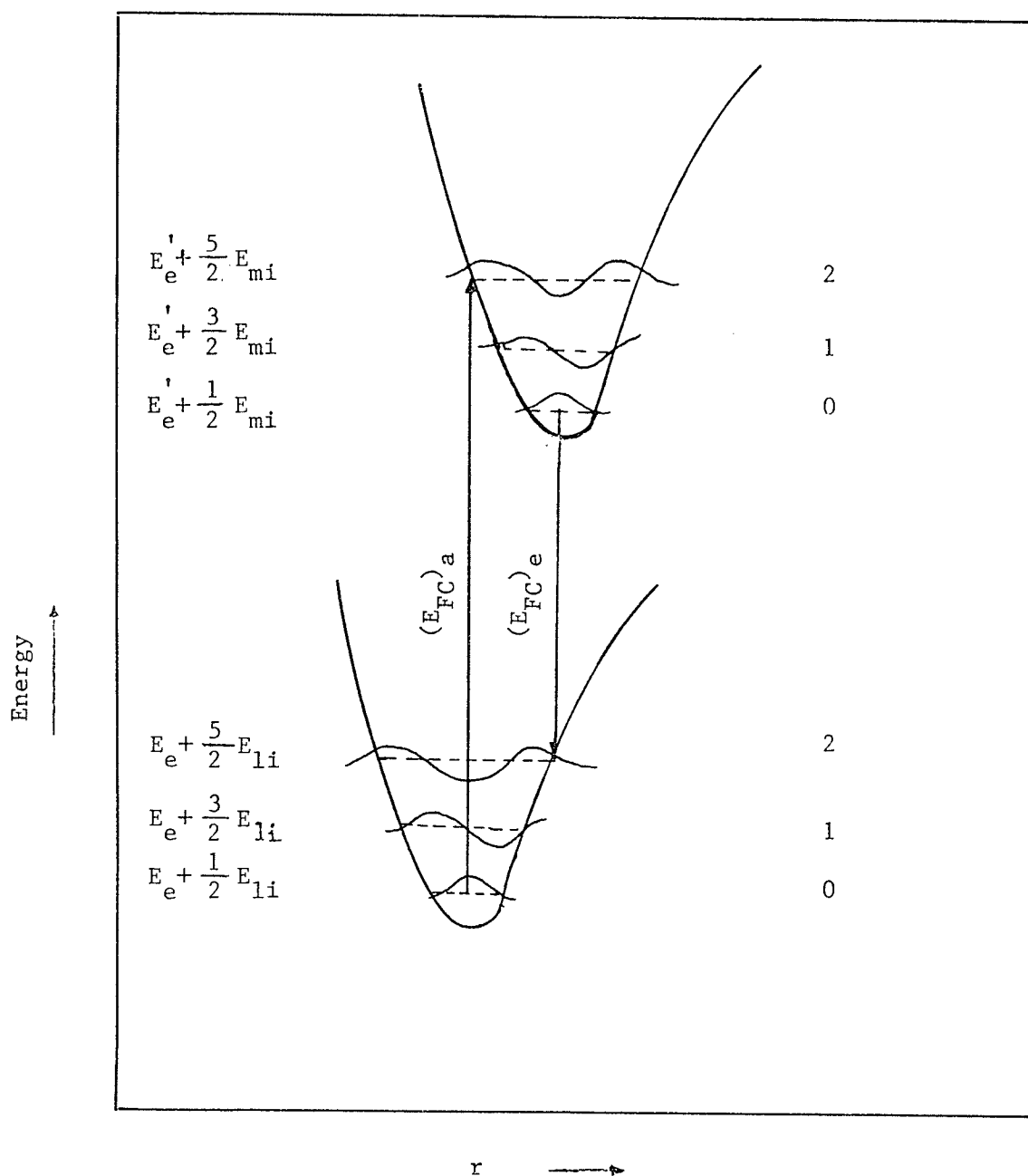


Fig. 2.2 - The potential energy diagram of a diatomic molecule. The total energy (electronic and vibrational energy) of the molecules as a function of the nuclear separation, r . $(E_{FC})_a$, Franck-Condon maximum is absorption; $(E_{FC})_e$, Franck-Condon minimum is emission.

$$H_{m\ell} = \langle \Phi_{mj} | J_{m\ell} | \Phi_{\ell} \rangle \quad (2.22)$$

$$J_{m\ell} = \langle \theta_m | J_N | \theta_{\ell} \rangle \quad (2.23)$$

where J_N is the nuclear kinetic energy operator and $P = \frac{4\pi^2 \rho_E}{h^2}$ is the density of state factor and $C_{m\ell} = |J_{m\ell}|^2$ is the electronic factor.

From equations (2.19), (2.22) and (2.23), the electronic and vibrational components can be separated. The electronic factor $|J_{\ell m}|^2$ and the Einstein coefficient $A_{\ell m}$ (or $|M_{\ell m}|^2$) involve the wavefunctions of the initial and final electronic states, so that non-radiative transitions are subject to the same multiplicity, same symmetry and same parity selection rules as radiative transitions [17]. For example, the electric-dipole transition between electronic states of different multiplicity is spin-forbidden, thus the transition from first triplet state to the ground singlet state is also spin-forbidden, while the transition from the first excited singlet state to the ground singlet state is spin-allowed.

The basic difference between the radiative and non-radiative transitions is that the former involves the electric dipole operator M' and it occurs between vibronic states that differ in energy, while the latter involves the kinetic energy operator J_N and it occurs between vibronic states of the same energy (with $\pm \frac{1}{2} \rho_E$). It can be seen from a potential energy diagram (see Fig. 2.2) that a radiative transition is a vertical transition between the potential surfaces corresponding to different electronic states, while a non-radiative transition is a horizontal transition, which involves crossing or tunneling from the potential surface of initial electronic state ℓ to the continuum of isoenergetic

vibrational levels of the potential surface associated with the final electronic state m . In the following we shall review the efficiency of radiative transition only.

(ii) The efficiency of radiative transition

There are three bimolecular processes which commonly compete with each other in the radiative transitions in organic semiconductors, and therefore the electroluminescent phenomena depend greatly on these processes.

(a) Exciton-exciton interactions

In organic semiconductors, the probability of radiative emission depends not only on monomolecular decay but also on bimolecular recombination processes. The exciton-exciton interactions can be divided into (1) free exciton-free exciton interactions and (2) free exciton-trapped exciton interactions. The free-free exciton interactions have been discussed in Section 2.2.1, so in here we shall briefly review the exciton-trapped exciton interactions. In real crystals, there are always traps capturing excitons. Exciton traps are sites capable of holding the energy that, otherwise, propagates through the lattice. These traps are generally localized and non-periodic states in the crystal. Thus, the radiative transition rate is determined by the specific electronic structure of the trap site. The presence of the traps changes the spectral energy distribution, especially the fluorescence and electroluminescence, and also changes the time dependence of population and depopulation processes in the specimen. In organic semiconductors, three types of traps have been identified [52,115,173] and they are:

- (1) guest molecules such as tetracene doped in anthracene - the guest

molecules can be identified by their spectral properties, which are normally different from those of the host crystal;

(2) defect or lattice imperfections - these have been considered to be responsible for vibronic series in the luminescence spectra of the crystal, which are identical to the spectra of the intrinsic host emission but shifted to the lower energy side by a certain amount of energy;

(3) self-trapping - the self-trapping of an exciton is a process in which the exciton induces a lattice relaxation, which causes some energy loss.

The way in which these exciton-exciton interactions affect the efficiency of electroluminescence are still not clear. In Chapter IV we shall present our approach to this problem for both perfect crystals and real crystals.

(b) Exciton-carrier interactions

The nonradiative destruction of triplet excitons and singlet excitons by excess electrons and holes in organic semiconductors have been investigated by many investigators [39,41,53,110,154,160,161]. The first experimental study by Helfrich [53] have showed that the excess electrons induced into anthracene crystals by carrier injection cause a decrease of triplet lifetime. More recently, Williams et al [160,161] have reported that the excitons are quenched by carriers and have suggested that the interaction of the singlet excitons with charge carriers provides an additional mechanism for non-radiative exciton decay. The change of quantum yield of fluorescence due to the exciton-carrier interactions may be written as [160,161]

$$\eta_f = \frac{\alpha_1}{\alpha_1 + \alpha_2 + k_s} \quad (2.24)$$

where α_1 and α_2 represent, respectively, the radiative transition with the emission of photons and the non-radiative transition with the emission of phonons, and k_s is the singlet exciton-carrier reaction rate which is given by [160,161]

$$\begin{aligned} k_s &= N_t (1 - \theta) \alpha_v + N_t \theta \sigma (u + v^2/3u) \quad u > v \\ &= N_t (1 - \theta) \sigma v + N_t \theta \sigma (v + u^2/3v) \quad u < v \end{aligned} \quad (2.25)$$

where σ is the reaction cross-section between a carrier and a singlet exciton, u and v are, respectively, the thermal velocities of carrier and singlet excitons.

(c) Exciton-surface interactions

There are two processes for quenching the mobile molecular excitons at the boundary between an organic semiconductor and an electrode, They are: (1) Charge transfer - an exciton can transfer an electron to an adjacent trapping center at the interface, producing a free hole in organic semiconductor (for example, oxygen molecules adsorbed at the surface can act as electron trap centers) and (2) Energy transfer - an exciton can transfer its energy to the acceptor molecules present at or adjacent to the surface of the organic semiconductors. Usually, such an electron transfer is a rather slow process as compared with the energy transfer between organic semiconductor and an electrode.

A metal on the surface of a molecular crystal can influence the electronic states of the surface molecules in two ways: first, it can modify their energetic position and secondly, it can affect the lifetime of excited states. The first effect results from the discontinuity of the dielectric constant across the interface, which leads to a change in the

molecular polarization energy. If the polarization is enhanced, surface molecules may act as traps for excitons. The second effect results from non-radiative transitions induced by metal electrons.

In general, the exciton quenching zone at the surface is very narrow (about 20 Å) [110]. In the case of electroluminescence, the excitons are generated from the electron-hole recombination inside the crystals and the recombination zone width is estimated to be at least about 10^3 Å. Hence the exciton-surface interactions may not be so important as compared with other non-radiative transitions. But in the case of photoconduction, the disassociation of excitons at the boundary, which generates carriers, is one of the important processes for photocarrier generation mechanisms. This will be discussed in Section 2.3.

2.2.3 Experimental results in anthracene

In this section, we shall briefly review some of the important experimental results as follows:

(i) Effects of doping impurities

Electroluminescence from pure anthracene occurs primarily in the range of 4000-4500 Å (blue light) and is the same as those of the normal anthracene fluorescence (see Table 2.5). But for the anthracene doped with tetracene, the electroluminescence may be either only that of the dopant in the range of 5000-5500 Å (green light) or a mixture of anthracene and tetracene emission, the intensity ratio depending upon the concentration of the dopant [33,66,119,124,125,167,175]. By adding a suitable amount of tetracene, the color of the electroluminescence of anthracene can be controlled from blue to green. The anthracene-tetracene

TABLE 2.5

THE ABSORPTION AND EMISSION SPECTRUM RANGES OF NAPHTHALENE,
ANTHRACENE AND TETRACENE CRYSTALS

Organic Semiconductors	Absorption- Spectrum	Emission- Spectrum (fluorescence)	Reference
Naphthalene	2300-3300 Å	3000-3700 Å	[17,52]
Anthracene	2300-4000 Å	3800-5100 Å	[17,52]
Tetracene	3300-4360 Å	4700-5800 Å	[17,52]

system involves transfer of excitation energy from the host crystal to the guest molecule. At room temperature the fluorescence efficiency is approximately 10^5 times higher for the guest (tetracene) than for the host (anthracene)

$$\eta_T/\eta_A = 10^5 C_T \quad (2.26)$$

where η_T and η_A are, respectively, the quantum yield for the fluorescence of tetracene and anthracene, C_T is the mole fraction of tetracene in anthracene. Equation (2.26) shows that for $C_T = 10^{-5}$, both partners have the same intensity of fluorescence.

Figure 2.3 shows the spectral dependence of fluorescence and electroluminescence for undoped and tetracene-doped anthracene crystals. In Fig. 2.3(a), the dash-line indicates that the fluorescence of anthracene doped with about 5×10^{-6} mole tetracene, and therefore the guest and host have about the same intensity of fluorescence. In Fig. 2.3(b) the solid line represents the undoped anthracene electroluminescence spectrum and the dash lines that of anthracene doped with tetracene of about 10^{-3} mole. In this case all the observed electroluminescence spectrum is almost that of tetracene.

(ii) Field dependence of electroluminescence:

(a) D.C. electroluminescence

D.C. electroluminescence can be observed either using single injection electrodes [109,119,168] or double injection electrodes [32, 33,51,54,92,124,125,167,168]. However, the threshold field for the onset of electroluminescence would be different in two cases. In general, the threshold field for the case of double injection is much smaller than

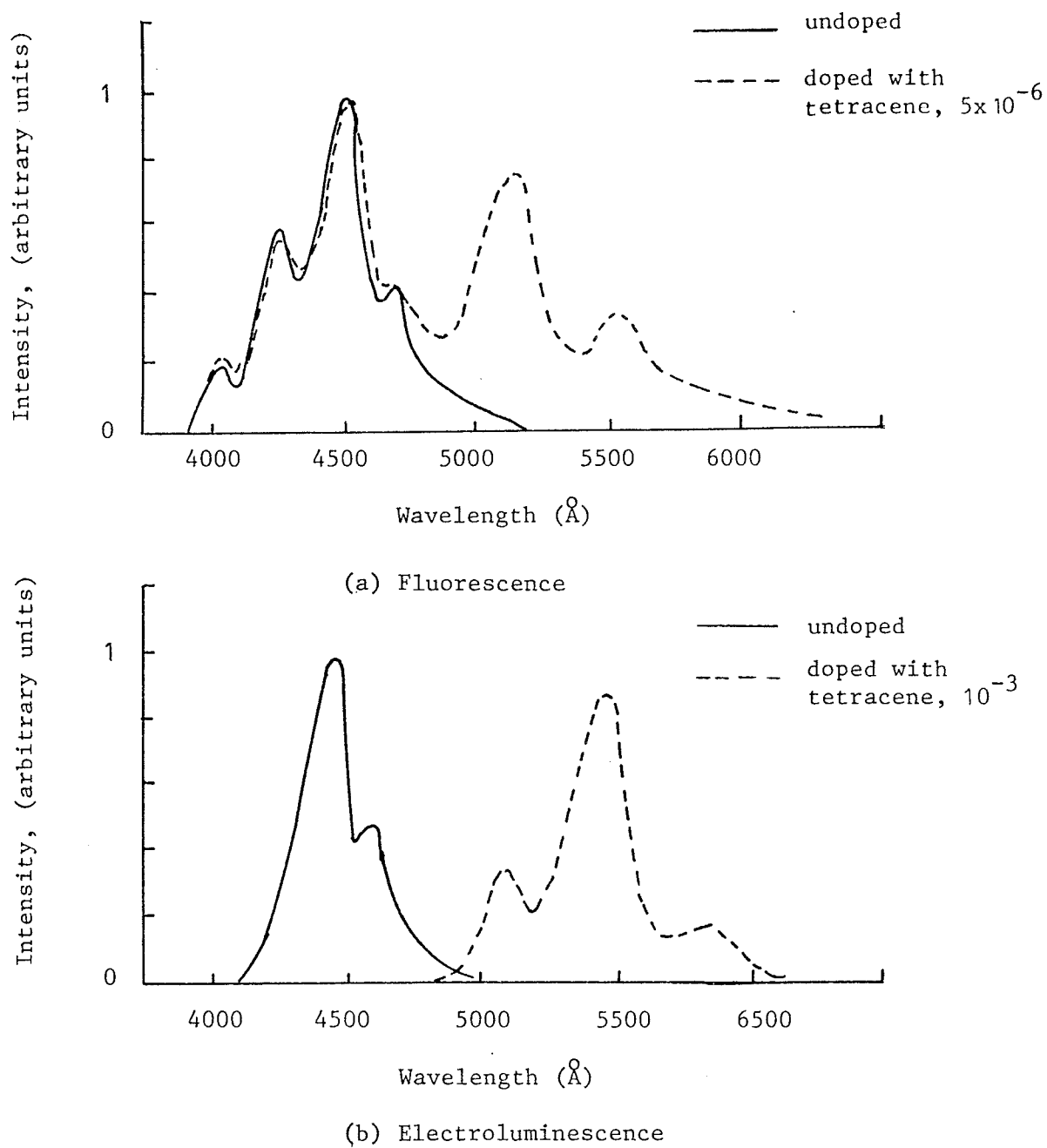


Fig. 2.3 - The spectra of fluorescence and electroluminescence for undoped anthracene and doped with tetracene. (after Zschokke-Gränacher [175]).

that for the case of single injection. Table 2.6 shows some materials which have been used for injecting contact electrodes for anthracene.

It is well known [51,54] that at high injection current level, the brightness is linearly proportional to the current; and at low injection current level, the brightness is proportional to the square of the current. The location of the luminous zone inside the specimen depends on the concentration of electron-hole pairs distribution. The luminous zone is usually considered as the carrier recombination width. Some important experimental results of d.c. electroluminescence are summarized in Table 2.7.

(b) Pulsed electroluminescence

Pulsed electroluminescence has been observed by many investigators [14,54,168,176] using pulsed-voltage techniques. They have reported that the electroluminescence consists of two components; one is "fast component", generally called "prompt electroluminescence", and the other is "slow component", generally called "delayed electroluminescence". The fast component is due to the singlet excitons generated by direct electron-hole recombination. The "fast" light transient marks the time when the two leading carrier fronts meet in the specimen. It is this time together with the "fast" current that enables the calculation of the carrier recombination rate constant. The slow component is due to the singlet excitons generated indirectly by triplet-triplet annihilation. The "slow" light transient enables us to distinguish the delayed fluorescence of the directly generated singlet excitons. The "slow" current transient can be used to monitor any change of exciton generation rate which may arise from a decrease of current due to trapping. It should be noted that electron and hole detrapping will also give rise to a slow light transient.

TABLE 2.6

MATERIALS USED AS CARRIER INJECTING CONTACTS TO ANTHRACENE

Electrodes Form	Electron Injection Materials (Cathode)	Hole Injection Materials (Anode)	Ref.
Liquid Contacts	A solution of negative anthracene ion Sodium + anthracene + tetrahydrofuran	A solution of positive anthracene ion (1) $\text{KI} + \text{I}_2$ in water (2) AlCl_3 + anthracene + nitromethane	[51,54]
	Lithium + anthracene + nitromethane	AlCl_3 + anthracene + ethylenediamine	[175]
Solid Contacts	Sodium-potassium alloy	Evaporated gold	[92]
	Na + tetrahydrofuran + anthracene	(1) AlCl_3 + anthracene + nitromethane (2) Silver paste (3) Gold paste (4) Evaporated silver (5) Evaporated Al (6) Conducting glass (SnO_2)	[168]
	(1) n^+ -Si wafers covered with 20-40 Å SiO_2 (2) A fine grid structure of evaporated Al on a glass substrate oxidized to approximately 50 Å of Al_2O_3	(1) Evaporated transparent films of $\text{Cu}_2\text{O} - \text{CuI}$ (2) Evaporated Se-Te alloy (3) Colloidal black Pt paste (4) Iodized Cu paste	[33]
	Carbon-fibres	Evaporated indium	[170]

TABLE 2.7
SUMMARY OF PREVIOUS EXPERIMENTAL RESULTS OF ELECTROLUMINESCENCE IN ANTHRACENE CRYSTALS

Specimen Preparation	Specimen Thickness	Form of Contacts	Light Emission Peak Wavelength	Threshold Field	Current-voltage dependence $J \propto V^n$	Temp. Range	Remarks	Reference
Single crystals (Solution grown)	10-20 μ	Liquid contacts, Single injection	4210 Å 4440 Å	4×10^5 V/cm	$n > 10$	293°K	D.C. EL Pulsed EL A.C. EL	[109, 119]
Single crystals (Melt grown)	1-5 mm	Liquid contacts, Double injection	4300 Å	Unspecified	$n > 2$	293°K	D.C. EL Pulsed EL A.C. EL	[51,54]
Single crystals doped with tetracene	1.5 mm	Liquid contacts, Double injection	4230 Å 4450 Å 4740 Å 4792 Å 5300 Å	Unspecified	$n > 2$	293°K	D.C. EL	[175]
Films (vacuum evaporated)	10 μ	Solid contacts, Double injection	4100Å-5400Å	Unspecified	$n > 3$	293°K	D.C. EL	[32,33]
Single crystals (zone-refined)	2 mm	Solid contacts, Double injection	4500 Å	350 V/cm	$n > 2$	100°K-350°K	D.C. EL	[167,168]
Single crystals doped with tetracene	Unspecified	Liquid contacts, Double injection	4340 Å 5480 Å		$n > 3$	293°K	D.C. EL	[124,125]
Single crystals doped with tetracene	Unspecified	Solid contacts, Double injection	4250 Å 4950 Å 5250 Å	7000 V/cm	$n > 6$	293°K	D.C. EL	[66]
Single crystals (zone-refined)	2.2 mm - 5 mm	Solid contacts, Double injection	4300 Å	6×10^3 V/cm	$6 < n < 12$	293°K	D.C. EL	[170]
Single crystals	50 μ	Solid contacts, Double injection	4450 Å	1×10^5 V/cm		293°K	A.C. EL	[17]

(c) A.C. electroluminescence

The experimental results of electroluminescence as a function of frequency and voltage are very scarce. Some investigators [117] have found that the light output is in phase with applied voltage in the frequency range of 0-4000 Hz, and that using the same materials for both electrodes, the wave form of electroluminescence is symmetrical, but if the two electrode materials are different, the wave form is unsymmetrical [17]. These results indicate that the injection of both majority and minority carriers depends greatly on the electrode material, or on the ohmic properties of the contact.

(iii) Temperature dependence of electroluminescence:

There are very few results available on the temperature dependence of electroluminescence. The electroluminescent brightness has been found to be linearly proportional to the current, but independent of temperature for the temperature range between 350°K and 150°K [108]. Williams et al [108] have reported that the melt-grown crystals show a considerable portion of defect emission in the electroluminescence spectra, especially at low temperatures. Although the carrier injection efficiency slightly improves, the internal quantum yields of electroluminescence decreases [170] at high temperatures.

The basic mechanisms of temperature dependence of electroluminescence is still not fully understood. In Chapter IV, we shall present our experimental results and theoretical approach on this subject.

2.3 PHOTOELECTRIC EFFECT

The processes of charge carrier generation in organic semiconductors resulting from the interaction of semiconductors with light have been studied by many investigators [17,19,22,28,29,48,71,80,115,139]. The observed photoconductivity and photovoltage have been found to be strongly dependent on a number of parameters, among the most important of these being (i) the wavelength and intensity of the incident light, (ii) the magnitude and polarity of the applied field, (iii) the state of illuminated surface, (iv) the ambient atmosphere and (v) the temperature of the specimen.

Considering the photogeneration of free carriers in organic semiconductors, it is well known that in addition to the direct-ionization process, carriers can be generated by such other processes as the interaction of singlet and triplet excitons, and the interaction of excitons with surface states at electrode surfaces or with impurity or defect sites near the surfaces. This may be the reason that experimental results reported by different investigators differ widely in magnitude and temperature dependence of the photocurrents. In the following, we shall discuss the photoconduction process and photovoltaic phenomena separately.

2.3.1 Photoconduction processes

In this section, we shall discuss only the following three important photogeneration processes.

(i) One-quantum processes

A one-quantum process means that the process involves only one photon or exciton in a single interaction process. The following processes are on-quantum processes.

(a) Collision of singlet excitons with impurity or defect sites near and at the surfaces

This process is the most common one for organic semiconductors, such as anthracene or tetracene when excited in the region of the strongest optical absorption. Hence the specimen is excited by the light within the range between 3100 Å and 4000 Å, the singlet excitons will be generated. Then the singlet excitons in motion collide with impurity or defect sites near or at the surface, causing dissociation of excitons, which generate one type of carriers (say, holes) and traps the other type of carriers (say, electrons) at impurity or defect sites. The nature of the dissociation centers near or at the surfaces has been studied by Johnston and Lyons [62]. They found that the removal of the original surface layer (with original impurity or defect sites) from the crystal under ultra-high vacuum reduces markedly the transient photocurrent in the low intensities, and that the reintroduction of oxygen on the crystal surfaces results in an increase in hole current, indicating clearly that oxygen is responsible for the dissociation centers. They concluded that the exciton dissociation at impurity sites is the major generation process when the crystal is exposed in the air.

The generation rate of this process is given [37] by

$$g_{bo} = Q \zeta \left[\frac{\epsilon_a \lambda_s}{1 + \epsilon_a \lambda_s} \frac{1}{1 + x_s / \lambda_s} \right] \quad (2.27)$$

where ϵ_a is the absorption coefficient, Q is the quantum yield of carrier generation, ζ is the illumination light intensity, λ_s is the diffusion

length of singlet excitons, and x_s is the surface path length of singlet excitons.

(b) Collision of triplet excitons with trapping centers in the bulk of the crystal

This process is important in anthracene crystals when the specimen is excited in the fluorescence re-absorption region (3900-4500 Å). The trapped carriers in the bulk would be liberated by triplet excitons. This process has been studied by many investigators [13,48,55]. The enhancement of photoconduction by this process can be expressed as a function of applied voltage, specimen thickness and light intensity or the concentration of triplet excitons [13]. The photoconduction current is given by

$$J_{ph} \sim \zeta^n \frac{v^2}{d^3} = \frac{9}{8} \mu_p k_{ph} (\epsilon_a) [T] \frac{v^2}{d^3} \quad (2.28)$$

where ζ is the light intensity; n is numerical constants ($0.5 \leq n \leq 1$); k_{ph} is the empirical constant which is a function of absorption coefficient, ϵ_a ; and $[T]$ is the triplet exciton concentration which can be calculated [13] using equation (2.26) on the basis of the assumptions: (1) the absorption coefficient in the fluorescent spectral region change exponentially with light wavelength; (2) triplet excitons are generated near the illuminated surface.

(c) Photoionization by one photon

This process implies that the absorbed photons create directly free electron-hole pairs without intermediate steps which involve excitons. This process is also called the intrinsic process. Castro and Horning [19] were the first to perform an experiment showing a direct photocarrier

generation process. They studied quantum yield in anthracene using pulse techniques, and observed a peak of photocurrent at 2800 \AA which they attributed to intrinsic charge-carrier generation by a single-photon process. Evidence for the intrinsic character of the 2800 \AA photocurrent is based primarily on the fact that the peak in the photocurrent spectral-response curve does not correspond to any known optical transition, and the magnitude of the 2800 \AA electron photocurrent is relatively insensitive to the condition of the crystal surface [19]. The intrinsic photoconduction in anthracene crystals have also been investigated by Chaiken et al [22] using steady state current measuring techniques. They have found that the direct ionization (i.e., a crystal band-to-band transition) occurs at a threshold excitation energy of 4.0 eV ($\sim 3100 \text{ \AA}$), and it results in a maximum intrinsic photocurrent yield at 4.4 eV ($\sim 2800 \text{ \AA}$). Many investigators have confirmed that the energy level 4.0 eV corresponds to the first narrow conduction band and 4.4 eV corresponds to the second wide conduction band [22, 7,139]. The field dependence of quantum yield for intrinsic photocarrier generation has been investigated by many investigators [11,22,23,108]. They have reported that at electric fields higher than $2 \times 10^5 \text{ v/cm}$, the quantum yield of carrier generation increases very rapidly with field (at least 10 times higher than that at low fields).

(ii) Two quantum processes:

A two quantum process means that the process involves two photons or two excitons, or one photon and one exciton in a single collision process (see Fig. 2.4). There are several possible mechanisms for these

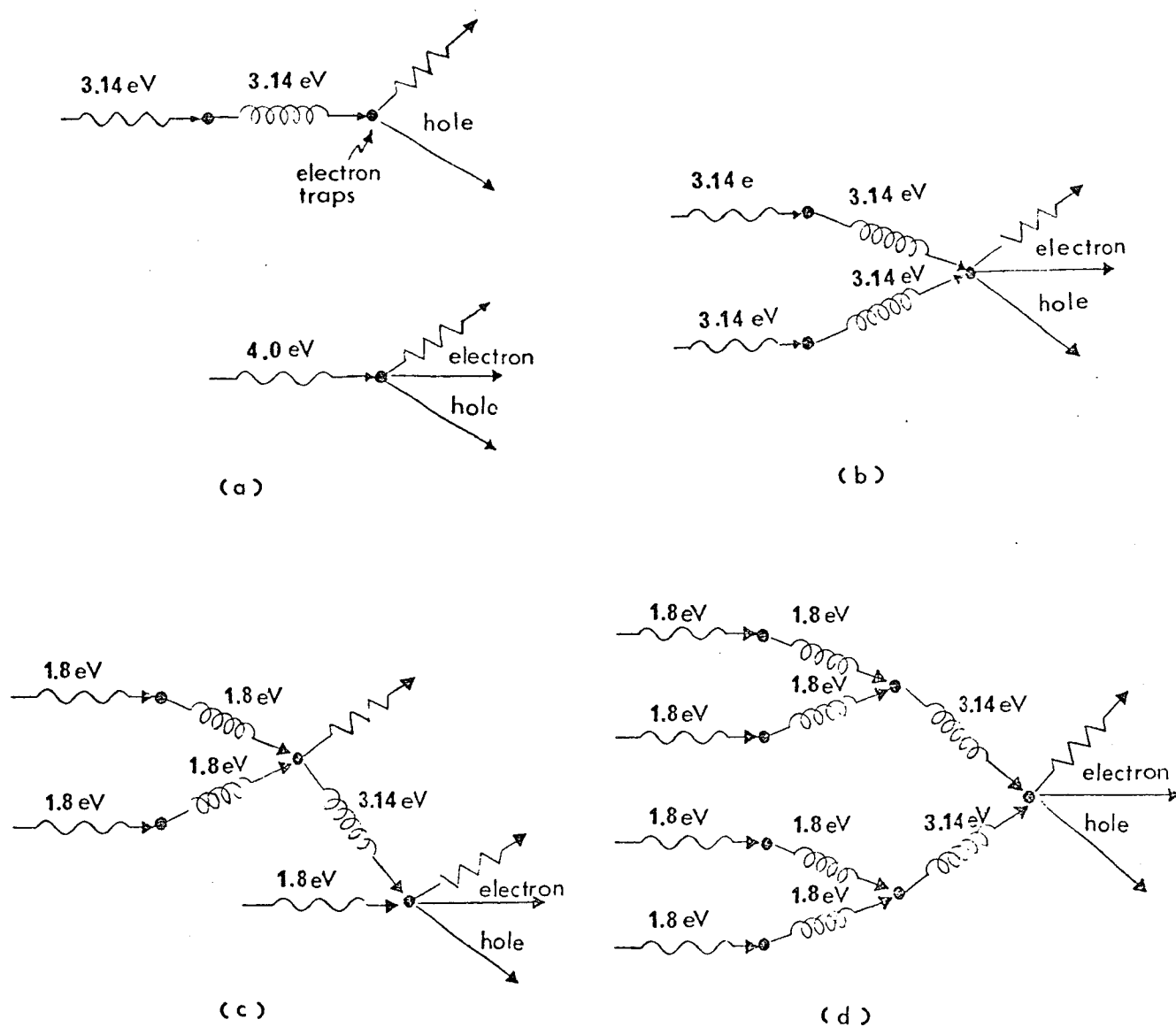


Fig. 2.4 - Photocarrier generation processes.

—→ represents electron or hole; ———→ represents phonon; —~~~~→ represents photon; —(o)(o)(o)→ represents exciton.

- (a) One-quantum process; (b) Two-quantum process;
(c) Three-quantum process; (d) Four-quantum process.

processes to occur in molecular crystals [48,80], but the most probable mechanism for the carrier generation in the bulk is the collision of two singlet excitons, which generate electron-hole pairs [24,26,62,71,79,136,139]. This mechanism was first proposed by Choi and Rice [24] who, using perturbation theory, have calculated the rate constant for singlet-exciton annihilation in the first excited state of anthracene crystals. Their theoretically calculated results have been confirmed experimentally by Silver et al [136] and by Johnston and Lyons [62] by using pulse techniques. They [62] found that the generation rate of charge carrier is given by

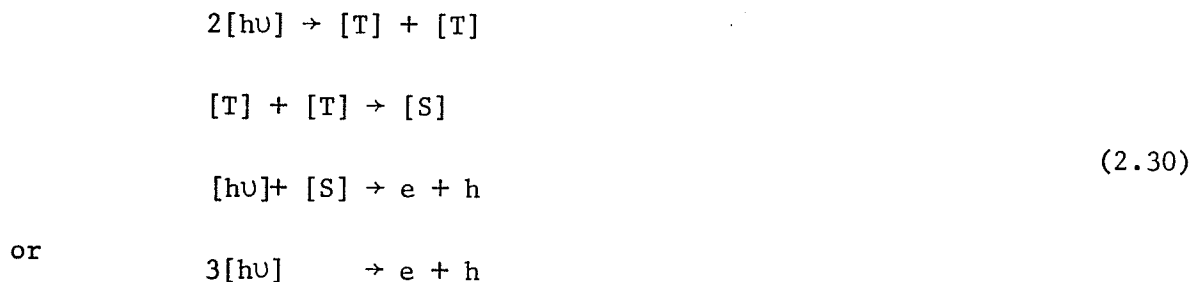
$$\frac{dn}{dt} = k_{ss}[S]^2 \quad (2.29)$$

where $[S]$ denotes the equilibrium concentration of excitons during the light flash, n is the concentration of carriers, and k_{ss} is the bimolecular rate constant for carrier generation by exciton-exciton collision. For light of wavelength 4000 Å and of intensity 3×10^{12} photons/cm² incident on the crystal, the number of carriers generated in one flash, calculated from equation (2.29), is 2×10^7 cm⁻³. This agrees well with experimental results of Johnston et al [62].

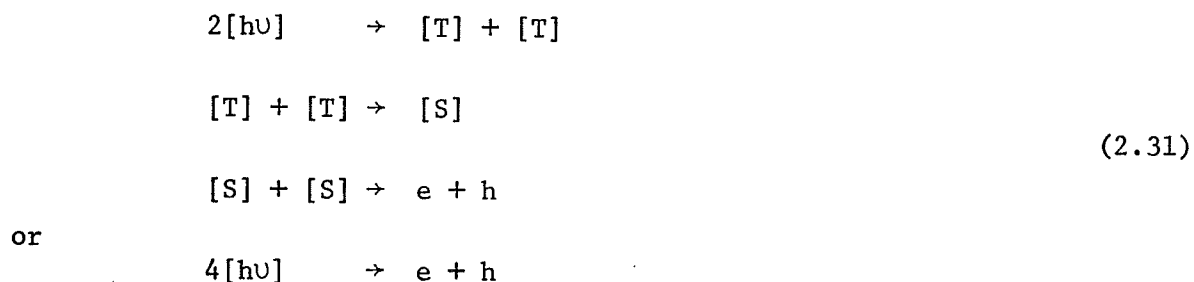
(iii) Multi-quantum processes

A multi-quantum process means that the process involves more than two quanta (each of which can be either a photon or an exciton) in a single interaction process (see Fig. 2.4). Three quantum generation processes in anthracene have been reported by Singh et al [134] and Kepler et al [71]. When a high-intensity light (such as Q-switched ruby laser ($\lambda = 6940$ Å)) is used as the photogeneration source, charge carriers are

generated by a three photon process [71,134], and the dominant mechanism for the generation of charge carriers involves the photoionization of singlet-exciton states. The basic dynamics of this process can be described as follows



Four quantum processes have been reported by Hasegawa et al [50]. Using Q-switched ruby laser of photon energy 1.79 eV, they found that carriers were generated from interactions represented by the following equation:



But their proposed mechanism has been criticized by both Kepler [71] and Strome [141], who suggested that the results could be better approximated by three quantum processes.

2.3.2. Photovoltaic phenomena

It is well known that the bulk photovoltage (Dember photovoltage) arises when a light produces a concentration gradient of the non-

equilibrium carriers because of the difference between the electron and hole mobilities. The photovoltage may also be affected by the surface states which may capture photocarriers. Thus, the total photovoltage should be the sum of the bulk photovoltage and the surface photovoltage. In this section, we shall discuss briefly (i) the general theory of photovoltaic effects in solids and (ii) the experimental results of photovoltaic phenomena in organic semiconductors.

(i) The general theory of photovoltaic effect in solids

The photovoltaic effect in solids may be caused by (a) bulk photovoltaic effect (Dember photovoltaic effect), (b) surface photovoltaic effect, and (c) depletion-layer photovoltaic effect, of which only (c) is associated with a p-n junction (either homo- or hetero- p-n junction). The photovoltaic effect in p-n junction has been studied in detail by many investigators [96,150]. Hence, we shall discuss only the bulk and surface photovoltaic effects as follows:

(a) The bulk photovoltaic effect

This effect in general is referred to as the Dember effect [31, 95,150], which arises due to the diffusion of non-equilibrium photocarriers in the bulk of the crystal. On the basis of the following assumptions (1) the local charge is neutral and there are no traps in the bulk of the specimen, (2) the thickness of the specimen is much larger than the diffusion length of the carriers, and (3) there is recombination at the surface, Moss [95] derived the open-circuit photovoltage for small illumination light intensity (or for the excess photo-carrier concentration much less than the equilibrium carrier concentration)

based on the small-signal theory as

$$V_{ph} = \frac{\zeta(D_p s)(\mu_p - \mu_n)}{\mu_n n_{fo}} \times \frac{\sinh(d/L_p) + s(D_p/L_p)[\cosh(d/L_p) - 1]}{[s^2 + (D_p/L_p)^2] \sinh(D_p/L_p) + 2s(D_p/L_p) \cosh(d/L_p)} \quad (2.32)$$

For large illumination light intensity (or for excess photo-carrier concentration much larger than the equilibrium carrier concentration) based on the large signal theory Moss obtained [95]

$$V_{ph} = \left(\frac{\mu_p - \mu_n}{\mu_n + \mu_p} \right) \left(\frac{kT}{q} \right) \ln [1 + sd/2D_p (1 + \mu_p/\mu_n)] \quad (2.33)$$

where ζ is the illuminated light intensity, D_p is the diffusion constant of holes, s is the surface recombination velocity, and L_p is the diffusion length of holes. It can be seen when μ_n equals μ_p and when the surface recombination velocity s equals 0, $V_{ph} = 0$. It can be imagined that as there are always traps in solids, and as the local charge may not be neutral because of the different mobilities of the two types of carriers (electrons and holes), the photovoltage would be a function of specimen thickness and its absorption coefficient. These effects have not been taken into account in equation (2.32). Therefore, we shall present our unified approach to this problem, taking these effects into account in Chapter V.

(b) The surface photovoltaic effect

On the surface of semiconductors there are always local states. This gives rise to photo-diffusion effects. For example, in the case of strong surface recombination there will be the photodiffusion difference between the surface and the bulk, which is similar in nature to the bulk

photovoltaic effect. In contrast to the bulk photovoltages, this surface photovoltage might be due to the spacially non-uniformly distribution of surface states or recombination impurities. However, the nature of the surface photovoltaic effect is still unclear. So far, the general theory for the surface photovoltaic effect is not available. The general qualitative consideration is that the light can affect the contact potential between the metallic electrode and the semiconductor because the excitation of electrons into the conduction band would raise the Fermi-level by ΔE_f according to the following relation [48]

$$\Delta E_f = kT \ln \left(\frac{n_L}{n_D} \right) \quad (2.34)$$

where n_D and n_L refer to the density of free electron in the dark and under light illumination, respectively. The energy band at surface would bend upward or downward with respect to the bulk Fermi-level. Thus, the surface potential, ϕ_s , is strongly dependent on the surface states or surface conditions. The experimental results related to the bulk photovoltaic effect or surface photovoltaic effect in organic semiconductors will be reviewed in the next subsection.

(ii) The experimental results of photovoltaic phenomena in organic semiconductors

The number of experimental results on photovoltage effect is much less than those on photoconductivity, probably because it has been recognized that the photovoltage depends strongly on illuminated light wavelength and specimen surface conditions.

(a) Light wavelength dependence

In general, the spectral distribution of photovoltage correlates well with the absorption spectrum as shown in Fig. 2.5. An increase in

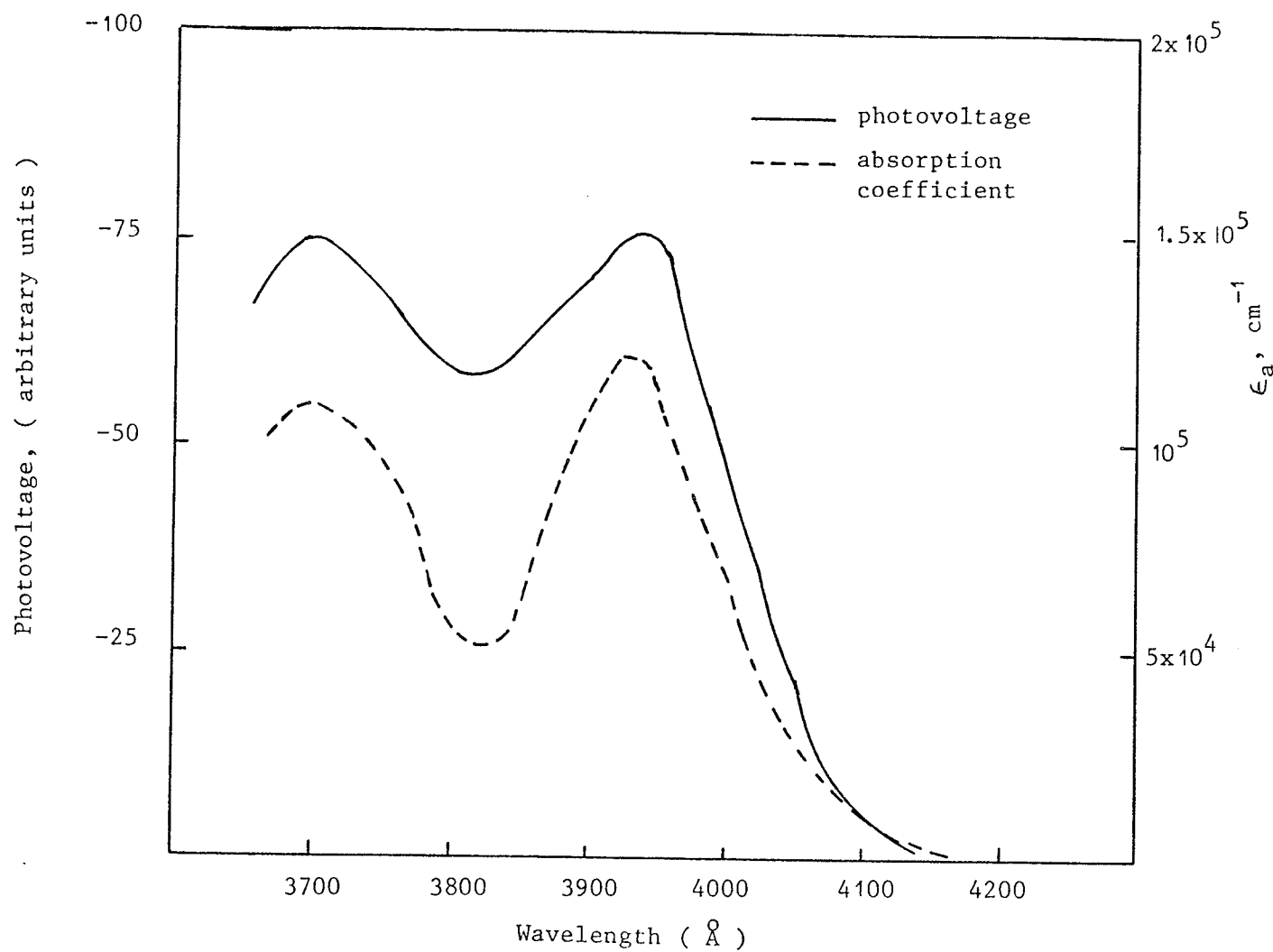
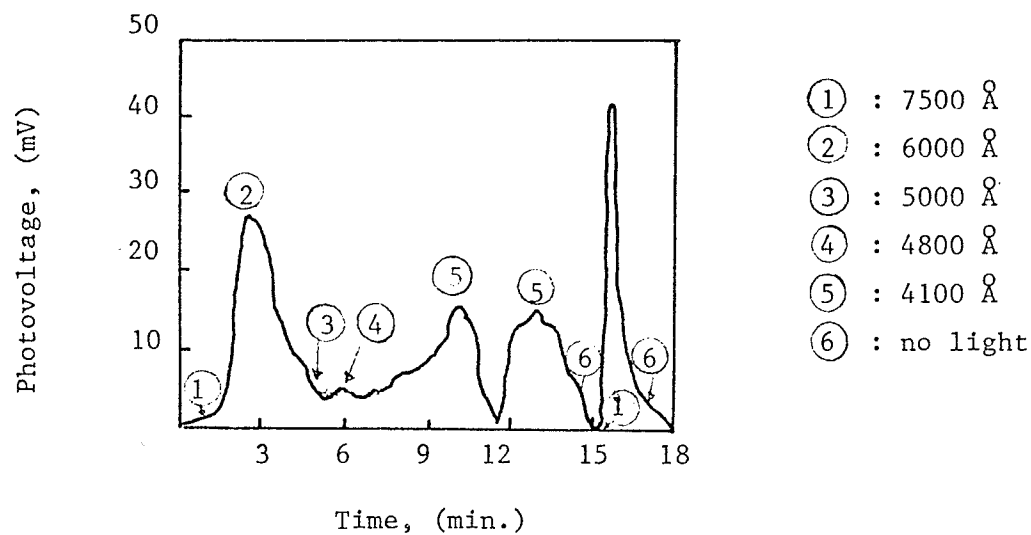


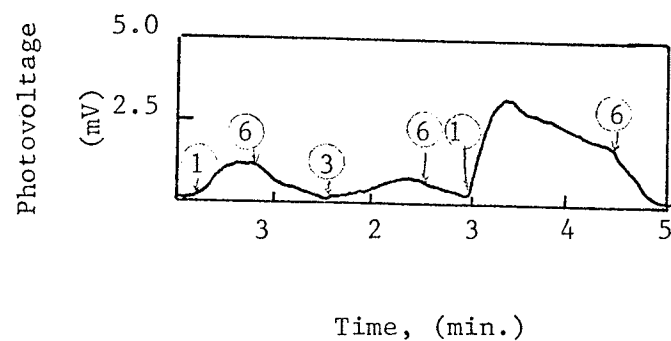
Fig. 2.5 - Spectral dependence of the photovoltage of anthracene crystals and spectral dependence of absorption coefficients. (After Vertsimaka [157])

light intensity changes only the magnitude of photovoltage, but does not disturb the correlation between the spectral distribution of photovoltage and the absorption spectrum. The absorption can be roughly divided into two regions, namely, (1) strong absorption region and (2) weak absorption region. In the strong absorption region, the photovoltage may be increased up to a certain maximum limiting value and its sign indicates the sign of majority carrier; but in the weak absorption region, the photovoltage may be reduced to zero, or even cause its sign to reverse. Vladimirov [159] has observed that when anthracene crystal is illuminated within the strong absorption region ($\lambda < 4000 \text{ \AA}$), the magnitude of photovoltage correlates well with the absorption spectrum and its sign indicates a p-type conductivity; but when anthracene crystal is illuminated with weak absorption region ($\lambda > 4000 \text{ \AA}$), its sign indicates an n-type conductivity, and this inversion occurs at $\lambda = 4000 \text{ \AA}$ at room temperatures. Recently, the photovoltaic effect in naphthalene crystals as a function of light wavelength has been studied by Tavares [149]. He observed that the magnitude of photovoltage in naphthalene for red light (7500 \AA) is strongly enhanced if the specimen is previously illuminated by violet light (4100 \AA) or by green light (5100 \AA) as shown in Fig. 2.6. These phenomena have been explained only qualitatively by Tavares [149]. It is believed that this enhanced effect of photovoltage is due to the local charge non-neutrality or space charge effect. The theoretical explanation of this effect will be presented in Chapter V based on our analysis.

The photovoltage in tetracene crystals as a function of specimen have been studied by Lyons et al [87]. They found that the thinner the



(a)



(b)

Fig. 2.6 - The enhancement of photovoltage due to local charge non-neutrality in naphthalene crystals.

(a) Red light produced by previously illuminating the specimen with violet light.

(b) Red light produced by previously illuminating the specimen with green light.

(after Tavares [149])

specimen the higher is the photovoltage generated in the region of the weak absorption, and that the photovoltage is almost independent of specimen thickness in the region of strong absorption. In Chapter V, we shall also present our theoretical explanation of these phenomena.

(b) Surface condition dependence

So far, investigators [48,102,157,159] have studied the effect of surface conditions on photovoltage by one of the following means:

(1) to expose the specimen in different ambient gases, (2) to allow the surface barrier by applied higher electric fields and, (3) to excite the specimen by increasing light intensity. It is possible that the surface photovoltage ϕ_s is due to the boundary bending of the energy bands, and thus its magnitude and sign depend strongly on the surface states of the specimen surface. (See Fig. 2.7.)

It has been reported that the adsorption of oxygen tend to decrease the photovoltage [102,157,159]. This phenomena might be explained [102,159] by the fact that the adsorbed oxygen produces on the anthracene surface negatively charged states, causing the corresponding change in the bending of the energy bands. Some important results of bulk and surface photovoltaic effects are summarized in Table 2.8.

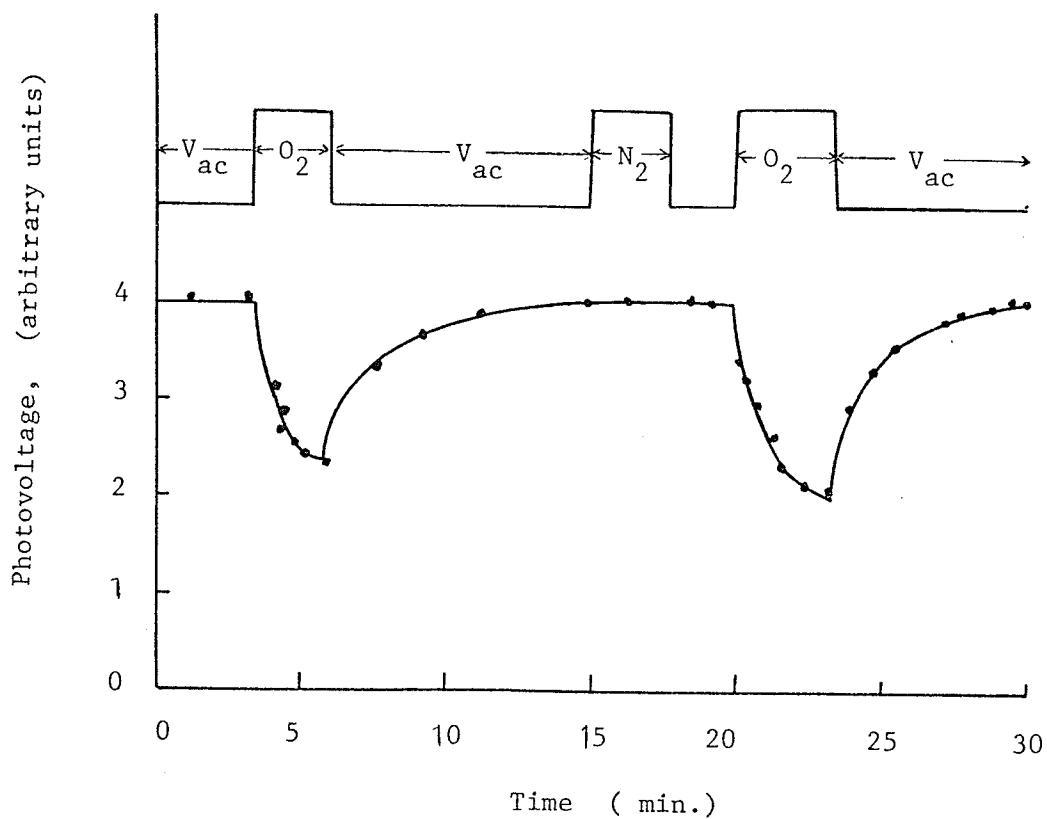


Fig. 2.7 - The change of the photovoltage in anthracene crystal
 due to change in the ambients.
 (after Nakada et al [102])

TABLE 2.8

SUMMARY OF PREVIOUS EXPERIMENTAL RESULTS OF PHOTOVOLTAIC EFFECT IN ANTHRACENE CRYSTALS

Crystal Preparation	Specimen Thickness	Front surface (First contact)	Back surface (Second contact)	Polarity of Front surface	Wave-length Range	Temperature Range	Remarks	Reference
Single crystals (solution grown)	5.1 μ -10 μ	Electrolyte -0.01M NaCl solution	Electrolyte -0.01M NaCl solution	Negative	3650 Å	293°K	Maximum photo-voltage = 0.2V	[63]
Single crystals and polycrystal	100 μ -300 μ	Conducting quartz-glass	Aluminum	Negative	3100 Å - 3650 Å	261°K - 328°K		[108]
Sublimation films	50 μ	SnO ₂	Metal	Negative		300°K	Surface photo-voltage	[102]
Single crystals (zone refined)	30 μ -50 μ	SnO ₂	SnO ₂	Negative Positive	<4000 Å >4000 Å	300°K - 375°K	Sign inversion of photovoltage occurs at $\lambda = 4000$ Å	[139]
Single crystals (zone refined)	40 μ	SnO ₂	SnO ₂	Negative or Positive	3700 Å - 4200 Å	300°K	Spectral distribution same as absorption spectrum	[157]

CHAPTER III

UNIFIED APPROACHES TO THE THEORY OF CURRENT INJECTION IN SOLIDS

In this chapter, we present a new unified approach to the theory of one-carrier current injection in a solid having an arbitrary distribution of traps in energy and in space and some experimental results to show the relation between the size effects and the spatial trap distribution. The space-charge-limited currents in both organic and inorganic crystals have been discussed at length by many investigators [55,77], but little has been reported on organic materials, particularly in film form. We chose anthracene films for the present investigation partly because they are easy to fabricate for various film thicknesses. We also present a new unified approach to the theory of double-carrier current injection in a solid having traps distributed uniformly or nonuniformly in energy but homogeneously in space, and present some computed results to compare presently available experimental results.

These two approaches also enable the study of the energy distribution of the traps in a solid from the measurements of J-V characteristics since the expressions for the latter can be easily deduced to the expression for any particular conditions.

A. SINGLE INJECTION

3.1 THEORY OF SINGLE INJECTION

In single crystals the trap energy levels, if there are any, are generally discrete; while in amorphous and polycrystalline materials

they are distributed in accordance with certain distribution functions [143]. The latter has been attributed to the intrinsic disorder of the lattice, which is possibly due to the variation of the nearest neighbour distances. Material specimens in film form produced either by vacuum deposition or by other means are likely to be polycrystalline, and therefore, traps created by defects are generally distributed and their density is rather high even if the material itself is very pure chemically. Furthermore, material specimens always have boundaries such as their surfaces with metallic contacts. The trap distribution near such boundaries would be different from that in the bulk. In the theoretical analysis we make the following assumptions, but the treatment is general and therefore can be applied to thick or thin specimens in crystal or in film form of any materials.

(i) The energy band model can be used to treat the behaviour of injected carriers.

(ii) Only injected hole carriers are considered and the ohmic contact to inject them is perfect. (A similar treatment can be easily extended to the case for only injected electron carriers.)

(iii) The electric field is so large that the current components due to diffusion and due to carriers thermally generated in the specimen can be neglected.

(iv) The treatment is one dimensional with the plane at $x = 0$ as the injecting contact and that at $x = d$ as the collecting contact, and the specimen thickness is d .

The distribution function for the trap density as a function of energy level E above the edge of the valence band and distance x from the

injecting contact for hole carriers can be written as

$$h(E, x) = N_t(E) S(x) \quad (3.1)$$

where $N_t(E)$ and $S(x)$ represent respectively the energy and spatial distribution functions of traps. If the traps capture only holes, the electric field $F(x)$ inside the specimen follows the Poisson's equation

$$\frac{dF(x)}{dx} = - \frac{q[P_f(x) + P_t(x)]}{\epsilon} \quad (3.2)$$

and the current density may be written as

$$J = q \mu P_f(x) F(x) \quad (3.3)$$

where ϵ is the permittivity, μ is the hole mobility, q is the electronic charge, $P_t(x)$ and $P_f(x)$ are, respectively, the densities of injected trapped and injected free holes. $P_t(x)$ and $P_f(x)$ are given by

$$P_t(x) = \int_0^{E_g} h(E, x) f(E) dE \quad (3.4)$$

and

$$P_f(x) = N_V \exp(-E_F/kT) \quad (3.5)$$

where E_g is the energy band gap, N_V is the effective density of states in the valence band, k is the Boltzmann constant, T is the absolute temperature, and E_F is the quasi-Fermi level for holes, and $f(E)$ is the Fermi-Dirac distribution function which is given by

$$f(E) = \frac{1}{1 + g \exp[(E_F - E)/kT]} \quad (3.6)$$

where g is the degeneracy factor of the trap state. In the following we shall consider three general cases:

3.1.1 The traps confined in a single discrete energy level.

For this case, equation (3.1) becomes

$$h(E, x) = H_a \delta(E - E_t) S(x) \quad (3.7)$$

where H_a is the density of traps, E_t is the trap energy level above the edge of the valence band and $\delta(E - E_t)$ is the Dirac delta function.

From equations (3.4) and (3.6) we obtain

$$P_t(x) = \int_0^{E_g} \frac{H_a \delta(E - E_t) S(x) dE}{1 + g \exp [(E_F - E)/kT]} \quad (3.8)$$

$$\approx \frac{H_a S(x)}{1 + \frac{H_a \theta_a}{P_f(x)}} \quad (3.8)$$

in which

$$\theta_a = \frac{gN_V}{H_a} \exp (-E_t/kT) \quad (3.9)$$

Substitution of equation (3.9) into equation (3.2) gives

$$\frac{dF(x)}{dx} = - \frac{q}{\epsilon} \left[P_f + \frac{H_a S(x)}{1 + \frac{H_a \theta_a}{P_f(x)}} \right] \quad (3.10)$$

An analytical solution of equation (3.10) for J as a function of applied voltage is not possible, although a numerical solution can be obtained for all possible cases separately. For simplicity, we assume that E_t is a shallow trap level located below E_F . This implies that $H_a \theta_a \gg P_f(x)$. On the basis of this assumption and by multiplying both sides of equation (3.10) with $2F(x)$ and substituting equation (3.3) into it, we obtain

$$2F(x) \frac{dF(x)}{dx} = \frac{d[F(x)]^2}{dx} = - \frac{2J}{\epsilon \mu \theta_a} [\theta_a + S(x)] \quad (3.11)$$

Integration of equation (3.11) and use of the boundary condition

$$V = - \int_0^d F(x) dx \quad \text{give}$$

$$J = \frac{9}{8} \epsilon \mu \theta_a \frac{V^2}{d_{\text{eff}}^3} \quad (3.12)$$

in which V is the applied voltage and

$$d_{\text{eff}} = \left\{ \frac{3}{2} \int_0^d \left(\int_0^t [\theta_a + S(x)] dx \right)^{1/2} dt \right\}^{2/3} \quad (3.13)$$

Equation (3.12) is similar in form to that derived by Lampert [75] except that d has been replaced with d_{eff} which can be considered as "effective thickness". The difference between d_{eff} and d can be attributed to the inhomogeneous spatial distribution of free and trapped carriers.

3.1.2 The traps distributed exponentially within the forbidden energy gap.

For this case equation (3.1) becomes

$$h(E, x) = \frac{H_b}{kT_c} \exp \left(- \frac{E}{kT_c} \right) S(x) \quad (3.14)$$

where H_b is the density of traps per unit energy interval and T_c is a characteristic constant of the distribution. If $T_c > T$ we can assume that [89] $f(E) = 1$ for $E_F < E < \infty$ and $f(E) = 0$ for $E < E_F$ as if we take $T = 0$. This is a good approximation particularly when T_c is much larger than T . With this assumption we obtain

$$\begin{aligned} P_t(x) &= \int_{E_F}^{\infty} \frac{H_b}{kT_c} \exp \left(- \frac{E}{kT_c} \right) S(x) dE \\ &= H_b \exp \left(- \frac{E_F}{kT_c} \right) S(x) \\ &= H_b \left(\frac{P_f}{N_V} \right)^{T/T_c} S(x) \end{aligned} \quad (3.15)$$

The upper limit of the integral has been extended to infinity. This is permissible if $E_F(x)$ is far enough removed from the Fermi level of the neutral region. By substituting equation (3.15) into equation (3.2), letting $T_c/T = \ell$, and multiplying both sides with $(\frac{\ell+1}{\ell}) [F(x)]^{1/\ell}$, we obtain

$$\begin{aligned} \left(\frac{\ell+1}{\ell}\right) [F(x)]^{1/\ell} \frac{dF(x)}{dx} &= \frac{d[F(x)]^{(\ell+1)/\ell}}{dx} \\ &= -\left(\frac{\ell+1}{\ell}\right) \frac{q}{\epsilon} [P_f F(x)]^{1/\ell} [P_f]^{(\ell-1)/\ell} + H_b N_V^{-1/\ell} S(x) \\ &= -\left(\frac{\ell+1}{\ell}\right) \frac{q H_b}{\epsilon} \left(\frac{J}{q \mu N_V}\right)^{1/\ell} [\theta_b + S(x)] \end{aligned} \quad (3.16)$$

in which

$$\theta_b = \frac{N_V}{H_b} \exp \left[-\frac{E_F}{kT} \left(\frac{\ell-1}{\ell} \right) \right] \quad (3.17)$$

Integration of equation (3.16) and use of the boundary condition

$$\begin{aligned} V = -\int_0^d F(x) dx \quad \text{give} \\ J = q^{1-\ell} \mu N_V \left(\frac{2\ell+1}{\ell+1} \right)^{\ell+1} \left(\frac{\ell}{\ell+1} \frac{\epsilon}{H_b} \right)^{\ell} \frac{V}{d_{\text{eff}}^{\ell+1}} \end{aligned} \quad (3.18)$$

in which

$$d_{\text{eff}} = \left\{ \frac{2\ell+1}{\ell+1} \int_0^d \left(\int_0^t [\theta_b + S(x)] dx \right)^{\ell/(\ell+1)} dt \right\}^{(\ell+1)/(2\ell+1)} \quad (3.19)$$

Equation (3.18) is similar in form to that derived by Mark and Helfrich [89] except that d has been replaced with d_{eff} . Again, the difference between d_{eff} and d is caused by the inhomogeneous spatial distribution of free and trapped carriers.

3.1.3 The traps distributed uniformly within the forbidden energy gap.

For this case, equation (3.1) becomes

$$h(E, x) = H_c S(x) \quad (3.20)$$

where H_c is the density of traps per unit energy interval. From equations (3.4) and (3.5) we obtain

$$\begin{aligned} P_t(x) &= \int_0^{E_g} \frac{H_c S(x) dE}{1 + g \exp [(E_F - E)/kT]} \\ &= H_c \{E_g + kT \ln \frac{1 + g \exp [(E_F - E_g)/kT]}{1 + g \exp (E_F/kT)}\} S(x) \\ &\approx H_c kT \left(\frac{E_g - E_F}{kT} - \ln g \right) S(x) \end{aligned} \quad (3.21)$$

since $E_g > E_F$. Substitution of equation (3.21) into equation (3.2) gives

$$\begin{aligned} \frac{dF}{dx} &= -\frac{q}{\epsilon} \{P_f + H_c kT \left(\frac{E_g - E_F}{kT} - \ln g \right) S(x)\} \\ &= -\frac{qH_c kT}{\epsilon} [\theta_c + S(x)] \ln \left[\frac{q\mu N_V g \exp (-E_g/kT)}{J} F \right] \end{aligned} \quad (3.22)$$

in which

$$\theta_c = \frac{N_V \exp (-E_F/kT)}{H_c kT \left(\frac{E_g - E_F}{kT} - \ln g \right)} \quad (3.23)$$

Integration of equation (3.22) and use of the boundary condition

$$V = - \int_0^d F(x) dx \quad \text{gives (see Appendix)}$$

$$J = 2q\mu N_V g \frac{V}{d_{\text{eff}}} \exp \left(-\frac{E_g}{kT} \right) \exp \left(-\frac{2\epsilon V}{qH_c kT d_{\text{eff}}^2} \right) \quad (3.24)$$

in which

$$d_{\text{eff}} = \left\{ 2 \int_0^d \int_0^t [\theta_c + S(x)] dx dt \right\}^{1/2} \quad (3.25)$$

Equation (3.24) is similar in form to that derived by Muller [98] except that d has been replaced with d_{eff} . Again the difference between d_{eff} and d is caused by the inhomogeneous spatial distribution of free and trapped carriers.

The above three general cases can be extended to many other cases for other possible distribution functions through an appropriate approximation procedure. However, once $S(x)$ is known, d_{eff} can be easily calculated and then the I-V characteristics can be determined.

3.2 EXPERIMENTAL AND COMPUTED RESULTS FOR SINGLE INJECTION

Anthracene film specimens were fabricated by evaporating the anthracene material of scintillation grade and depositing it onto a silver-coated glass substrate under a vacuum of 10^{-6} torr, the temperature of the substrate being kept at -60°C during deposition [104]. On the other surface of the film was vacuum-deposited a silver layer to form a sandwich type specimen, the silver electrode size on both film surfaces being 2 mm in diameter. The film thickness was measured with an interferometer and checked with the microbalance weighing method. Figure 3.1 shows the I-V characteristics for various film thicknesses. For a given thickness, I is proportional to V^3 indicating that the traps are distributed exponentially within the forbidden energy gap following equation (3.18) with $\ell = 2$. This is reasonable because the structure of anthracene films is likely to be polycrystalline, and the traps created by defects due to such a structure generally have an exponential distribution in energy [52]. Since the carriers injected from silver electrodes to anthracene are holes [61,120], we can now use equation (3.19) to

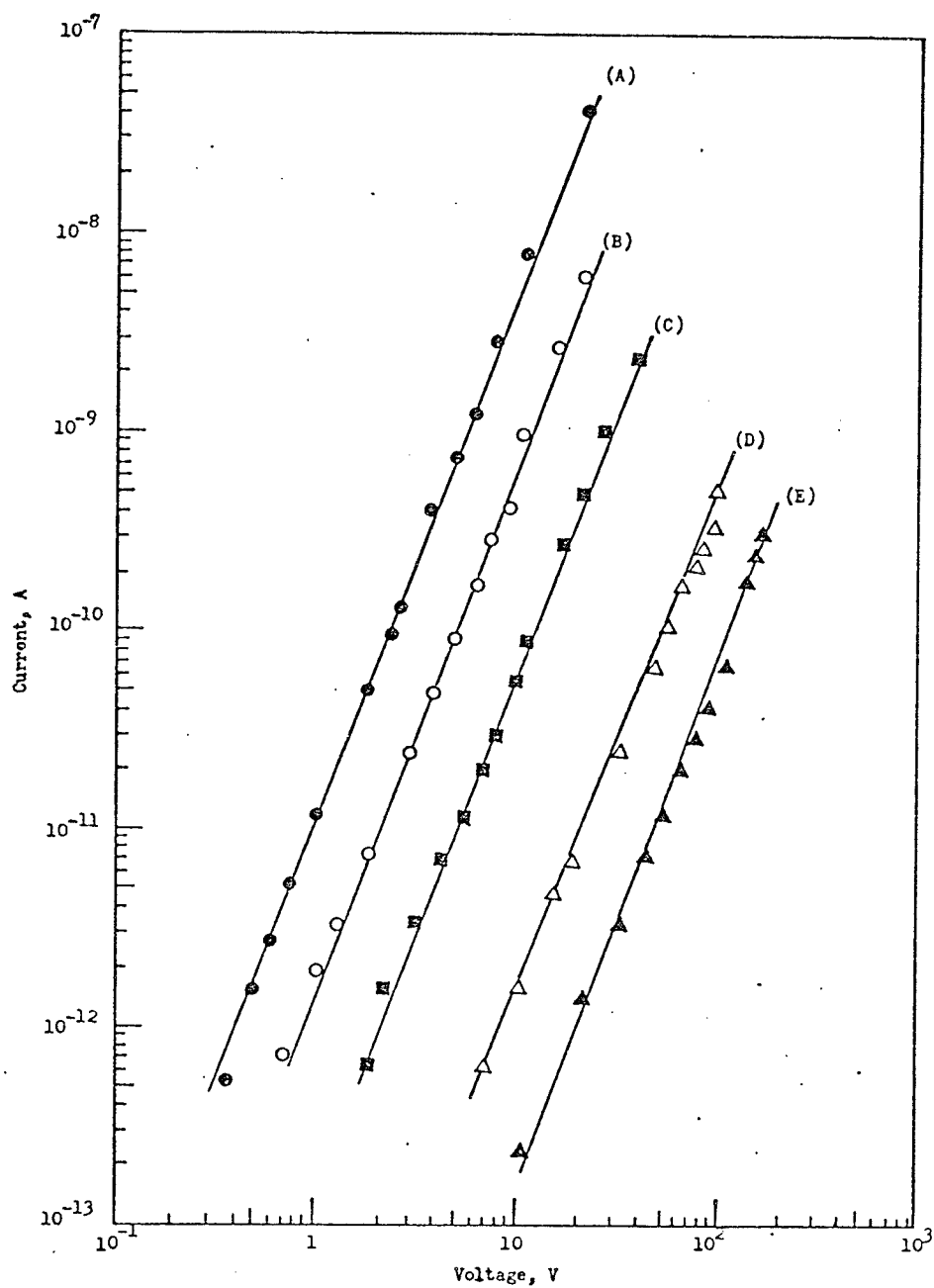


Fig. 3.1: The current-voltage characteristics of anthracene films of thickness (A) 1.62 μ , (B) 2.49 μ , (C) 3.90 μ , (D) 8.80 μ , and (E) 11.50 μ .

calculate d_{eff} and then determine $S(x)$ from the thickness dependence of I for a given applied voltage V . We shall first compute d_{eff} for three most probable distribution functions of $S(x)$ as follows. For simplicity the contribution of the free carriers to d_{eff} is ignored, so that equation (3.19) reduces to

$$d_{\text{eff}} = \left[\frac{2\ell + 1}{\ell + 1} \int_0^d \left(\int_0^t S(x) dx \right)^{\frac{\ell}{\ell+1}} dt \right]^{\frac{\ell+1}{2\ell+1}} \quad (3.26)$$

3.2.1 Uniform spatial distribution.

The distribution function may be written as

$$S(x) = 1 \quad (3.27)$$

d_{eff} for this distribution function is therefore

$$\begin{aligned} d_{\text{eff}} &= \left[\frac{2\ell+1}{\ell+1} \int_0^d \left(\int_0^t dx \right)^{\frac{\ell}{\ell+1}} dt \right]^{\frac{\ell+1}{2\ell+1}} \\ &= d \end{aligned} \quad (3.28)$$

3.2.2 Exponential spatial distribution with the maximum density at the injecting electrode (at $x = 0$).

The distribution function may be written as

$$S(x) = 1 + A \exp \left(-\frac{x}{x_0} \right) \quad (3.29)$$

where A and x_0 are constants. Substitution of equation (3.29) into equation (3.26) gives

$$d_{\text{eff}} = \left\{ \frac{2\ell+1}{\ell+1} \int_0^d \left[\int_0^t \left(1 + A \exp \left(-\frac{x}{x_0} \right) dx \right)^{\frac{\ell}{\ell+1}} dt \right]^{\frac{\ell+1}{2\ell+1}} \right.$$

By setting

$$p = \frac{\ell}{\ell+1}, \quad w = \exp\left(-\frac{t}{x_0}\right) \quad \text{and} \quad w_d = \exp\left(-\frac{d}{x_0}\right), \quad \text{we obtain}$$

$$\frac{d_{\text{eff}}}{d} = \frac{x_0}{d} \cdot (1+p)^{\frac{p}{1+p}} \cdot \left\{ \int_{w_d}^1 \frac{[\Lambda(1-w) - \ln w]^p}{w} dw \right\}^{\frac{1}{p+1}} \quad (3.30)$$

which can be easily evaluated.

3.2.3 Exponential spatial distribution with the maximum density at both electrodes (at $x = 0$ and $x = d$).

The distribution function may be written as

$$S(x) = 1 + B \left[\exp\left(-\frac{x}{x_0}\right) + \exp\left(-\frac{d-x}{x_0}\right) \right] \quad (3.31)$$

where B is a constant. Similarly, substituting equation (3.31) into equation (3.26) and simplifying it, we obtain

$$\frac{d_{\text{eff}}}{d} = \frac{x_0}{d} (1+p)^{\frac{p}{1+p}} \cdot \left\{ \int_{w_d}^1 \frac{[B(1-w-w_d + \frac{w_d}{w}) - \ln w]^p}{w} dw \right\}^{\frac{1}{p+1}} \quad (3.32)$$

From the experimental results given in Fig. 3.1 we have $\ell = 2$. Using this value for ℓ , we have computed d_{eff}/d as a function of d/x_0 and the results are given in Fig. 3.2 for various $S(x)$. From Fig. 3.1 and equation (3.18) we would expect I to be proportional to d^{-5} for a given V if the spatial distribution of traps is uniform. But the plot of I as a function of d for a given V in Fig. 3.3 shows that I is proportional to d^{-n} , in which n is dependent on d . This indicates that the trap distribution in the anthracene films under investigation is spatially inhomogeneous. Since I can be simply expressed as $I = Md^{-n} = Md_{\text{eff}}^{-5}$ for

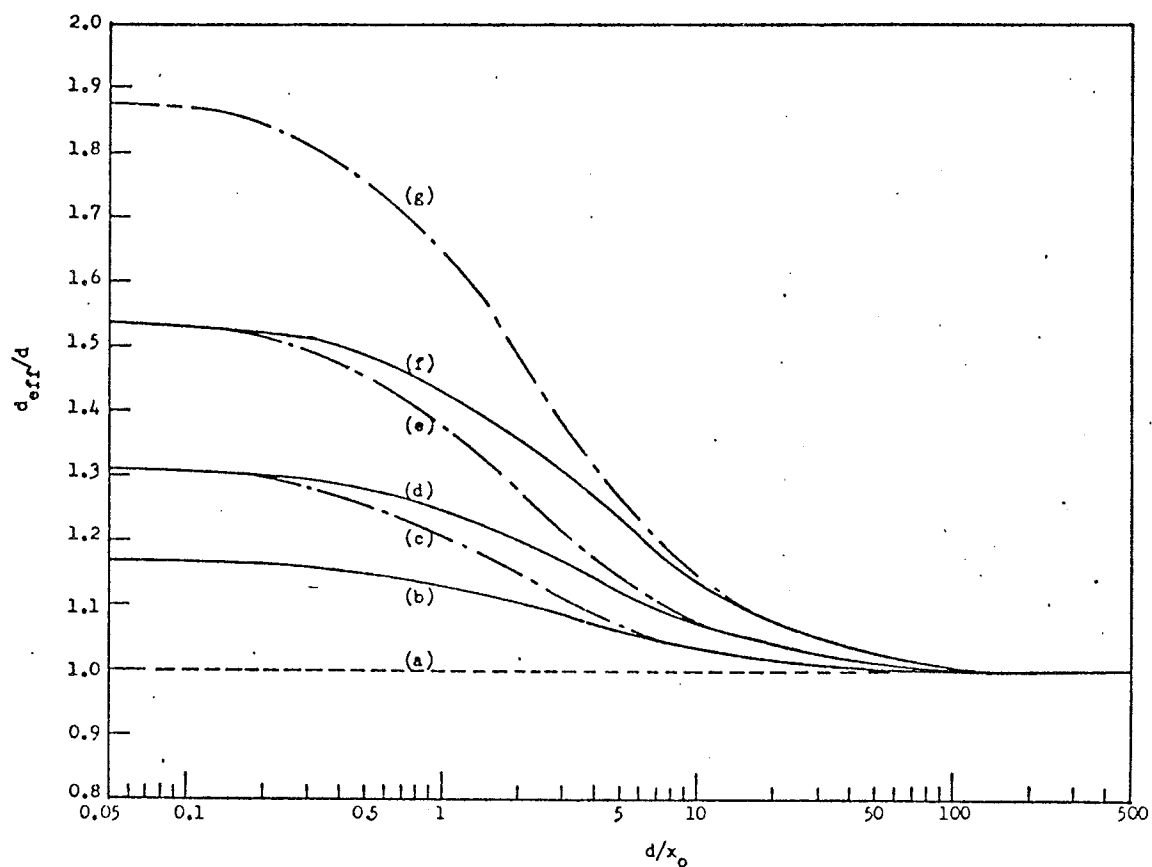


Fig. 3.2: d_{eff}/d as a function of d/x_0 for

- (a) $S(x) = 1$,
- (b) $S(x) = 1 + 0.5 \exp(-x/x_0)$,
- (c) $S(x) = 1 + 0.5\{\exp(-x/x_0) + \exp[-(d-x)/x_0]\}$,
- (d) $S(x) = 1 + \exp(-x/x_0)$,
- (e) $S(x) = 1 + \{\exp(-x/x_0) + \exp[-(d-x)/x_0]\}$,
- (f) $S(x) = 1 + 2 \exp(-x/x_0)$,
- (g) $S(x) = 1 + 2\{\exp(-x/x_0) + \exp[-(d-x)/x_0]\}$.

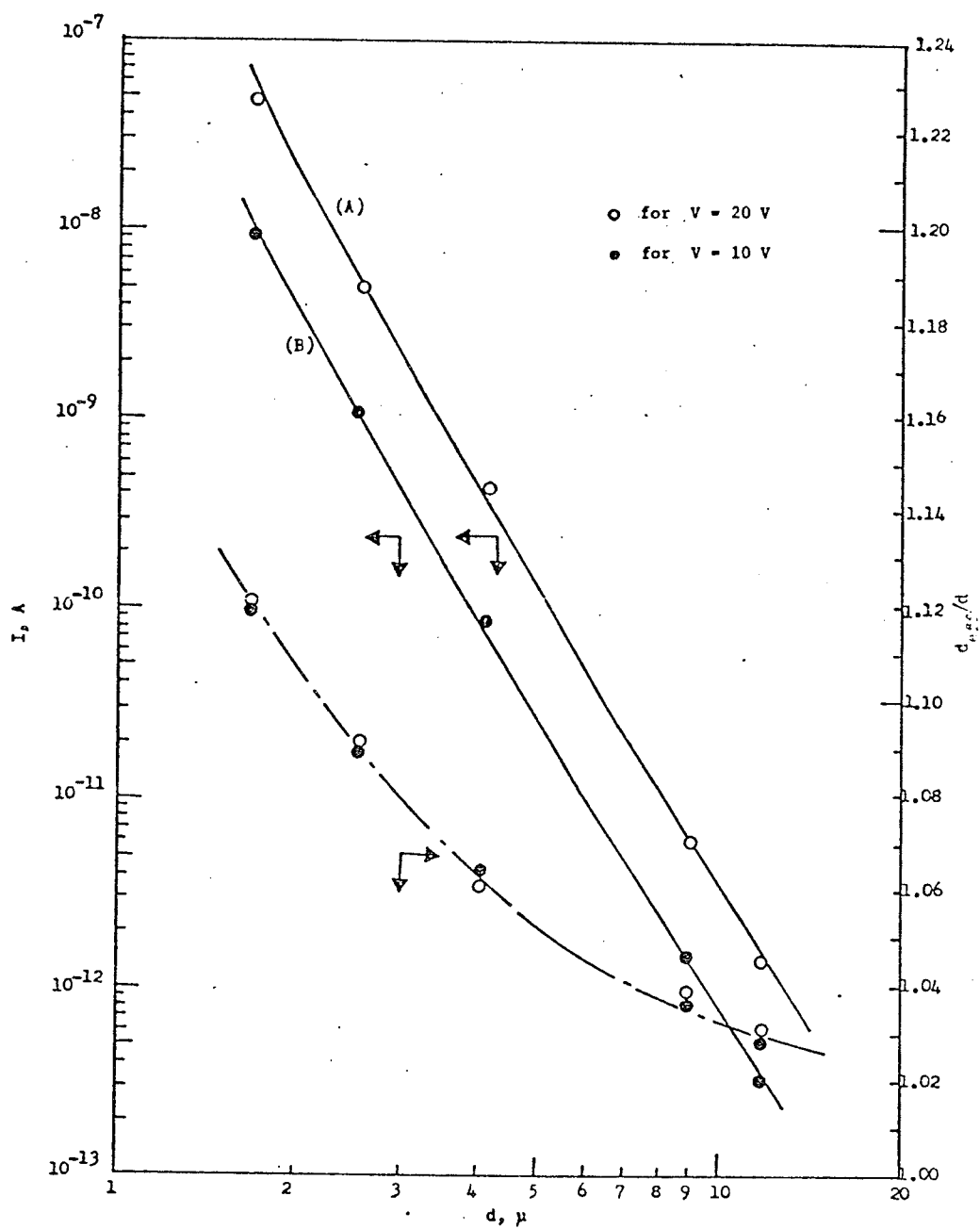


Fig. 3.3: I and d_{eff}/d as functions of film thickness for
(A) $V = 20$ V, and (B) $V = 10$ V.

a given V and $\ell = 2$, we can determine from Fig. 3.3 the values of n and d_{eff}/d for various values of d . The result of the latter is also plotted in the same figure.

It is reasonable to assume that if the inhomogeneity of the spatial trap distribution is caused by the metal-anthracene contacts, then the distribution function should be independent of film thickness because the same technique was used to fabricate all specimens. Since the material used for both electrodes is silver, we would expect that the trap distribution at $x = 0$ should be symmetrical with that at $x = d$. Thus the most probable spatial distribution function would be exponential with the maximum trap density at $x = 0$ and $x = d$. From Figs. 3.2 and 3.3 we have estimated that for $S(x)$ independent of d , the value of x_0 is between 0.3 and 0.4μ , and the value of B is between 1 and 2 . It should be noted that the number of thicknesses used for the present experimental investigation is only 5 , the curves drawn in Fig. 3.3 are clearly not unique. For accurate determination of $S(x)$ more results on thickness dependence of I - V characteristics and an iterative procedure to find x_0 , B or A are necessary.

3.3 CONCLUDING REMARK FOR SINGLE INJECTION

The general expressions for the current-voltage characteristics in a solid with traps uniformly and non-uniformly distributed in space and in energy have been derived using a unified mathematical approach. The analysis technique discussed in this chapter may, in principle, be used to analyse any distribution of traps with space and energy. However, it should be noted that in the derivation both the permittivity and the

carrier mobility have been assumed to be constant. For a more rigorous treatment, these two physical parameters may have to be considered to be altered by the charge exchange in traps [107].

B. DOUBLE INJECTION

3.4 THEORY OF DOUBLE INJECTION

In the theoretical analysis we make the following assumptions:

(i) The energy band model can be used to treat the behaviour of injected carriers.

(ii) Both injected electron and hole carriers are considered and the ohmic contacts at the cathode and at the anode to inject them are perfect.

(iii) The electric field is so large that the current components due to diffusion and due to carriers thermally generated in the specimen can be neglected.

(iv) The treatment is one dimensional with the plane at $x = 0$ as the electron-injecting contact and that at $x = d$ as the hole-injecting contact, the specimen thickness being d .

(v) The free electron and hole densities follow the Maxwell-Boltzmann statistics, while the trapped electron and hole densities follow the Fermi-Dirac statistics.

(vi) The mobilities of the free electrons and free holes are not affected by the presence of traps.

(vii) The fields at both injecting contacts are zero under all conditions. That is

$$F(x=0) = F(x=d) = 0 \quad (3.33)$$

(viii) The indirect recombination through traps is predominant so that the direct band recombination can be ignored.

The behaviour of double injection in a solid is governed by the current flow equations:

$$J_n = q\mu_n n_f F \quad (3.34)$$

$$J_p = q\mu_p p_f F \quad (3.35)$$

$$J = J_n + J_p \quad (3.36)$$

the continuity equations:

$$-(1/q)(dJ_n/dx) = r = np\langle v\sigma_R \rangle \quad (3.37)$$

$$(1/q)(dJ_p/dx) = r = np\langle v\sigma_R \rangle \quad (3.38)$$

and the Poisson equation:

$$dF/dx = (q/\epsilon)[p_f(x) + p_t - n_f(x) - n_t] \quad (3.39)$$

Based on the assumptions given above, the densities of free electrons and holes are given by

$$n_f(x) = N_c \exp[-(E_c - E_{Fn})/kT] \quad (3.40)$$

$$p_f(x) = N_v \exp[-(E_{Fp} - E_v)/kT] \quad (3.41)$$

and those of trapped electrons and holes by

$$n_t = \int_{E_\ell}^E h_n(E) f_n(E) dE \quad (3.42)$$

$$p_t = \int_{E_\ell}^E h_p(E) f_p(E) dE \quad (3.43)$$

where

$$f_n(E) = \frac{1}{1 + g_n^{-1} \exp[(E - E_{Fn})/kT]} \quad (3.44)$$

$$f_p(E) = \frac{1}{1 + g_p \exp[(E_{Fp} - E)/kT]} \quad (3.45)$$

and $h_n(E)$ and $h_p(E)$ are, respectively, the electron and hole trap distribution functions which are functions of energy level E between the two limiting levels E_ℓ and E_u . To evaluate n_t and p_t , and to derive the expressions for the J-V characteristics it is convenient to consider three general cases as follows:

3.4.1 The traps confined in a single discrete energy level.

(i) Shallow traps:

The electron traps are considered to be shallow if $E_{tn} > E_{Fn}$ (or $E_{tp} < E_{Fp}$ for shallow hole traps). For this case the trap distribution function is given by

$$h_n(E) = H_{an} \delta(E - E_{tn}) . \quad (3.46)$$

If E_{tn} is not too close to E_{Fn} for shallow traps, substitution of equations (3.44) and (3.46) into equation (3.42) gives

$$n_{at} \approx H_{an} g_n \exp[(E_{Fn} - E_{tn})/kT] . \quad (3.47)$$

Similarly, we can obtain $h_p(E)$ and P_{at} as follows:

$$h_p(E) = H_{ap} \delta(E - E_{tp}) \quad (3.48)$$

$$p_{at} \approx H_{ap} g_p^{-1} \exp[(E_{tp} - E_{Fp})/kT] . \quad (3.49)$$

From equations (3.40), (3.41), (3.47) and (3.49) we can write

and $n = n_f + n_{at} = K_{an} n_f$ (3.50)

$$p = p_f + p_{at} = K_{ap} p_f \quad (3.51)$$

in which

$$K_{an} = 1 + \frac{g_n H_{an}}{N_c} \exp[(E_c - E_{tn})/kT] \quad (3.52)$$

$$K_{ap} = 1 + \frac{H_{ap}}{g_p N_v} \exp[(E_{tp} - E_v)/kT] \quad (3.53)$$

By introducing the following parameters for the solids without traps (denoted by the subscript "0")

$$\mu_{R0} = e \langle v \sigma_R \rangle_0 / 2q \quad (3.54)$$

$$v_{R0} = \mu_u / \mu_{R0} \quad (3.55)$$

$$v_{p0} = \mu_p / \mu_{R0} \quad (3.56)$$

and the corresponding parameters for the solids with traps

$$\mu_{Ra} = \frac{\mu_{R0}}{K_{an} K_{ap}} = \frac{e \langle v \sigma_R \rangle_0}{2q} \frac{1}{K_{an} K_{ap}} \quad (3.57)$$

$$v_{an} = K_{ap} v_{n0} \quad (3.58)$$

$$v_{ap} = K_{an} v_{p0} \quad (3.59)$$

and also the following parameters

$$\alpha_a = \frac{\mu_n \mu_p e}{2 K_{an} K_{ap} \mu_{Ra} J} \quad (3.60)$$

$$\beta_a = q \mu_n / K_{an} J \quad (3.61)$$

$$\gamma_a = q \mu_p / K_{ap} J \quad (3.62)$$

$$U_a = \alpha_a F^2 \quad (3.63)$$

$$S_a = \beta_a n F = \beta_a K_{an} n_f F \quad (3.64)$$

$$T_a = \gamma_a p F = \gamma_a K_{ap} p_f F \quad (3.65)$$

equations (3.36), (3.37), (3.38) and (3.39) can be written as

$$S_a + T_a = 1 \quad (3.66)$$

$$dS_a/dx = -S_a T_a / U_a \quad (3.67)$$

$$dT_a/dx = S_a T_a / U_a \quad (3.68)$$

$$dU_a/dx = v_{an} T_a - v_{ap} S_a \quad (3.69)$$

Integration of equation (3.69) with the aid of equations (3.66), (3.67) and (3.68) gives

$$U_a = D_a (1 - S_a)^{v_{ap}} S_a^{v_{an}} \quad (3.70)$$

where D_a is the integration constant which is determined by differentiating equation (3.70) with respect to x and comparing it with equation (3.69). By doing so, we obtain

$$dS_a/dx = -S_a (1 - S_a) / U_a. \quad (3.71)$$

Since the entire current at the anode is carried by holes, thus $S_a = 0$; and the entire current at the cathode is carried by electrons, thus

$S_a = 1$. So integration of equation (3.71) gives

$$D_a = d / \int_{S_a=0}^{S_a=1} S_a^{v_{an}-1} (1-S_a)^{v_{ap}-1} dS_a. \quad (3.72)$$

Using equation (3.63) and the boundary condition $V = - \int_0^d F(x) dx$, it

can easily be shown that the relation between J and V is

$$J = \frac{9}{8} \epsilon \mu_{\text{eff}} \frac{V^2}{d^3} \quad (3.73)$$

where

$$\mu_{\text{eff}} = \frac{8}{9} \frac{q \mu_n \mu_p}{\langle v \sigma_R \rangle_0} \frac{\left[\int_0^1 S_a^{v_{an}-1} (1-S_a)^{v_{ap}-1} dS_a \right]^3}{\left[\int_0^1 S_a^{3v_{an}/2-1} (1-S_a)^{3v_{ap}/2-1} dS_a \right]^2}. \quad (3.74)$$

Equations (3.73) and (3.74) are similar to those derived by Parmenter and Reppel [106] except that v_{no} and v_{po} have been replaced with $v_n = K_{an} v_{no}$ and $v_p = K_{ap} v_{po}$. Thus, by putting $K_{an} = K_{ap} = 1$, this case will degenerate to the case for trap-free solids.

(ii) Deep traps:

The electron traps are considered to be deep if $E_{tn} < E_{Fn}$ (or $E_{tp} > E_{Fp}$ for deep hole traps). For this case all equations derived for the shallow trap case can be used except that n_{at} , p_{at} , K_{an} and K_{ap} have to be replaced with the following expressions:

$$n_{at} \approx H_{an} \quad (3.75)$$

$$p_{at} \approx H_{ap} \quad (3.76)$$

$$K_{an} = 1 + \frac{H_{an}}{N_c} \exp \left[\frac{(E_c - E_{Fn})}{kT} \right] \quad (3.77)$$

$$K_{ap} = 1 + \frac{H_{ap}}{N_v} \exp \left[\frac{(E_{Fp} - E_v)}{kT} \right] \quad (3.78)$$

3.4.2 The traps distributed exponentially within the forbidden energy gap.

For this case the electron and hole trap distribution functions are

$$h_n(E) = \frac{H_{bn}}{kT_c} \exp\left(\frac{E - E_c}{kT_c}\right) \quad (3.79)$$

$$h_p(E) = \frac{H_{bp}}{kT_c} \exp\left(\frac{E_r - E}{kT_c}\right). \quad (3.80)$$

If $T_c > T$ we can assume that $f_n(E) = 1$ for $-\infty < E < E_{Fn}$ and $f_n(E) = 0$ for $E > E_{Fn}$; and $f_p(E) = 1$ for $E_{Fp} < E < \infty$ and $f_p(E) = 0$ for $E < E_{Fp}$ as if we take $T = 0$. This is a good approximation particularly when T_c is much larger than T [89]. With this assumption and from equations (3.42), (3.43), (3.79) and (3.80) we obtain

$$\begin{aligned} n_{bt} &= \int_{E_c}^{E_{Fn}} \frac{H_{bn}}{kT_c} \exp\left(\frac{E - E_c}{kT_c}\right) dE \\ &\approx H_{bn}(n_f/N_c)^{1/l} \end{aligned} \quad (3.81)$$

and

$$\begin{aligned} p_{bt} &= \int_{E_{Fp}}^{E_c} \frac{H_{bp}}{kT_c} \exp\left(\frac{E_r - E}{kT_c}\right) dE \\ &\approx H_{bp}(p_f/N_c)^{1/l} \end{aligned} \quad (3.82)$$

where $\ell = T_c/T$. Following the same procedure as above, we can write

$$n = n_f + n_{bt} = N_{bn} n_f^{1/\ell} \quad (3.83)$$

$$p = p_f + p_{bt} = K_{bp} p_f^{1/\ell} \quad (3.84)$$

$$K_{bn} = \left\{ 1 + \frac{N_c}{H_{bn}} \exp\left[\left(\frac{\ell-1}{\ell}\right) \left(\frac{E_{Fn} - E_c}{kT}\right)\right] \right\} \frac{H_{bn}}{N_c^{1/l}} \quad (3.85)$$

$$K_{bp} = \left\{ 1 + \frac{N_c}{H_{bp}} \exp\left[\left(\frac{\ell-1}{\ell}\right) \left(\frac{E_r - E_{Fp}}{kT}\right)\right] \right\} \frac{H_{bp}}{N_c^{1/l}} \quad (3.86)$$

To simplify matters, we introduce the following parameters:

$$\alpha_b = \frac{(\mu_n'''/K_{bn}) (\mu_n'''/K_{bn}) \epsilon}{[(l+1)/l] \mu_{Rb} l'''} \quad (3.87)$$

$$\beta_b = q \mu_n / K_{bn}^\ell J \quad (3.88)$$

$$\gamma_b = q \mu_p / K_{bp}^\ell J \quad (3.89)$$

$$U_b = \alpha_b F^{(\ell+1)/\ell} \quad (3.90)$$

$$S_b = \beta_b K_{bn}^\ell n_f F \quad (3.91)$$

$$T_b = \gamma_b K_{bp}^\ell p_f F \quad (3.92)$$

$$v_{bn} = (\mu_n^{1/\ell} / K_{bn}) / \mu_{Rb} \quad (3.93)$$

$$v_{bp} = (\mu_p^{1/\ell} / K_{bp}) / \mu_{Rb} \quad (3.94)$$

$$\mu_{Rb} = \frac{\epsilon \langle v \sigma \rangle_{Rb}}{[(\ell+1)/\ell] q (\mu_n n_f + \mu_p p_f)^{1-1/\ell}} \quad (3.95)$$

Using these parameters, substituting equations (3.83) and (3.84) into equation (3.39), and multiplying both sides with $\alpha_b (\frac{\ell+1}{\ell}) [F(x)]^{1/\ell}$ and then simplifying it, we obtain

$$dU_b/dx = v_{bn} T_b^{1/\ell} - v_{bp} S_b^{1/\ell} \quad (3.96)$$

Since

$$S_b + T_b = 1 \quad (3.97)$$

$$dS_b/dx = S_b^{1/\ell} T_b^{1/\ell} / U_b \quad (3.98)$$

$$dT_b/dx = -S_b^{1/\ell} T_b^{1/\ell} / U_b \quad (3.99)$$

integration of equation (3.96) gives

$$U_b = D_b \exp\{[\ell/(\ell+1)] [\nu_{bn} S_b^{(\ell-1)/\ell} + \nu_{bp} (1-S_b)^{(\ell-1)/\ell}]\} \quad (3.100)$$

where D_b is the integration constant which can be determined by integrating equation (3.95). Thus we have

$$D_b = d \int_0^1 \frac{\exp\{[\ell/(\ell+1)] [\nu_{bn} S_b^{(\ell-1)/\ell} + \nu_{bp} (1-S_b)^{(\ell-1)/\ell}]\} dS_b}{S_b^{1/\ell} (1-S_b)^{1/\ell}} \quad (3.101)$$

Using equations (3.90) and (3.100) and the boundary condition

$V = - \int_0^d F(x) dx$, it can be easily be shown that the relation between J and V is

$$J = q^{l+1} \mu'_{\text{eff}} \left(\frac{2l+1}{l+1} \right)^{l+1} \left(\frac{l\epsilon}{l+1} \right)^l \frac{V^{l+1}}{d^{2l+1}} \quad (3.102)$$

where

$$\begin{aligned} \mu'_{\text{eff}} = & [(l+1)/(2l+1)]^{l+1} \mu'_{Rb} \nu'_{bp} \nu'_{bn} \\ & \times \frac{\left(\int_0^1 \exp\left\{\left(\frac{l}{l+1}\right) [\nu_{bn} S_b^{(\ell-1)/\ell} + \nu_{bp} (1-S_b)^{(\ell-1)/\ell}]\right\} [S_b^{1/\ell} (1-S_b)^{1/\ell}]^{-1} dS_b \right)^{l+1}}{\left(\int_0^1 \exp\left\{\left(\frac{2l^2+1}{l^2-1}\right) [\nu_{bn} S_b^{(\ell-1)/\ell} + \nu_{bp} (1-S_b)^{(\ell-1)/\ell}]\right\} [S_b^{1/\ell} (1-S_b)^{1/\ell}]^{-1} dS_b \right)^{l+1}} \end{aligned} \quad (3.103)$$

Equation (3.102) is similar in form to that derived by Mark and Helfrich [89] for one-carrier current injection except that $\mu_p N_v / H_{bp}$ has been replaced with μ'_{eff} for double carrier current injection.

3.4.3 The traps distributed uniformly within the forbidden energy gap.

For this case the electron and hole trap distribution functions are

$$h_n(E) = H_{an} \quad (3.104)$$

$$h_p(E) = H_{dp} \quad (3.105)$$

From equations (3.42), (3.43), (3.104), and (3.105); and on the assumption that $f_n(E) = 1$ for $-\infty < E < E_{Fn}$, and $f_p(E) = 1$ for $E_{Fp} < E < \infty$; and $f_n(E) = f_p(E) = 0$, otherwise; we obtain

$$n_{dt} \approx H_{dn}(E_{Fn} - E_v) \quad (3.106)$$

and

$$p_{dt} \approx H_{dp}(E_c - E_{Fp}) \quad (3.107)$$

Thus we can write

$$n = n_f + n_{dt} = K_{dn} \ln \left(n_f / N_c e^{-E_g/kT} \right) \quad (3.108)$$

$$p = p_f + p_{dt} = K_{dp} \ln \left(p_f / N_v e^{-E_g/kT} \right) \quad (3.109)$$

in which

$$K_{dn} = \left\{ 1 + \frac{N_c \exp[(E_{Fn} - E_c)/kT]}{H_{dn}(E_{Fn} - E_v)} \right\} H_{dn} kT \quad (3.110)$$

$$K_{dp} = \left\{ 1 + \frac{N_v \exp[(E_c - E_{Fp})/kT]}{H_{dp}(E_c - E_{Fp})} \right\} H_{dp} kT. \quad (3.111)$$

Similarly, we introduce the following parameters for mathematical simplicity:

$$\alpha_d = J/qK_{dn}K_{dp}\langle v\sigma_R \rangle_d \quad (3.112)$$

$$\beta_d = q\mu_n/J \quad (3.113)$$

$$\gamma_d = q\mu_p/J \quad (3.114)$$

$$U_d = \alpha_d \ln F \quad (3.115)$$

$$S_d = \beta_d n_f F \quad (3.116)$$

$$T_d = \gamma_d p_f F \quad (3.117)$$

$$S_0 = \beta_d N_c \exp(-E_g/kT) F \quad (3.118)$$

$$T_0 = \gamma_d N_v \exp(-E_g/kT) F \quad (3.119)$$

$$v_{dn} = 1/K_{dn} \mu_{Rd} \quad (3.120)$$

$$v_{dp} = 1/K_{dp} \mu_{Rd} \quad (3.121)$$

$$\mu_{Rd} = \epsilon \langle v \sigma \rangle_0 / q (\mu_n n_f + \mu_p p_f) \quad (3.122)$$

Using these parameters, and substituting equations (3.108) and (3.109) into equations (3.37), (3.38) and (3.39); we obtain

$$\frac{dS_d}{dx} = \ln(T_d/T_0) \ln(S_d/S_0) / \alpha_d \quad (3.123)$$

$$-\frac{dT_d}{dx} = \ln(T_d/T_0) \ln(S_d/S_0) / \alpha_d \quad (3.124)$$

$$\frac{dF}{dx} = \frac{q}{\epsilon} [K_{dp} \ln(T_d/T_0) - K_{dn} \ln(S_d/S_0)] \quad (3.125)$$

Substitution of equations (3.123) and (3.124) into equation (3.125) and integration give

$$F = D_d \left\{ \exp[v_{dn} S_0 E_1 \ln(S_d/S_0) + v_{dp} T_0 E_1 \ln(T_d/T_0)] \right\} \quad (3.126)$$

where E_1 is the exponential integral and D_d is the integration constant.

From equations (3.125) and (3.126) and based on $V = - \int_0^d F(x) dx$, the value

of D_d can be determined and it is

$$D_d = \frac{\alpha_d \left(\frac{V}{d^2} \right) \left\{ \int_0^1 \left[\left(\ln \frac{S_d}{S_0} \right) \left(\ln \frac{1-S_d}{S_0} \right) \right]^{-1} dS_d \right\}^2}{\int_0^1 \frac{\left\{ \exp \left[\nu_{dn} S_0 E_1 \left(\ln \frac{S_d}{S_0} \right) + \nu_{dp} T_0 E_1 \left(\ln \frac{1-S_d}{T_0} \right) \right] \right\}}{\left(\ln \frac{1-S_d}{T_0} \right) \left(\ln \frac{S_d}{S_0} \right)} dS_d} \quad (3.127)$$

Thus the relation between J and V is

$$J = 2q\mu_{\text{eff}}'' (V/d) \exp[C(V/d^2)] \quad (3.128)$$

where

$$\mu_{\text{eff}}'' = \frac{dK_{dn}K_{dp} \langle v\sigma_R \rangle_d}{2 \int_0^1 \frac{\left\{ \exp \left[\nu_{dn} S_0 E_1 \left(\ln \frac{S_d}{S_0} \right) + \nu_{dp} T_0 E_1 \left(\ln \frac{1-S_d}{T_0} \right) \right] \right\}}{\left(\ln \frac{1-S_d}{T_0} \right) \left(\ln \frac{S_d}{S_0} \right)} dS_d} \quad (3.129)$$

and

$$C = \frac{d^2}{V} \ln \frac{d^2}{V} \frac{\int_0^1 \frac{\exp \left[\nu_{dn} S_0 E_1 \left(\ln \frac{S_d}{S_0} \right) + \nu_{dp} T_0 E_1 \left(\ln \frac{1-S_d}{T_0} \right) \right]}{\ln[(1-S_d)/T_0] \ln(S_d/S_0)} dS_d}{\alpha_d \left\{ \int_0^1 \left[\left(\ln \frac{S_d}{S_0} \right) \ln \left(\frac{1-S_d}{T_0} \right) \right]^{-1} dS_d \right\}^2} \quad (3.130)$$

Equation (3.128) is similar in form to that derived by Muller [98] for one-carrier current injection except that μn_0 has been replaced with μ_{eff}'' and $2e/qHkT$ with C for double carrier current injection.

It should be noted that an alternative approach to this double-injection problem can also be obtained by employing free carrier densities instead of local coordinates as the independent variables. Based

on this alternative approach, we can easily deduce from equations (3.34) - (3.39) the following equation

$$\frac{d(\ln n_f)}{d(\ln p_f)} = \frac{\rho - \epsilon r / \mu_n n_f}{\rho + \epsilon r / \mu_p p_f} \quad (3.131)$$

If the recombination rate constant, trap densities and their distribution function are known, n_f can be calculated in terms of p_f . Thus we can write

$$n_f = G(p_f) \quad (3.132)$$

and the crystal specimen thickness and the applied voltage in the form

$$d = \int_0^d dx = -\frac{J\epsilon}{q} \int_{p_f(x=d)}^{p_f(x=0)} \frac{\mu_p dp_f}{(\mu_n n_f + \mu_p p_f)(\mu_p p_f \rho + \epsilon r)} \quad (3.133)$$

$$V = -\int_0^d F dx = -\frac{J^2 \epsilon}{q^2} \int_{p_f(x=d)}^{p_f(x=0)} \frac{\mu_p dp_f}{(\mu_n n_f + \mu_p p_f)^2 (\mu_p p_f \rho + \epsilon r)} \quad (3.134)$$

From equations (3.131) - (3.134) we can easily deduce expressions of J-V characteristics for all types of trap distribution described above.

3.5 COMPUTED RESULTS FOR DOUBLE INJECTION

In order to show the effect of traps on the double injection J-V characteristics, we take anthracene crystal as an example. Generally, in this material the electron and hole mobilities are small, and the recombination rate constant is large resulting in a small space charge overlap. Thus the steady state double injection current in a solid without traps as a function of applied voltage is given by [55,57].

$$J = \frac{9}{8} \epsilon \mu_0 \frac{V^2}{d^3} \quad (3.135)$$

where $\mu_0 = \mu_n + \mu_p$. The presence of traps in the material alters this expression as has been discussed in Section 3.4. In the following we shall present some computed results which are computed by finite difference method, to show the effect of traps for two most probable types of trap distribution using the following physical parameters for anthracene

$$\begin{aligned} \mu_n &= 0.4 \text{ cm}^2/\text{V-sec} \\ \mu_p &= 0.8 \text{ cm}^2/\text{V-sec} \\ \langle v\sigma_R \rangle_0 &= 10^{-6} \text{ cm}^3/\text{sec} \end{aligned}$$

There is so far no experimental evidence that the traps are distributed uniformly within the forbidden energy gap. Physically, the uniform distribution of traps is unlikely to occur in a solid. We include it in our theoretical analysis just for the completeness of this unified approach, and, for the present, no computed results are presented for this type of trap distribution.

3.5.1 The traps confined in a single discrete energy level

For this case, the expression for the J-V characteristics [equation (3.73)] is similar to equation (3.135) except that μ_0 is replaced with μ_{eff} which is a function of μ_n , μ_p , h_n , h_p , r and F ; and may be simply expressed as

$$\mu_{\text{eff}} = \frac{\mu_n}{K_{\text{an}}} + \frac{\mu_p}{K_{\text{ap}}} \quad (3.136)$$

Figure 3.4 shows the ratio μ_{eff}/μ_0 as a function of H_{an}/N_c and the trapping level $(E_c - E_{\text{tn}})/kT$ [which is for electron traps and which is assumed

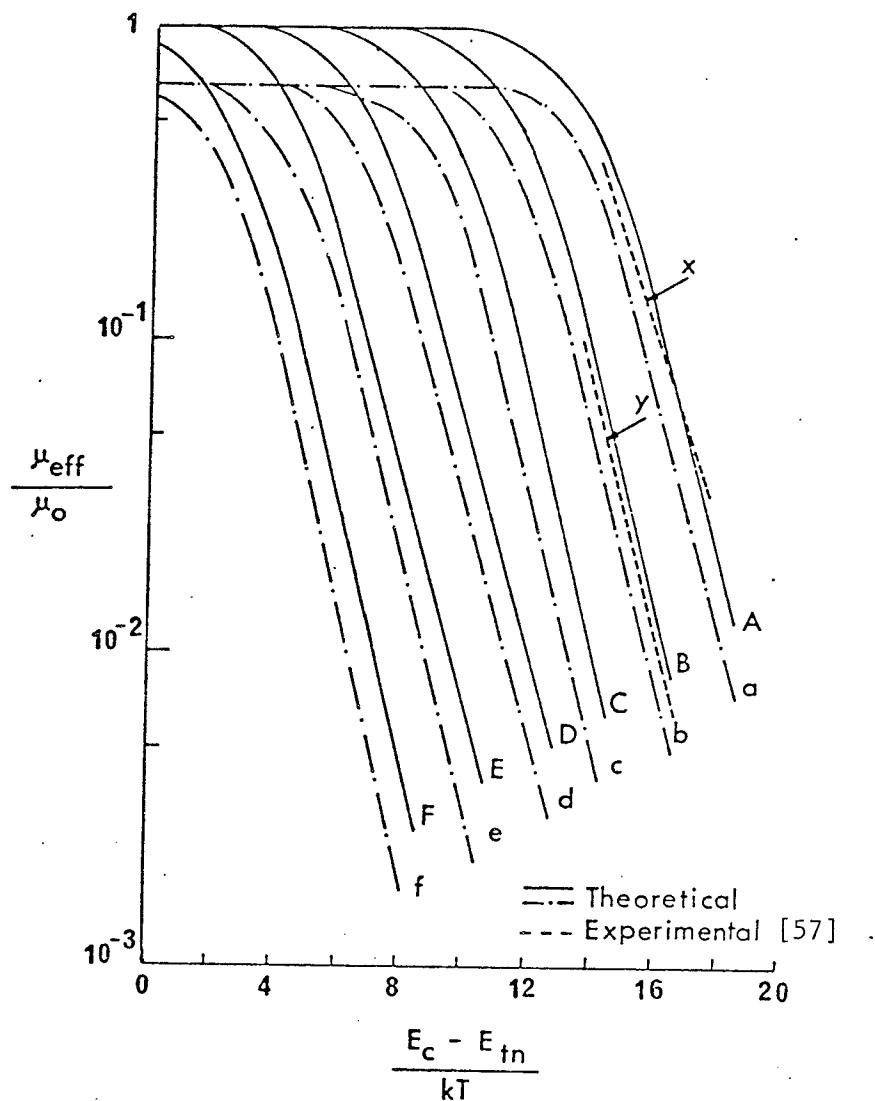


Fig. 3.4: μ_{eff}/μ_o as a function of $(E_c - E_{tn})/kT$ for traps confined in a single discrete energy level.

Solid lines for $K_{\text{an}}/K_{\text{ap}}=1$ and semi-dashed lines for $K_{\text{an}}/K_{\text{ap}}=0.5$.

A and a: $H_{\text{an}}/N_c = 10^{-6}$, B and b: $H_{\text{an}}/N_c = 10^{-5}$,

C and c: $H_{\text{an}}/N_c = 10^{-4}$, D and d: $H_{\text{an}}/N_c = 10^{-3}$,

E and e: $H_{\text{an}}/N_c = 10^{-2}$, F and f: $H_{\text{an}}/N_c = 10^{-1}$.

x: tetracene concentration = 1ppm equivalent to $H_{\text{an}}/N_c = 10^{-6}$.

y: tetracene concentration = 10ppm equivalent to $H_{\text{an}}/N_c = 10^{-5}$.

to be equal to $(E_{tp} - E_v)/kT$ for hole traps] for $K_{an}/K_{ap} = 1$ and 0.5. These results indicate that for a fixed trapping level the double injection current decreases with increasing trap density, and for a fixed trap density it decreases with increasing value of $(E_c - E_{tn})/kT$. This also implies that the shallow traps are less effective in reducing the current than the deep traps. These computed results are in good agreement with the experimental results of Hoesterey et al [57] and those of Schwob et al [124] for anthracene heavily doped with tetracene as shown in Fig. 3.4. This indicates that for traps created by dopants alone the traps are likely to be confined in a single discrete energy level.

3.5.2 The traps distributed exponentially within the forbidden energy gap.

For this case the J-V characteristics is given in equation (3.102), in which μ'_{eff} does not have the same dimension as μ_o but has the dimension of $(cm^2 V^{-1} sec^{-1}) (cm^3)^{\ell-1} (eV)^\ell$. However, to show the effect of traps, results are shown in Fig. 3.5. It can be seen that for a given value of ℓ the ratio μ'_{eff}/μ_o increases with increasing V, and for a given V it decreases with increasing value of ℓ . The higher the applied voltage, the less is the effect of traps, and this agrees well with the experimental results of Schwob et al [125] for tetracene-doped anthracene and those of Dresner [32] for undoped anthracene as shown in Fig. 3.5. This also indicates that in most anthracene crystals with imperfections the traps created by them are distributed exponentially within the forbidden energy gap with ℓ approximately equal to 2 at room temperature.

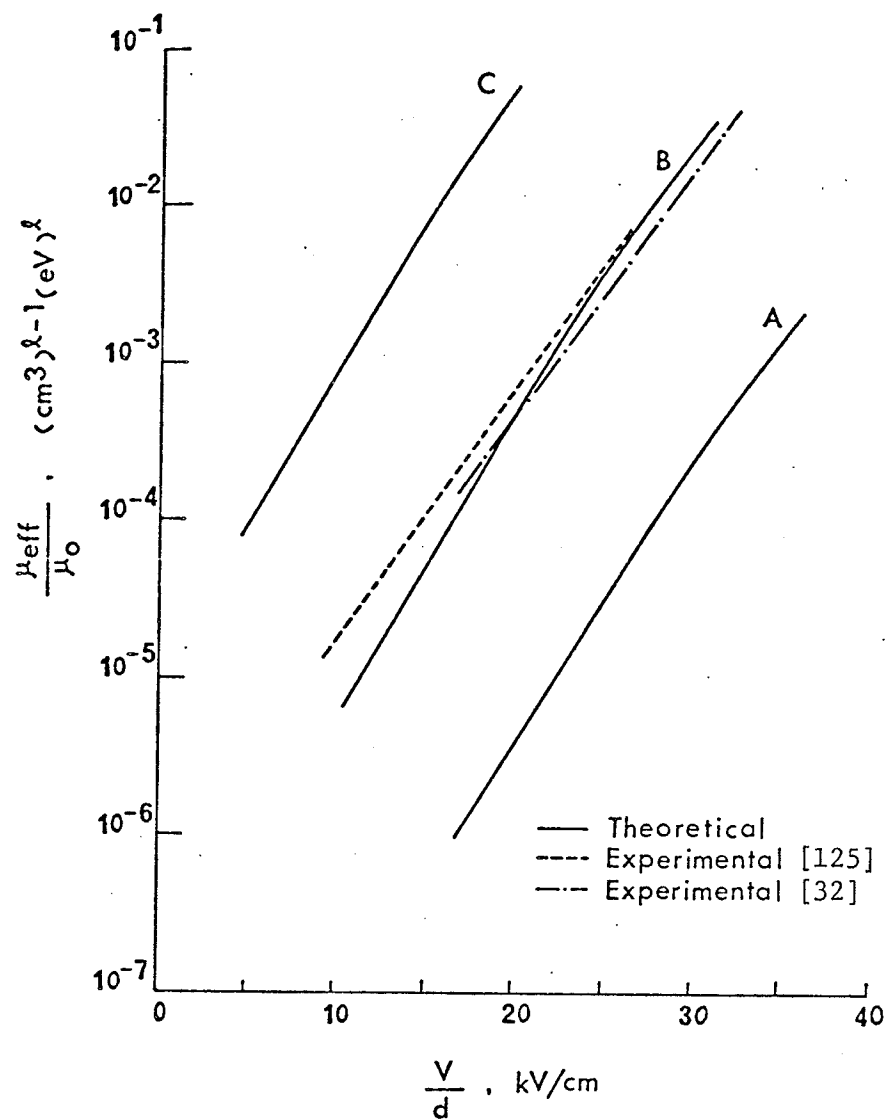


Fig: 3.5: μ_{eff}'/μ_0 as a function of V/d for traps distributed exponentially within the forbidden energy gap.

A: $\ell = 2.5$, B: $\ell = 2.0$, and C: $\ell = 1.5$.

3.6 CONCLUDING REMARKS FOR DOUBLE INJECTION

The general expressions for the double injection current-voltage characteristics in a solid with traps uniformly and non-uniformly distributed in energy have been derived using a unified mathematical approach. An alternative approach using free carrier densities instead of local coordinates as the independent variables has also been discussed. The analysis techniques described in this chapter may, in principle, be used to analyze any distribution of traps with energy since any type of distribution can always be resolved into components to fit these three general distribution functions. The computed results are in good agreement with the experimental results for anthracene containing traps either confined in a single discrete energy level or distributed exponentially within the forbidden energy gap. The effect of traps on the J-V characteristics can be used as a tool to determine the purity of a crystal. However, it should be noted that in the derivation both the permittivity and the carrier mobilities have been assumed to be constant. For a more rigorous treatment these physical parameters may have to be considered to be altered by the charge exchange in traps [107].

CHAPTER IV

THEORY OF

FILAMENTARY DOUBLE INJECTION

AND ELECTROLUMINESCENT PHENOMENA

In general, the interface between an electrode and a crystal surface which is not microscopically identical from domain to domain, is never homogeneous and uniform. Thus, there must be one or more microregions at which the potential barrier has a profile more favourable to carrier injection than at other regions of the interface. Furthermore, the crystal itself is never microscopically homogeneous and uniform. For all these unavoidable imperfections the current-passing through a crystal specimen is filamentary at least from a microscopic point of view. For an electrical field applied to the specimen longitudinally, the field will not be uniform longitudinally due to the effect of space charge and the current density will not be uniform radially due to the formation of filamentary paths. The current filaments formed in Si, GaAs, ZnTe, $\text{GaAs}_{1-x}\text{P}_x$ and polycrystalline Si have been observed by Barnett et al [8,9].

This chapter is to present a theoretical model for the filamentary injection and to show that the expressions derived on the basis of this model can explain quantitatively some important experimental aspects of electroluminescence in undoped and doped anthracene crystals.

4.1 THEORY OF FILAMENTARY DOUBLE INJECTION

In the theoretical analysis we make the following assumptions:

(i) At the voltage of or higher than the threshold voltage for the onset of electroluminescence, there may be one or more than one filaments formed between electrodes. But for mathematical simplicity we use cylindrical coordinates and consider only one filament formed along the z -axis which coincides with the central line joining the two circular plane electrodes of radius r_d . The whole system is symmetrical about the z -axis.

(ii) In the filament the longitudinal component of the diffusion current can be ignored because of the large longitudinal component of the electric field and the radial component of the drift current can be ignored because of the small radial component of the electric field.

(iii) The free electron and hole densities follow the Maxwell-Boltzmann statistics, while the trapped electron and hole densities follow the Fermi-Dirac statistics.

(iv) The mobility of the free electrons, μ_n , and that of the free holes, μ_p , are not affected by the presence of traps, nor by the high electric field.

(v) The treatment is two-dimensional with plane at $z = 0$ as the hole-injecting contact and that at $z = d$ as the electron-injecting contact, the specimen thickness being d .

(vi) The simply extrinsic (through traps) and intrinsic indirect recombinations are equally important and the recombination rate, R , consists of a longitudinal component, R_z , and a radial component, R_r .

The behaviour of double injection in a crystal is governed by the current flow equations

$$\begin{aligned}
\vec{J}_n &= \vec{J}_{nz} + \vec{J}_{nr} \\
&= q \mu_n n_f F \vec{i}_z + q D_n \frac{\partial n_f}{\partial r} \vec{i}_r
\end{aligned} \tag{4.1}$$

$$\begin{aligned}
\vec{J}_p &= \vec{J}_{pz} + \vec{J}_{pr} \\
&= q \mu_p p_f F \vec{i}_z - q D_p \frac{\partial p_f}{\partial r} \vec{i}_r
\end{aligned} \tag{4.2}$$

$$\vec{J} = \vec{J}_n + \vec{J}_p = \vec{J}_z + \vec{J}_r \tag{4.3}$$

the continuity equations

$$\mu_n \frac{\partial}{\partial z} (n_f F) = - \mu_p \frac{\partial}{\partial z} (p_f F) = R_z \tag{4.4}$$

$$\frac{D_n}{r} \frac{\partial}{\partial r} \left(r \frac{\partial n_f}{\partial r} \right) = \frac{D_p}{r} \frac{\partial}{\partial r} \left(r \frac{\partial p_f}{\partial r} \right) = R_r \tag{4.5}$$

and the Poisson equation

$$\nabla \cdot F = \frac{q}{\epsilon} [p_f + p_t - n_f - n_t] \tag{4.6}$$

The densities of free electrons and holes are, respectively, given by

$$n_f = N_c \exp[-(E_c - E_{Fn})/kT] \tag{4.7}$$

$$p_f = N_v \exp[-(E_{Fp} - E_v)/kT] \tag{4.8}$$

where J , J_n and J_p are, respectively, the total, electron and hole current densities; n_t and p_t are, respectively, the trapped electron and trapped hole densities; F is the electric field; ϵ is the permittivity of the crystal; D_n and D_p are, respectively, the diffusion coefficients for electrons and holes; E_c and E_v are, respectively, the energy levels at conduction and valence band edges; E_{Fn} and E_{Fp} are, respectively, quasi-

Fermi levels for electrons and holes; N_c and N_v are, respectively, the effective densities of states in the conduction and the valence bands; q is the electronic charge; k is the Boltzmann constant; T is the absolute temperature; \vec{i}_z and \vec{i}_r are, respectively, the unit vectors in the directions of z-axis and r-axis; and subscripts z and r refer, respectively to z- and r-direction. To derive the expressions for the current-voltage (I-V) characteristics it is convenient to consider two general cases as follows:

4.1.1 The traps confined in a single discrete energy level.

For this case the trap density distribution function for electrons is given by

$$h_n(E) = H_{an} \delta(E - E_{tn}) \quad (4.9)$$

thus

$$n_t = \int_{E_l}^{E_u} \frac{h_n(E) dE}{1 + g_n^{-1} \exp[(E - E_{Fn})/kT]} \quad (4.10)$$

Similarly, we have the trap density distribution function for holes

$$h_p(E) = H_{ap} \delta(E - E_{tp}) \quad (4.11)$$

and

$$p_t = \int_{E_l}^{E_u} \frac{h_p(E) dE}{1 + g_p \exp[(E_{Fp} - E)/kT]} \quad (4.12)$$

where H_{an} and H_{ap} are, respectively, the trap densities for electrons and holes for the trap distribution function following a delta function; g_n and g_p are, respectively, the degeneracy factors of trap states for electrons and holes; E_u and E_l are, respectively, the upper and the lower

limits of the trapping energy levels; and E_{tn} and E_{tp} are, respectively, electron and hole trapping energy levels.

For simplicity, we introduce the following parameters

$$K_{an} = 1 + \frac{n_t}{n_f} \quad (4.13)$$

$$K_{ap} = 1 + \frac{p_t}{p_f} \quad (4.14)$$

$$\mu_{Ra} = \frac{\epsilon R_o}{2q} \frac{1}{K_{an} K_{ap}} \quad (4.15)$$

$$v_{an} = K_{ap} \mu_n \left(\frac{2q}{\epsilon R_o} \right) \quad (4.16)$$

$$v_{ap} = K_{an} \mu_p \left(\frac{2q}{\epsilon R_o} \right) \quad (4.17)$$

$$\alpha_a = \frac{\mu_n \mu_p \epsilon}{2 K_{an} K_{ap} \mu_{Ra} J_{zo}} \quad (4.18)$$

$$\beta_a = \frac{q \mu_n}{K_{an} J_{zo}} \quad (4.19)$$

$$\gamma_a = \frac{q \mu_p}{K_{ap} J_{zo}} \quad (4.20)$$

$$U_a = \alpha_a F_z^2 = C_a / J_{zo} \quad (4.21)$$

$$S_a = \beta_a K_{an} n_f F_z \quad (4.22)$$

$$T_a = \gamma_a K_{ap} p_f F_z \quad (4.23)$$

$$W_a = \frac{J_z(r)}{J_{zo}} = \frac{J_{nz}(r) + J_{pz}(r)}{J_{nzo} + J_{pzo}} \quad (4.24)$$

Where R_o is the electron-hole recombination coefficient without traps,

J_{zo} is J_z at $r = 0$ (the center of the filament), and F_z is the electric field in the z -direction. Using these parameters the current density in z direction can be written as

$$W_a = S_a + T_a \quad (4.25)$$

Assuming that the radial variation of F_z is negligible, then equation (4.6) becomes

$$\frac{dU}{dr} = v_{an} T_a - v_{ap} S_a = 0 \quad (4.26)$$

thus

$$T_a = \left(\frac{v_{ap}}{v_{an}} \right) S_a \quad (4.27)$$

Substitution of equation (4.27) into equation (4.25) gives

$$S_a = \frac{W_a}{1 + \frac{v_{ap}}{v_{an}}} \quad (4.28)$$

$$T_a = \frac{(v_{ap}/v_{an}) W_a}{1 + \frac{v_{ap}}{v_{an}}} \quad (4.29)$$

Equation (4.5) can be written as

$$\frac{1}{r} \frac{\partial}{\partial r} \left(r \frac{\partial W_a}{\partial r} \right) = (AF_z^{-1} J_{zo}) W_a^2 \quad (4.30)$$

This equation indicates that the radial distribution of W_a is a function of z ; therefore, to obtain an equation for an average profile, we average the parameter over the specimen thickness of d . Thus, we can write

$$\left[\frac{1}{d} \int_0^d \frac{F_z dz}{AJ_{zo}} \right] \left[\frac{1}{W_a^2} \frac{1}{r} \frac{\partial}{\partial r} \left(r \frac{\partial W_a}{\partial r} \right) \right] = 1$$

or

$$\frac{\partial^2 \bar{W}_a}{\partial r^2} + \frac{1}{r} \frac{\partial \bar{W}_a}{\partial r} = (\lambda_a J_{zo}) \bar{W}_a^2 \quad (4.31)$$

in which \bar{W}_a is the average value of W_a in the z -direction, and

$$\left. \begin{aligned} A &= \frac{v_{ap}/v_{an}}{(1 + v_{ap}/v_{an})^2} \cdot \frac{2 K_{ap} K_{an} \mu_{Ra}}{\mu_p \mu_n \epsilon} \cdot \frac{\mu_p D_n + \mu_n D_p}{D_p D_n} \\ \lambda_a &= \frac{A}{\frac{1}{d} \int_0^d F_z dz} = \frac{A}{\langle F_z \rangle} \end{aligned} \right\} \quad (4.32)$$

An examination of equation (4.31) shows that the solution for \bar{W}_a would approach infinity as r approaches to zero. Physical reality requires a finite solution for all values of r , and this demands that $\partial \bar{W}_a / \partial r$ must approach to zero when r approaches to zero. Thus the term $1/r \partial \bar{W}_a / \partial r$ can be neglected, and equation (4.31) reduces to

$$\frac{d^2 \bar{W}_a}{dr^2} = \lambda_a J_{zo} \bar{W}_a^2 \quad (4.33)$$

Using the boundary conditions

$$\begin{aligned} r \rightarrow 0 & \quad \bar{W}_a \rightarrow 1 \\ r \rightarrow \infty & \quad \bar{W}_a \rightarrow 0 \quad \text{and} \quad \frac{d\bar{W}_a}{dr} \rightarrow 0 \end{aligned}$$

the solution of equation (4.33) gives

$$\bar{W}_a = \left[1 + \left(\frac{\lambda_a J_{zo}}{6} \right)^{1/2} r \right]^{-2} \quad (4.34)$$

From equations (4.24) and (4.34) the average current density over the specimen thickness d is given by

$$\bar{J}_z(r) = J_{zo} \left[1 + \left(\frac{\lambda_a J_{zo}}{6} \right)^{1/2} r \right]^{-2} \quad (4.35)$$

and the total current

$$\begin{aligned}
 I &= \int_0^{2\pi} \int_0^{r_d} \bar{J}_z(r) r dr d\theta \\
 &= \frac{12\pi}{\lambda_a} \left\{ \ln \left[1 + \left(\frac{\lambda_a J_{zo}}{6} \right)^{1/2} r_d \right] + \left[1 + \left(\frac{\lambda_a J_{zo}}{6} \right)^{1/2} r_d \right]^{-1} - 1 \right\}
 \end{aligned} \quad (4.36)$$

where J_{zo} is the filamentary current density at the centre. It is likely that the carriers are mainly injected from some asperities on the electrode surfaces and that each of such asperities has a very small injection area. One asperity on the cathode and the other on the anode will form a double-injection current filament. It is therefore reasonable to assume that J_{zo} follows the normal expression for space charge limited currents because the density of carriers diffusing away from $r = 0$ would be very small as compared with that at $r = 0$. In equation (4.35) $\bar{J}_z(r)$ decreases abruptly with increasing r indicating that $\bar{J}_z(r)$ becomes less space-charge-limited as r is increased. On the basis of this argument, J_{zo} for this case is the same as J given by equations (3.73) and (3.74), and for convenience, they are rewritten as follows:

$$J_{zo} = \frac{9}{8} \epsilon \mu_{\text{eff}} \frac{V^2}{d^3} \quad (4.37)$$

in which

$$\mu_{\text{eff}} = \frac{8}{9} \frac{q \mu_n \mu_p}{\mathcal{R}_0} \frac{\left[\int_0^1 s_a^{v_{\text{an}}-1} (1-s_a)^{v_{\text{ap}}-1} ds_a \right]^3}{\left[\int_0^1 s_a^{\frac{3v_{\text{an}}}{2}-1} (1-s_a)^{\frac{3v_{\text{ap}}}{2}-1} ds_a \right]^2} \quad (4.38)$$

and V is the applied voltage across the electrodes.

4.1.2 The traps distributed exponentially within the forbidden energy gap.

For this case the trap density distribution functions for electrons and holes are, respectively,

$$h_n(E) = \frac{H_{bn}}{kT_c} \exp\left(-\frac{E - E_c}{kT_c}\right) \quad (4.39)$$

$$h_p(E) = \frac{H_{bp}}{kT_c} \exp\left(-\frac{E_v - E}{kT_c}\right) \quad (4.40)$$

where T_c is the characteristic constant of the trap distribution, and H_{bn} and H_{bp} are, respectively, the trap densities per unit energy interval for electrons and holes. If $T_c > 1$ we can assume that the electron distribution function $f_n(E) = 1$ for $-\infty < E < E_{Fn}$ and $f_n(E) = 0$ for $E > E_{Fn}$; and the hole distribution function $f_p(E) = 1$ for $E_{Fp} < E < \infty$ and $f_p(E) = 0$ for $E < E_{Fp}$ as if we take $T = 0$. This is a good approximation [77] particularly when T_c is much larger than T . With this assumption we obtain

$$\begin{aligned} n_t &= \int_{E_v}^{E_{Fn}} \frac{H_{bn}}{kT_c} \exp\left(-\frac{E - E_c}{kT_c}\right) dE \\ &\approx H_{bn} (n_f/N_c)^{1/\ell} \end{aligned} \quad (4.41)$$

and

$$\begin{aligned} p_t &= \int_{E_{Fp}}^{E_c} \frac{H_{bp}}{kT_c} \exp\left(-\frac{E_v - E}{kT_c}\right) dE \\ &\approx H_{bp} (p_f/N_v)^{1/\ell} \end{aligned} \quad (4.42)$$

where $\ell = T_c/T$.

Following the same procedure as above we introduce the following parameters.

$$K_{bn} = (n_f + n_t)/n_f^{1/\ell} \quad (4.43)$$

$$K_{bp} = (p_f + p_t)/p_f^{1/\ell} \quad (4.44)$$

$$\mu_{Rb} = \frac{\varepsilon \omega_b^2}{[(\ell + 1)/\ell] q} \frac{1}{(\mu_n n_f + \mu_p p_f)^{1 - 1/\ell}} \quad (4.45)$$

$$v_{bn} = (\mu_n^{1/\ell} / K_{bn}) / \mu_{Rb} \quad (4.46)$$

$$v_{bp} = (\mu_p^{1/\ell} / K_{bp}) / \mu_{Rb} \quad (4.47)$$

$$\alpha_b = \frac{(\mu_p^{1/\ell} / K_{bp}) (\mu_n^{1/\ell} / K_{bn}) \varepsilon}{[(\ell + 1)/\ell] \mu_{Rb} J_{zo}^{1/\ell}} \quad (4.48)$$

$$\beta_b = q \mu_n / K_{bn}^\ell J_{zo} \quad (4.49)$$

$$\gamma_b = q \mu_p / K_{bp}^\ell J_{zo} \quad (4.50)$$

$$u_b = \alpha_b F_z^{(\ell + 1)/\ell} = c_b / J_{zo}^{1/\ell} \quad (4.51)$$

$$s_b = \beta_b K_{bn}^\ell n_f F_z \quad (4.52)$$

$$t_b = \gamma_b K_{bp}^\ell p_f F_z \quad (4.53)$$

$$w_b = \frac{J_z(r)}{J_{zo}} = \frac{J_{nz}(r) + J_{pz}(r)}{J_{nzo} + J_{pzo}} \quad (4.54)$$

Where R_b is electron-hole recombination coefficient for the traps distributed exponentially within the forbidden energy gap. Using these parameters, the current density in z-direction can be written as

$$W_b = S_b + T_b \quad (4.55)$$

Again, by assuming the radial variation of F_z to be negligible, we have

$$\frac{dW_b}{dr} = v_{bn} T_b^{1/\ell} - v_{bp} S_b^{1/\ell} = 0 \quad (4.56)$$

Thus

$$T_b = \left(\frac{v_{bp}}{v_{bn}} \right)^\ell S_b \quad (4.57)$$

Substitution of equation (4.57) into equation (4.55) gives

$$S_b = \frac{W_b}{1 + (v_{bp}/v_{bn})^\ell} \quad (4.58)$$

$$T_b = \frac{(v_{bp}/v_{bn})^\ell W_b}{1 + (v_{bp}/v_{bn})^\ell} \quad (4.59)$$

Equation (4.5) can be written as

$$\frac{1}{r} \frac{\partial}{\partial r} \left(r \frac{\partial W_b}{\partial r} \right) = (B F_z^{-1/\ell} J_{zo}^{1/\ell}) W_b^{2/\ell} \quad (4.60)$$

Following the same argument for obtaining equation (4.31), we can write the differential equation for the average value of W_b in the z-direction as

as

$$\left[\frac{1}{d} \int_0^d \frac{F_z^{1/\ell} dz}{B J_{zo}^{1/\ell}} \right] \left[\frac{1}{W_b^{2/\ell}} \frac{1}{r} \frac{\partial}{\partial r} \left(r \frac{\partial W_b}{\partial r} \right) \right] = 1$$

or

$$\frac{\partial^2 \bar{W}_b}{\partial r^2} + \frac{1}{r} \frac{\partial \bar{W}_b}{\partial r} = (\lambda_b J_{zo}^{1/\ell}) \bar{W}_b^{2/\ell} \quad (4.61)$$

in which

$$B = \frac{v_{bp}/v_{bn}}{[1 + (v_{bp}/v_{bn})^\ell]^{2/\ell}} \cdot \frac{(\frac{\ell+1}{\ell}) K_{bp} K_{bn} \mu_{Rb}}{\mu_p^{1/\ell} \mu_n^{1/\ell} \epsilon} \cdot \frac{\mu_p^{D_n} + \mu_n^{D_p}}{D_p D_n} \quad \left. \vphantom{\frac{v_{bp}/v_{bn}}{[1 + (v_{bp}/v_{bn})^\ell]^{2/\ell}}} \right\} \quad (4.62)$$

$$\lambda_b = \frac{B}{\frac{1}{d} \int_0^d F_z^{1/\ell} dz} = \frac{B}{\langle F_z^{1/\ell} \rangle}$$

Using the same boundary conditions for solving equation (4.33), the solution of equation (4.61) gives

$$\begin{aligned} \bar{W}_b &= \exp[-(\lambda_b J_{zo}^{1/2})^{1/2} r] \quad \text{for} \quad \ell = 2 \\ &= \left[1 + \left(\frac{2-\ell}{2\ell} \right) \left(\frac{2\ell \lambda_b J_{zo}^{1/\ell}}{2+\ell} \right)^{1/2} r \right]^{\frac{-2\ell}{(2-\ell)}} \quad \begin{array}{l} \text{for } 1 < \ell < 2 \\ \text{and } \ell > 2 \end{array} \end{aligned} \quad (4.63)$$

From equation (4.54) we have

$$\bar{J}_z(r) = J_{zo} \bar{W}_b \quad (4.64)$$

and the total current

$$I = 2\pi J_{zo} \int_0^{r_d} \exp[-(\lambda_b J_{zo}^{1/2})^{1/2} r] r dr$$

for $\ell = 2$

$$= 2 J_{zo} \int_0^{r_d} \frac{r dr}{[1 + (\frac{2-\ell}{2\ell}) (\frac{2\ell\lambda_b}{2+\ell}) J_{zo}^{\frac{1}{2}\ell} r]^{2\ell/(2-\ell)}}$$

for $1 < \ell < 2$
and $\ell > 2$ (4.65)

where J_{zo} for this case is same as J given by equations (3.102) and (3.103) and for convenience, they are rewritten as follows:

$$J_{zo} = q^{\ell-1} \mu'_{eff} \left(\frac{2\ell+1}{\ell+1}\right)^{\ell+1} \left(\frac{\ell\epsilon}{\ell+1}\right)^{\ell} \frac{V^{\ell+1}}{d^{2\ell+1}} \quad (4.66)$$

and

$$\mu'_{eff} = [(\ell+1)/(2\ell+1)]^{\ell+1} \mu_{Rb}^{\ell} v_{bp}^{\ell} v_{bn}^{\ell}$$

$$\times \frac{\left\{ \int_0^1 \exp\left\{ \left(\frac{\ell}{\ell-1}\right) [v_{bn} s_b^{(\ell-1)/\ell} + v_{bp} (1-s_b)^{(\ell-1)/\ell}] \right\} [s_b^{1/\ell} (1-s_b)^{1/\ell}]^{-1} ds_b \right\}^{\ell+1}}{\left\{ \int_0^1 \exp\left\{ \frac{2\ell^2+1}{\ell^2-1} [v_{bn} s_b^{(\ell-1)/\ell} + v_{bp} (1-s_b)^{(\ell-1)/\ell}] \right\} [s_b^{1/\ell} (1-s_b)^{1/\ell}]^{-1} ds_b \right\}^{\ell+1}}$$

(4.67)

As the uniform distribution of traps is unlikely to occur in a crystal, we shall not analyze this case. The above theory of filamentary double injection will be used as the basis for the development of the theory of electroluminescence.

4.2 ELECTROLUMINESCENCE IN MOLECULAR CRYSTALS DUE TO DOUBLE INJECTION

It is likely that multiple current filaments may simultaneously exist between two paralleled plane electrodes. For such a case we can always consider that within a domain of radius r_d is enclosed only one current filament and that the total current between the plane electrodes may be expressed as

$$I_T = I_{\text{domain 1}} + I_{\text{domain 2}} + \dots$$

$$= \sum_n I_n \approx HI$$

This means that the total current can be represented by the current in one domain I multiplied by a constant H .

It should be noted that when $\left(\frac{\lambda_a J_{zo}}{6}\right)^{\frac{1}{2}} r_d \ll 1$ for the traps confined in a single discrete energy level or when $(\lambda_b J_{zo})^{\frac{1}{2}} r_d \ll 1$ for the traps distributed exponentially within the forbidden energy gap,

$I \approx (\pi r_d^2) J_{zo}$. This implies that the current is uniformly distributed within the area πr_d^2 provided that r_d is chosen small enough to satisfy this condition.

In molecular crystals, for example, in undoped and doped anthracene, both the electron and hole mobilities are generally small [69,80,100], and the recombination rate constant is large [54,94,138], resulting in a small space charge overlap. Thus, the simultaneous injection of electrons and holes from the contacting electrodes will produce two-carrier space charge limited currents within the filament, and lead to electroluminescence when two types of carriers meet and recombine radiatively. Using undoped anthracene crystals (supplied by Harshaw Chemical Company) cleaved along a-b plane with a pair of double-injection electrodes (Ag as anode and Na and anthracene in tetrahydrofuran as cathode) of 3 mm in diameter, we have measured the electroluminescent brightness as a function of current, applied electric voltage and temperature; and the results will be presented in Sections 4.2.1 to 4.2.3. We have also found that electroluminescence occurs first within a single filament and the brightness decreases with increasing distance from the centre of the

of the filament in a manner similar to the variation of $J_z(r)$ with r in equations (4.35) or (4.36) and that as the voltage is increased, multiple-filaments are observed, and the electroluminescent brightness increases. Since the normal parallel plane electrodes have sharp edges, the filaments are generally formed near the edges because the field is higher there. Some investigators [170] have used carbon fibres of $0.01 - 0.1 \mu$ in diameter as injecting electrodes possibly because the local field at the tips of such fibres is very high so as to enable carrier injection there.

After the onset of electroluminescence in a molecular crystal with a fixed emission spectrum, the electroluminescent brightness is governed by the external quantum efficiency [15], η_q given by

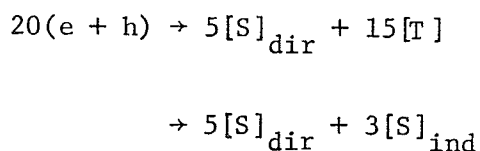
$$\eta_q = \eta_i \eta_g \eta_e = \eta_{int} \eta_e \quad (4.68)$$

where η_i is the carrier injection efficiency which is the ratio of the current due to minority carriers to the total current; and if we assume J_n is the current due to minority carriers, then

$$\eta_i = \frac{J_n}{J_n + J_p} ; \quad (4.69)$$

η_g is the light generation efficiency; $\eta_{int} = \eta_i \eta_g$ is the internal quantum efficiency which is a function of the total current density and temperature of the electroluminescence specimen; and η_e is the light extraction efficiency which is defined as the ratio of power loss due to the light transmission within the electroluminescence specimen to the total power losses which consist of both the losses in the bulk and on the surface, and can be considered to be fixed for a given specimen.

For double injection the recombination of the injected electrons with the injected holes at the recombination centers [94,127] will yield singlet and triplet excitons. It is generally accepted that the singlet excitons producing fluorescence are partly generated directly by electron-hole recombination and partly generated indirectly by triplet-triplet recombination in pairs according to the following relation [51,54].



where e and h represent, respectively, the electron and hole; $[S]_{\text{dir}}$ and $[S]_{\text{ind}}$ represent, respectively, the singlet excitons produced by the direct and the indirect processes; and $[T]$ represents the triplet excitons. It is the efficiency of generating $[S]_{\text{dir}}$ and $[S]_{\text{ind}}$ and their subsequent population in the crystal, which govern the electroluminescent intensity; but the threshold voltage is mainly governed by local field effects on the electrode surfaces. Since there is a great difference in lifetime between the singlet and the triplet excitons in molecular crystals (for example, they are 10^{-8} sec and 10^{-2} sec, respectively, in anthracene); the total electroluminescence consists of prompt electroluminescence due to $[S]_{\text{dir}}$ and delayed electroluminescence due to $[S]_{\text{ind}}$, and exhibits time constants corresponding to both of these decays. But in the steady state of electroluminescence is the combination of these two.

To develop a time dependent equation for excitons and hence for electroluminescence, we make the following assumptions.

(1) Singlet and triplet excitons generated due to the recombination of injected electrons and holes have the generation rates G_S and G_T , respectively.

(ii) Singlet and triplet excitons have, respectively, the rate constants α_1 and β_1 for the radiative transition with the emission of photons; and α_2 and β_2 for the non-radiative transition with the emission of phonons.

(iii) Singlet and triplet excitons may relax into traps at the levels ΔE_t lower in energy with the rate constants α_{HG} and β_{HG} , respectively.

(iv) Trapped excitons may be thermally detrapped, and then decay radiatively with the rate constants α_{G1} and β_{G1} , and non-radiatively with the rate constant α_{G2} and β_{G2} for singlet and triplet excitons, respectively.

(v) The effective rate constant for triplet-triplet annihilation is γ , and that for triplet-trapped annihilation is γ_G .

(vi) Excitons may be depopulated by the interactions between excitons and charge carriers or between excitons and surface states. But in the following analysis we assumed that the effect of these interactions is small [110] and can be neglected.

4.2.1 Current dependence of electroluminescent intensity.

(i) Prompt electroluminescence:

(a) Undoped crystals

On the assumption that in the deep traps $\Delta E_t \gg kT$ and that the intersystem crossing into the triplet states can be ignored, the rate equations for singlet-excitons generated directly by the electron-hole recombination may be written [5,173] as

$$\frac{d[S]_{dir}}{dt} = G_s - (\alpha_1 + \alpha_2) [S]_{dir} - \alpha_{HG} [S_G]_{dir} - K_s [S]_{dir} \quad (4.70)$$

$$\frac{d[S_G]_{\text{dir}}}{dt} = \alpha_{\text{HG}} [S]_{\text{dir}} - (\alpha_{\text{G1}} - \alpha_{\text{G2}}) [S_G]_{\text{dir}} \quad (4.71)$$

where $[S]$ and $[S_G]$ represent, respectively, the free and trapped singlet exciton; and K_s is the carrier-singlet exciton reaction rate. In the deep trap case α_{HG} is larger than K_s so that the last term in equation (4.70) may be neglected. In the steady state $d[S_G]_{\text{dir}}/dt = d[S]_{\text{dir}}/dt = 0$, and thus from equations (4.70) and (4.71) we obtain

$$[S]_{\text{dir}} = \frac{G_s}{\alpha_1 + \alpha_2 + \alpha_{\text{HG}}^2/\alpha_G} \quad (4.72)$$

where G_s is the number of singlet excitons per unit volume generated per unit time, and can be written as [51,54]

$$G_s = \frac{g_s J_z(r)}{q \lambda_s} \quad (4.73)$$

in which λ_s is the diffusion length of the singlet exciton, and g_s is the fraction of electron-hole pairs that produces the singlet-excitons immediately after recombination, and it is approximately equal to 1/4 for anthracene [51,54]. Thus the internal-quantum efficiency can be written as

$$\begin{aligned} \eta_{\text{int}} &= \alpha_1 \int_0^{2\pi} \int_0^d \int_0^r [S]_{\text{dir}} r d\theta dz dr \\ &= \frac{\alpha_1}{\alpha_1 + \alpha_2 + K(N_s)} \left(\frac{2\pi g_s d}{q \lambda_s} \right) I \end{aligned} \quad (4.74)$$

where

$$K(N_s) = \alpha_{\text{HG}}^2/\alpha_G \quad (4.75)$$

The brightness of the prompt electroluminescence, B , is proportional to η_q . If we assume η_e is a constant, then B is linearly proportional to the total current I .

$$\begin{aligned} B &\propto \eta_{\text{int}} \eta_e \\ &= b_1 I \end{aligned} \quad (4.76)$$

where b_1 is a constant.

(b) Doped crystals

In general, the doped guest molecules tend to quench the host molecular fluorescence and to emit the guest molecular fluorescence. Of course, the quantum yield of guest molecular fluorescence depends on the dopant concentration. For example, an anthracene crystal doped with 1 ppm of tetracene will emit green light from tetracene instead of blue light from anthracene. The rate equations (4.70) and (4.71) can be used for doped crystals. Thus in the steady state we have

$$[S_G]_{\text{dir}} = \frac{\alpha_{\text{HG}}}{(\alpha_{G1} + \alpha_{G2})} \frac{G_s}{(\alpha_1 + \alpha_2 + \alpha_{\text{HG}}^2/\alpha_G)} \quad (4.77)$$

In this case α_{HG} based on the hopping model can be defined [142,173] as

$$\alpha_{\text{HG}} = \frac{C_G}{t_{\text{hs}}} \quad (4.78)$$

where C_G is the dopant (guest molecule) concentration, and t_{hs} is the singlet exciton hopping time. Following the same procedure, the internal quantum efficiency for doped crystal can be written as

$$\eta_{\text{int}}^d = (K_{\text{es}} C_G) \frac{\alpha_1}{\alpha_1 + \alpha_2 + K(N_s)} \left(\frac{2\pi g_s^d}{q\lambda_s} \right) I \quad (4.79)$$

where K_{es} is defined as the energy transfer constant for singlet excitons [173], and is given by

$$K_{es} = \frac{\alpha_{G1}}{\alpha_1(\alpha_{G1} + \alpha_{G2})t_{hs}} \quad (4.80)$$

Thus, the brightness of the prompt electroluminescence is also linearly proportional to I

$$\begin{aligned} B^d &\propto \eta_{int}^d \eta_e \\ &= b_2 I \end{aligned} \quad (4.81)$$

where b_2 is a constant.

(ii) Delayed electroluminescence:

The rate equations for the free triplet $[T]$ and trapped triplet $[T_G]$ excitons and those for free singlet $[S]_{ind}$ and trapped singlet $[S_G]_{ind}$ created indirectly by triplet-triplet annihilation are given by

$$\frac{d[T]}{dt} = G_T - (\beta_1 + \beta_2)[T] - \beta_{HG}[T] - \gamma_G[T][T_G] - \gamma[T]^2 - K_T[T] \quad (4.82)$$

$$\frac{d[T_G]}{dt} = \beta_{HG}[T] - (\beta_{G1} + \beta_{G2})[T_G] - \gamma_G[T][T_G] \quad (4.83)$$

$$\frac{d[S]_{ind}}{dt} = \frac{1}{2} f \gamma[T]^2 - (\alpha_1 + \alpha_2)[S]_{ind} - K_s[S]_{ind} \quad (4.84)$$

$$\frac{d[S_G]_{ind}}{dt} = \frac{1}{2} f' \gamma_G[T][T_G] - (\alpha_{G1} + \alpha_{G2})[S_G]_{ind} \quad (4.85)$$

where f and f' are, respectively, the fractions of triplet-triplet and triplet-trapped triplet annihilations which create singlet excitons, and the value of f and f' is approximately 0.4 for anthracene; K_T is the carrier-triplet exciton reaction rate; and G_T is the number of triplet

excitons per unit volume generated per unit time and it is given [54] by

$$G_T = \frac{g_T J_z(r)}{q \lambda_T} \quad (4.86)$$

in which λ_T is the diffusion length of the triplet exciton, and g_T is the fraction of electron-hole pairs that produces the triplet excitons after recombination, and it is approximately equal to 3/4 for anthracene. It should be noted that in equations (4.82) and (4.84) γ is the effective overall rate constant for bimolecular triplet-triplet annihilation which includes the probability of producing [T] from this process [161]. In the deep trap case the last terms of equations (4.82) and (4.84) are very small and can be neglected and in the steady state $\frac{d[T]}{dt} = \frac{d[T_G]}{dt} = \frac{d[S]_{ind}}{dt} = \frac{d[S_G]_{ind}}{dt} = 0$. However, to solve the coupled equations (4.82) - (4.85), we have to make some approximations. It is therefore convenient to treat this problem for two cases as follows:

(1) Low injection (or low current) case

In this case we can assume that the monomolecular decay is dominant and therefore $[\beta_1 + \beta_2][T] \gg \gamma[T]^2$ and $[\beta_{G1} + \beta_{G2}][T_G] \gg \gamma_G[T][T_G]$.

For undoped crystals:

From equations (4.82) and (4.84) we have

$$[S]_{ind} = \frac{f\gamma}{2} \left(\frac{1}{\alpha_1 + \alpha_2} \right) [T]^2 \quad (4.87)$$

and

$$[T] = \frac{g_T/q\lambda_T}{\beta_1 + \beta_2 + \beta_{HG}} \cdot J_z(r) \quad (4.88)$$

Thus, the internal quantum efficiency is

$$\begin{aligned}
 \eta_{\text{int}} &= \alpha_1 \int_0^{2\pi} \int_0^d \int_0^{r_d} [S]_{\text{ind}} r \, \theta dz \, dr \\
 &= \frac{f\gamma}{2} \left(\frac{\alpha_1}{\alpha_1 + \alpha_2} \right) \left(\frac{1}{\beta_1 + \beta_2 + \beta_{\text{HG}}} \right)^2 (g_T/q\lambda_T)^2 2\pi d \int_0^{r_d} J_z^2(r) \, dr
 \end{aligned} \tag{4.89}$$

If we assume η_e is a constant, then the brightness of the delayed electroluminescence can be written as

$$\begin{aligned}
 B &\propto \eta_{\text{int}} \eta_e \\
 &= b_3 \int_0^{r_d} J_z^2(r) \, dr
 \end{aligned} \tag{4.90}$$

where b_3 is a constant.

For doped crystals:

In this case the guest molecules tend to quench the host molecular fluorescence. From equations (4.83) and (4.85) we have

$$[S_G]_{\text{ind}} = \frac{f\gamma_G}{2} \frac{[T][T_G]}{(\alpha_{G1} + \alpha_{G2})} \tag{4.91}$$

and

$$[T_G] = \left(\frac{\beta_{\text{HG}}}{\beta_{G1} + \beta_{G2}} \right) [T] \tag{4.92}$$

Based on the hopping model β_{HG} is given by [142,173]

$$\beta_{\text{HG}} = C_G/t_{\text{hT}} \tag{4.93}$$

where t_{hT} is the triplet exciton hopping time. Thus, from equations

(4.88), (4.91) and (4.92) the internal quantum efficiency for the doped crystals can be written as

$$\eta_{int}^d = (K_{eT} C_G) \frac{f\gamma}{2} \left(\frac{\alpha_1}{\alpha_1 + \alpha_2} \right) \left(\frac{1}{\beta_T + \beta_{HG}} \right)^2 (g_T / q\lambda_T)^2 2\pi d \int_0^{r_d} J_z^2(r) dr \quad (4.94)$$

where K_{eT} is the energy transfer constant for triplet excitons [173] and is given by

$$K_{eT} = \left(\frac{f\gamma_G}{f\gamma} \right) \left[\frac{\alpha_{G1}(\alpha_1 + \alpha_2)}{\alpha_1(\alpha_{G1} + \alpha_{G2})} \right] \frac{1}{t_{hT}} \quad (4.95)$$

Therefore, the brightness of the delayed electroluminescence can be written as

$$\begin{aligned} B^d &\propto \eta_{int}^d \eta_e \\ &= b_4 \int_0^{r_d} J_z^2(r) dr \end{aligned} \quad (4.96)$$

where b_4 is a constant.

(2) High injection (or high current) case

In this case we can assume that the bimolecular decay is dominant and therefore $(\beta_1 + \beta_2)[T] \ll \gamma[T]^2$ and $(\beta_{G1} + \beta_{G2})[T_G] \ll \gamma_G[T][T_G]$.

For undoped crystals:

By assuming that $[S_G]_{ind}$ is negligibly small, then from equations (4.82) and (4.85) and in the steady state, we obtain

$$[S]_{ind} = \frac{f\gamma}{2} \left(\frac{1}{\alpha_1 + \alpha_2} \right) [T]^2 \quad (4.97)$$

and

$$[T]^2 = \frac{1}{2} \frac{g_T J_z(r)}{q \lambda_T} \left(\frac{1 + 2\theta + \sqrt{1 + 4\theta}}{2\theta} \right) \quad (4.98)$$

where

$$\theta = \frac{g_T J_z(r) \gamma}{q \lambda_T} \left(\frac{t_{hT}}{C_G} \right)^2 \quad (4.99)$$

Since $\theta \gg 1$ for undoped crystals, we have

$$[T]^2 = \frac{1}{2} \frac{g_T J_z(r)}{q \lambda_T} \quad (4.100)$$

From Eqs. (4.94) and (4.100) we obtain

$$\begin{aligned} \eta_{int} &= \alpha_1 \int_0^{2\pi} \int_0^d \int_0^{r_d} [S]_{ind} r d\theta dz dr \\ &= \frac{f\gamma}{2} \left(\frac{\alpha_1}{\alpha_1 + \alpha_2} \right) \left(\frac{1}{2} \frac{g_T}{q\lambda_T} \right) 2\pi d I \end{aligned} \quad (4.101)$$

and thus the brightness of the delayed electroluminescence becomes

$$\begin{aligned} B &\propto \eta_{int} \eta_e \\ &= b_5 I \end{aligned} \quad (4.102)$$

where b_5 is a constant.

For doped crystals:

From equations (4.82) - (4.85) and in the steady state we have

$$[S_G]_{ind} = \frac{f'}{2} \frac{\beta_{HG}}{(\alpha_{G1} + \alpha_{G2})} [T] \quad (4.103)$$

and

$$[T] = \frac{\beta_{HG}}{2} [1 + \sqrt{1 + 4\theta}] \quad (4.104)$$

Since $\theta \ll 1$ for doped crystals, we have

$$[T] = \frac{1}{\sqrt{2}} \left(\frac{\gamma}{\beta_{HG}^2} \right)^{\frac{1}{2}} \frac{g_T J_z(r)}{q \lambda_T} \quad (4.105)$$

From equations (4.103) and (4.105) we have

$$\eta_{int}^d = \frac{f \gamma}{2\sqrt{2}} \frac{\alpha_{G1}}{(\alpha_{G1} + \alpha_{G2})^2} \left(\frac{g_T}{q \lambda_T} \right) 2\pi d I \quad (4.106)$$

and thus the brightness of the delayed electroluminescence is

$$\begin{aligned} B^d &\propto \eta_{int}^d \eta_e \\ &= b_6 I \end{aligned} \quad (4.107)$$

where b_6 is a constant.

In the steady state the brightness of electroluminescence is the sum of the brightness of prompt and delayed electroluminescence. Thus the brightness as a function of current can be deduced as follows.

(1) Low injection case

For undoped crystals:

$$B_T = b_1 I + b_3 \int_0^r J_z^2(r) dr \quad (4.108)$$

For doped crystals:

$$B_T = b_2 I + b_4 \int_0^r J_z^2(r) dr \quad (4.109)$$

(2) High injection case

For undoped crystals:

$$B_T = b_1 I + b_5 I \quad (4.110)$$

For doped crystals:

$$B_T = b_2 I + b_6 I \quad (4.111)$$

In general, for the high injection case the electroluminescent brightness is directly proportional to current according to equations (4.110) and (4.111), and this theoretical prediction agrees well with all presently available experimental results as shown in Fig. 4.1. For the low injection case, the B_T vs I relationship becomes non-linear according to equations (4.108) and (4.109). If $b_3 > b_1$ or $b_4 > b_2$, B_T becomes proportional to I^2 . Some experimental results following this square law are also shown in Fig. 4.1. For doped crystals, the presence of guest molecules quenches the host molecular fluorescence and exhibits the guest molecular fluorescence. But it should be noted that the electroluminescence yield from host and guest molecules changes with current and that the relative transfer of excitation energy from host to guest molecules decreases with increasing current [175]. Schwob et al [124, 175] have reported that under the low injection condition the tetracene fluorescence in tetracene-doped anthracene is dominant and the electroluminescent brightness is a function of dopant concentration. This is expected on the basis of equations (4.79), (4.94) and (4.109). It is possible that the brightness increases with increasing dopant concentration because under such a condition most recombinations occur in traps. However, as the current increases, the ratio of carriers being trapped by the guest to free carriers decreases, and so does the relative yield of guest fluorescence. Therefore, for the high injection case the host fluorescence of the tetracene-doped anthracene becomes dominant and its brightness

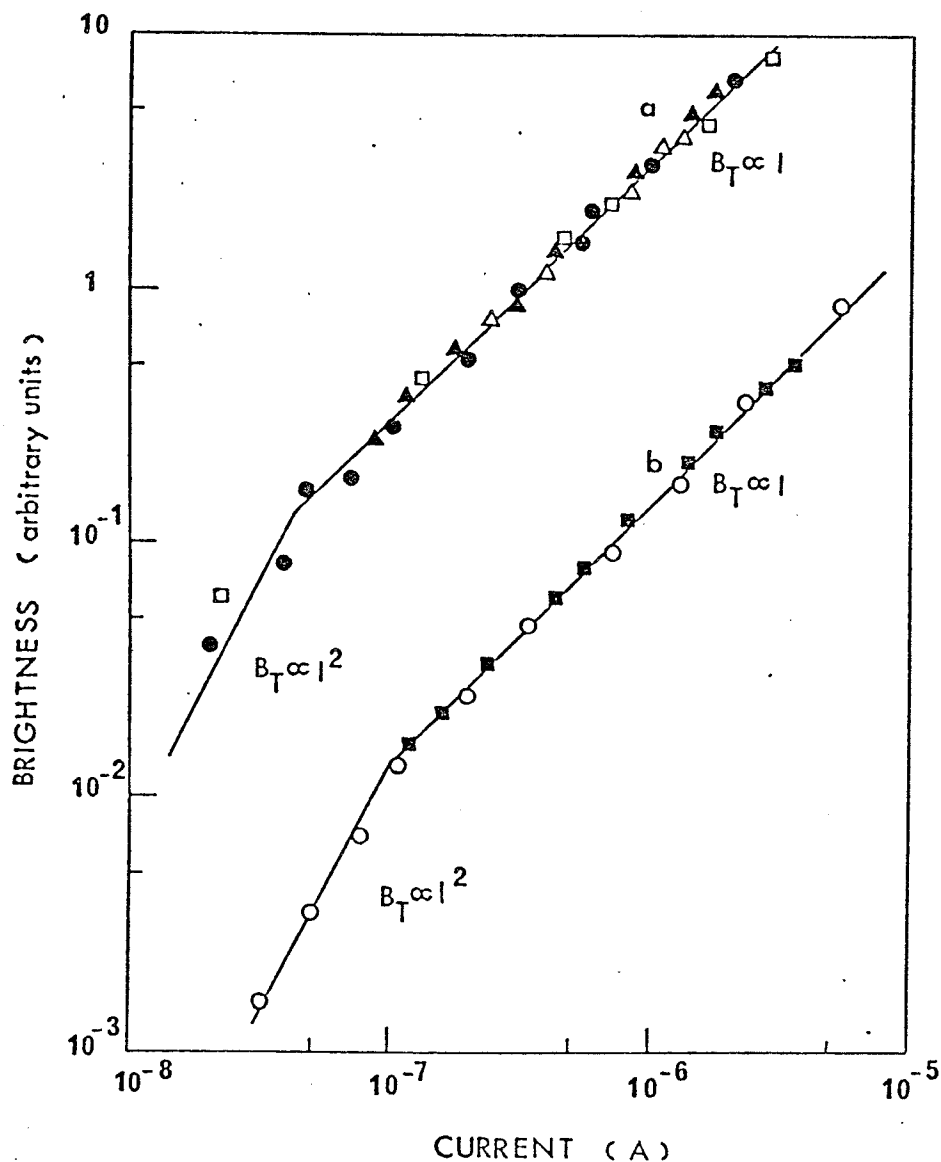


Fig. 4.1: Electroluminescent brightness as a function of current for (a) undoped anthracene crystals and (b) anthracene crystals doped with tetracene. Solid lines are based on the theory and experimental results are after William and Schadt Δ , Mehl and Funk \square , Hwang and Kao \bullet , Schwob and Zschokke-Granacher \circ , and Kawabe, Masuda and Namba Δ , \blacksquare .

increases to approximately linearly with current [124,175] as expected from equations (4.79), (4.106) and (4.111).

4.2.2 Voltage dependence of electroluminescent intensity.

From equations (4.36), (4.65) and (4.108) - (4.111), we can easily deduce the relationship of electroluminescent brightness with the applied voltage. In the following we consider two types of trap distribution under high injection condition.

(i) The traps confined in a single discrete energy level:

Substituting equation (4.37) into equation (4.36) and then into equation (4.111) and expanding it, we obtain

$$B_T \doteq A_a \frac{V^2}{d^3} \left(1 + a_1 \frac{V}{d^{3/2}} + a_2 \frac{V^2}{d^3} \right) \quad (4.112)$$

where

$$A_a = (b_2 + b_6) \left(\frac{9}{8} \varepsilon \mu_{\text{eff}} \right) \pi r_d^2$$

$$a_1 = - \frac{4}{3} \left(\frac{\lambda_a}{6} \right)^{1/2} \left(\frac{9}{8} \varepsilon \mu_{\text{eff}} \right)^{1/2} r_d$$

$$a_2 = \frac{3}{2} \left(\frac{\lambda_a}{6} \right) \left(\frac{9}{8} \varepsilon \mu_{\text{eff}} \right) r_d^2$$

Since r_d is small, $|a_2| < |a_1| < 1$.

(ii) The traps distributed exponentially within the forbidden energy gap:

Substituting equation (4.66) into equation (4.65) and then into equation (4.110), and expanding it, we obtain

$$\begin{aligned}
B_T &\doteq A_b \frac{V^{\ell+1}}{d^{2\ell+1}} \left[1 + b_{1\ell} \frac{V^{(\ell+1)/2\ell}}{d^{\frac{2\ell+1}{2\ell}}} + b_{2\ell} \frac{V^{(\ell+1)/\ell}}{d^{\frac{2\ell+1}{\ell}}} \right] \\
&\quad \text{for } \ell > 2, \text{ or } 1 < \ell < 2 \\
&\doteq A_b \frac{V^3}{d^5} \left(1 + b_{12} \frac{V^{3/4}}{d^{5/4}} + b_{22} \frac{V^{3/2}}{d^{5/2}} \right) \quad (4.113) \\
&\quad \text{for } \ell = 2
\end{aligned}$$

where

$$\begin{aligned}
A_b &= (b_1 + b_5) q^{\ell-1} \mu'_{\text{eff}} \left(\frac{2\ell+1}{\ell+1} \right)^{\ell+1} \left(\frac{\ell\epsilon}{\ell+1} \right)^\ell \pi r_d^2 \\
b_{1\ell} &= - \frac{2}{3} \left[q^{\ell-1} \mu'_{\text{eff}} \left(\frac{2\ell+1}{\ell+1} \right)^{\ell+1} \left(\frac{\ell\epsilon}{\ell+1} \right)^\ell \right]^{1/2\ell} \left(\frac{2\ell\lambda_b}{2+\ell} \right)^{1/2} r_d \\
b_{2\ell} &= \left[q^{\ell-1} \mu'_{\text{eff}} \left(\frac{2\ell+1}{\ell+1} \right) \left(\frac{\ell\epsilon}{\ell+1} \right)^\ell \right]^{1/\ell} \left(\frac{2\lambda_b}{2-\ell} \right) r_d^2 \\
b_{12} &= - \frac{1}{3} \left[q \mu'_{\text{eff}} \left(\frac{5}{3} \right)^3 \left(\frac{2\epsilon}{3} \right)^2 \right]^{1/4} \lambda_b^{1/2} r_d \\
b_{22} &= \frac{1}{6} \left[q \mu'_{\text{eff}} \left(\frac{5}{3} \right)^3 \left(\frac{2\epsilon}{3} \right)^2 \right]^{1/2} \lambda_b r_d^2
\end{aligned}$$

Since r_d is small, $|b_{2\ell}| < |b_{1\ell}| < 1$ and $|b_{22}| < |b_{12}| < 1$.

It is generally expected [57,114,120,151] that in doped crystals, such as tetracene doped in anthracene, the traps are created mainly by dopants, and are more likely to be confined in a single discrete energy level; and that in undoped crystals the traps may be the combination of the traps created by unavoidable impurities confined in single discrete energy levels, together with traps created by structural defects distributed exponentially in energy. Figure 4.2 shows the experimental results of the electroluminescent brightness as a function of applied voltage for undoped anthracene at room temperature. In this case it is

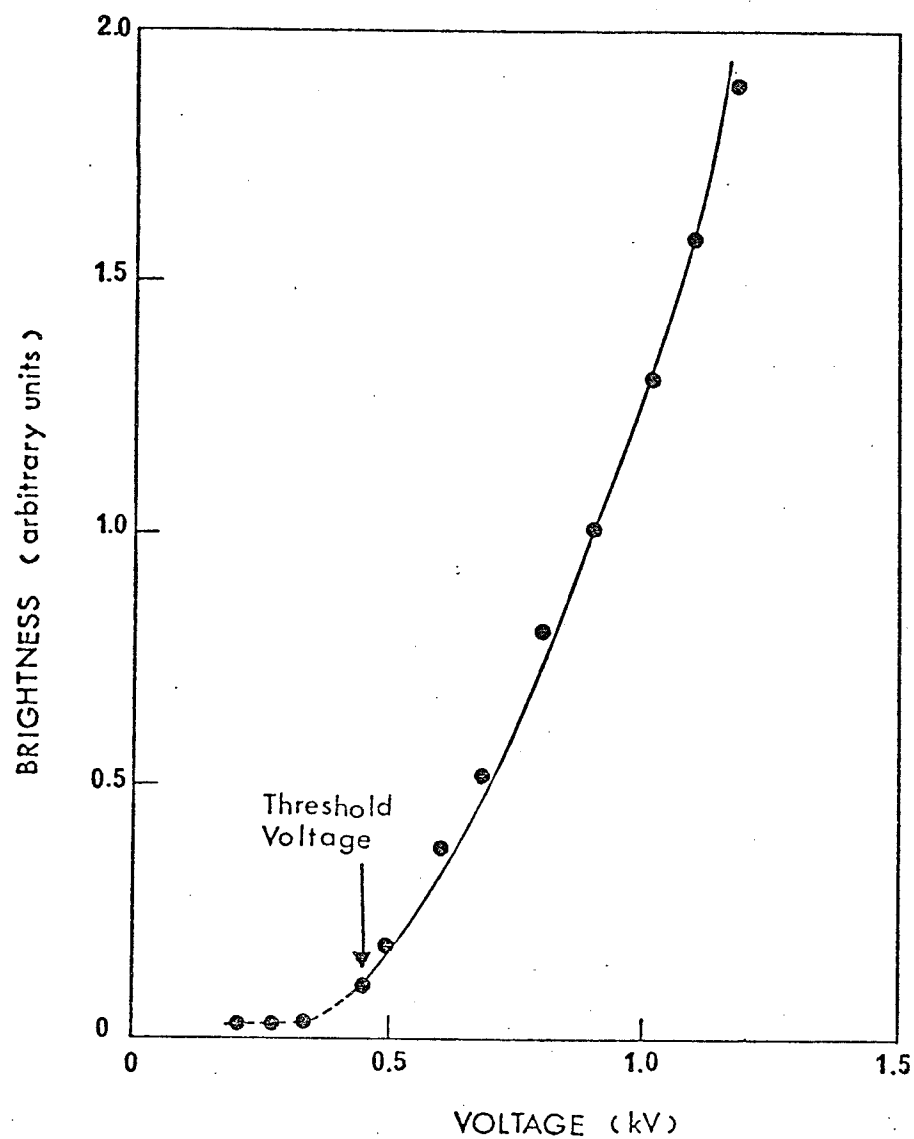


Fig. 4.2: Electroluminescent brightness as a function of applied voltage for undoped anthracene crystals at 20°C. Solid line is based on the theory and ● experimental results.

reasonable to assume that at voltages higher than the threshold voltage for the onset of electroluminescence most of exponentially distributed deep traps have been filled up and only shallow traps with single discrete energy levels left are dominant in the conduction process. Using the following parameters for our undoped anthracene sample: $\epsilon = 3.2 \times 10^{-11}$ F m⁻¹; $d = 1$ mm, $\mu_{\text{eff}} = 0.1 \text{ Cm}^2 \text{V}^{-1} \text{sec}^{-1}$, and $\lambda_a = 10^9 \text{ cm}^{-1}$; and assuming $r_d = 0.1$ mm, we have calculated the B_T vs V curve based on equation (4.113). It can be seen that the experimental results agree well with the theory. Since B_T is proportional to I , equation (4.112) and (4.113) explain also why current is not inversely proportional to $d^{2\ell+1}$ for crystals in which the exponential deep traps are dominant [170] and not inversely proportional to d^3 for crystals in which the discrete shallow traps are dominant [125]. We have mentioned in Section 4.1.1 that $\bar{J}_z(r)$ would be space-charge-limited only when r approaches to zero and become less space-charge-limited at larger r . If this is the case, the normally measured current density calculated by dividing the total measured current with the complete electrode area would not follow the normal expression for the space-charge limited currents, and this is the main reason why the measured current is not proportional to $d^{-(2\ell+1)}$ or to d^{-3} . Since the current density at $r = 0$ is much larger than the normally measured average current density, any calculations involving carrier densities, for example, the magnitude of the carrier-exciton interaction terms in equations (4.82) - (4.85), should take into account the effect of the non-uniformity of the current density distribution over the electrode area.

4.2.3 Temperature dependence of electroluminescent intensity.

Fig. 4.3 shows that the electroluminescent brightness of undoped anthracene increases with increasing temperature, reaches a certain peak value and then decreases with increasing temperature. This phenomenon has also been observed using a pair of single injection silver electrodes. This phenomenon may be explained in terms of three processes: (a) exciton-trapped exciton interactions [52,90,130,133,134,140], (b) exciton-carrier interactions [38,39,41,53,123,160-162], and (c) exciton-surface state interactions [65,72,95,110,115], which control the electroluminescent intensity and are temperature-dependent. It has been reported [65,97,155] that the surface states at the interface between the contacting electrode and the anthracene crystal quenches singlet excitons and that the quenching rate decreases with increasing temperature. However, the effect of surface states may be very small [111] as compared with those of processes (a) and (b), and therefore we ignore the process (c) for the present discussions.

If we define the temperature for the peak electroluminescent brightness as the brightness characteristic temperature T_b , then it is possible that for temperatures lower than T_b the process (a) is dominant, and for temperature higher than T_b the process (b) becomes important. The physical meaning of T_b can be thought of as the characteristic temperature of these processes, at which the singlet exciton-attempt-escape frequency is equal to the carrier-singlet exciton reaction rate,

$$\text{or} \quad \nu \exp \left(- \frac{E_{ti}}{kT_b} \right) = K_s = Z N_T$$

$$T_b = \frac{E_{ti}/k}{\ln [\nu/ZN_T]} \quad (4.114)$$

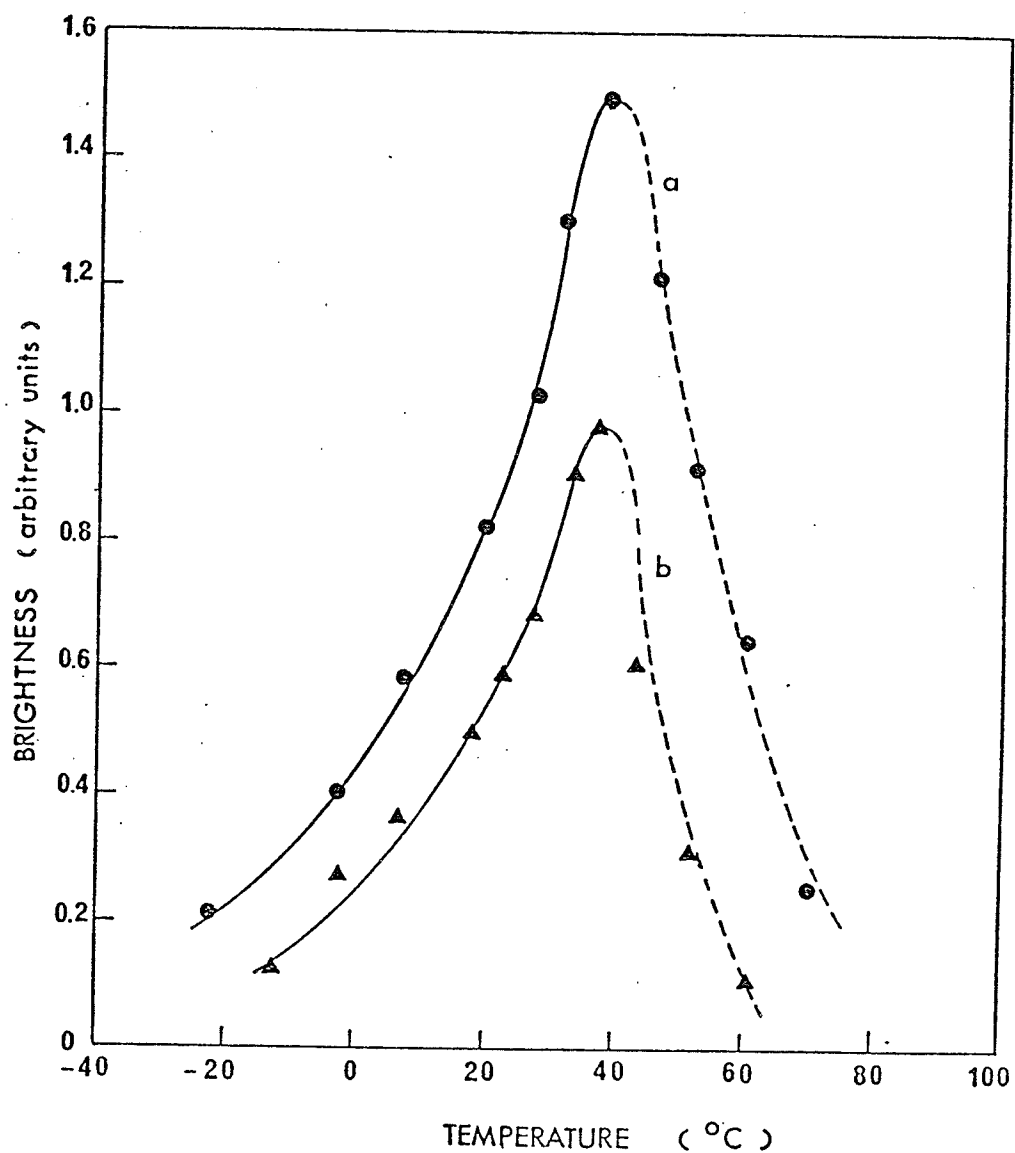


Fig. 4.3: Electroluminescent brightness as a function of temperature for undoped anthracene crystals for (a) applied voltage: 1.2 kV and (b) applied voltage: 1.0 kV. Solid lines are based on the theory and \bullet \blacktriangle and dash lines are experimental results.

where E_{ti} is the trapped singlet exciton energy measured from the singlet-exciton energy level, ν is the singlet-exciton-escape frequency factor, K_s and Z are, respectively, the rate and the rate constant of carrier-singlet exciton reactions. In anthracene it is generally accepted that the thermal velocity of carriers u is larger than that of singlet excitons v . If this is the case, K_s may be written [160] as

$$\begin{aligned} K_s &= N_T (1-\theta_t) \sigma \nu + N_T \theta_t \sigma (u+\nu^2/3u) \\ &= ZN_T \end{aligned} \quad (4.115)$$

where N_T is the total carrier density (electrons and holes); θ_t is the ratio of free carrier density to the total carrier density which includes both free and trapped carriers, and σ is the reaction cross section between a carrier and an exciton. The semi-logarithmic plot of B_T vs $1/T$ from the data given in Fig. 4.3 for the temperature range from -20°C to 40°C gives an activation energy E_{ti} of 0.21 eV. Using this value for E_{ti} , the value [97] of 10^7 sec^{-1} for ν and the value [123] of $10^{-8} \text{ cm}^3 \text{ sec}^{-1}$ for K_s and assuming N_T to be $3 \times 10^{11} \text{ cm}^{-3}$ (this value is of the same order of that used by other investigators [160,161]) T_b has been estimated to be about 313°K (or 40°C) which is in good agreement with experiment. It should be noted that the average value of 313°K for T_b was calculated using the average value of N_T which was determined and used by other investigators [160,161], assuming an average carrier distribution over the complete electrode area. This value of T_b should correspond to our measured peak value of B_T because we measured only the total electroluminescent brightness over the complete electrode area. Since J_{zo} in the filament is much larger than $\bar{J}_z(r)$ at $r > 0$, we can

expect that N_T inside the filament at $r = 0$ may be several orders of magnitude larger than the average value of N_T and also T_b at $r = 0$ would be much larger than the average value of T_b .

For temperatures lower than T_b and within the range from -20°C to 40°C , the brightness increases with increasing current and this has been discussed in Section 4.2.1. Since B_T is proportional to I for the high injection case, the temperature dependence of B_T can be explained in terms of the temperature dependence of I . By assuming $|H_{ap}| \gg |H_{an}|$ and $|E_c - E_{tn}| = |E_{tp} - E_v| = E_t$ for simplicity, μ_{eff} in equation (4.112) may be written as

$$\begin{aligned} \mu_{\text{eff}} &= \frac{\mu_n}{K_{an}} + \frac{\mu_p}{K_{ap}} \\ &\approx \frac{\mu_n N_c}{g_n H_{an}} \exp \left(- \frac{E_t}{K_T} \right) \\ &= \frac{\mu_n N_c}{g_n H_{an}} \exp \left[- \frac{E_c - E_s}{KT} \right] \exp \left[- \frac{E_{ti}}{KT} \right] \\ &= C \exp \left[- \frac{E_{ti}}{KT} \right] \end{aligned} \quad (4.116)$$

where E_s is the singlet exciton energy level measured from the conduction band edge. Substitution of equation (4.116) into (4.112) gives

$$\begin{aligned} B_T &= A_a \frac{V^2}{d^3} \left(1 + a_1 \frac{V}{d^{3/2}} + a_2 \frac{V^2}{d^3} \right) \\ &\approx (b_2 + b_6) \left(\frac{9}{8} \epsilon \mu_{\text{eff}} \right) \pi r_d^2 \frac{V^2}{d^3} \\ &= D \exp \left[- \frac{E_{ti}}{KT} \right] \end{aligned} \quad (4.117)$$

in which $|a_1|$ and $|a_2|$ are much less than 1. Equation (4.117) explains

the temperature dependence of B_T for temperatures below T_b .

For temperatures higher than T_b the brightness decreases though the current still increases with increasing temperature, and the electroluminescence disappears at a certain temperature depending on the applied voltage. It has been experimentally observed that the interaction of singlet excitons [160] or of triplet excitons [161] with charge carrier quenches the fluorescence. The change of temperature may not affect very much the carrier injection from the electrodes but it would affect the value of θ_t . For undoped anthracene crystals the brightness as a function of temperature for $T > T_b$ can be written as

$$B_T(T) = \frac{[b_1 I]_{T_b}}{1 + \frac{K_s}{\alpha_1 + \alpha_2 + K(N_s)}} + \frac{[b_3 \int_0^r dJ_z^2(r) dr]_{T_b}}{\left[1 + \frac{K_s}{\alpha_1 + \alpha_2}\right] \left[1 + \frac{K_T}{\beta_1 + \beta_2 + \beta_{HG}}\right]} \quad (4.118)$$

for low injection, and

$$B_T(T) = \frac{[b_1 I]_{T_b}}{\left[1 + \frac{K_s}{\alpha_1 + \alpha_2 + K(N_s)}\right]} + \frac{[b_5 I]_{T_b}}{\left[1 + \frac{K_s}{\alpha_1 + \alpha_2}\right]} \quad (4.119)$$

for high injection, where $[b_1 I]_{T_b}$, $[b_3 \int_0^r dJ_z^2(r) dr]_{T_b}$ and $[b_5 I]_{T_b}$ are defined in equations (4.76), (4.90) and (4.102) but at temperature T_b . The values of $K_s/[\alpha_1 + \alpha_2 + K(N_s)]$, $K_s/(\alpha_1 + \alpha_2)$ and $K_T/(\beta_1 + \beta_2 + \beta_{HG})$ generally increase with increasing temperature. Thus, equations (4.118) and (4.119) explains the phenomenon shown in Fig. 4.3 for $T > T_b$.

4.3 ELECTROLUMINESCENCE IN ANTHRACENE CRYSTALS DUE TO FIELD ENHANCED INJECTION

As has been mentioned in Section 4.2, electroluminescence has been observed in anthracene either with double-injection [32,33,51,167,168] or with field enhanced injection [17,109,168,176] electrodes. In this section we report some new phenomena in anthracene crystals cleaved along the a-b plane with vacuum-deposited silver [32,104] on both opposite surfaces as electrodes.

(1) Electroluminescence always appears first at the edges of both electrodes irrespective of electrode geometry and arrangement indicating that electroluminescence is associated with field-induced minority electrons in the high field regions since silver electrodes inject only holes at low fields.

(2) The voltage to maintain the self-sustaining electroluminescence after its onset is much smaller than the threshold voltage for its onset V_{th} . For example, V_{th} for a specimen of 0.5 mm in thickness at 20°C is 1.4 kV, while the minimum voltage required to maintain the electroluminescence is 0.6 kV, though the light brightness in this case is very small. The brightness increases with increasing applied voltage but it becomes practically independent of applied voltage for voltages between 0.6 and 0.9 kV.

(3) The spectrum of the electroluminescence ranges from 4,050 to 5,150 Å, which is close to that obtained with double-injection electrodes [33].

(4) The brightness increases with increasing current; and by adjusting the voltage to maintain a constant current, it is then independent of temperature for, at least, temperatures between -20°C and 20°C.

(5) The temperature dependence of V_{th} is shown in Fig. 4.4 and the current voltage (J-V) characteristics in Fig. 4.5, the dashed lines indicating the values of V_{th} .

(6) For voltages below V_{th} , J is proportional to V^2 following the relation for the single injection into a solid containing hole-traps in a discrete energy level [75]. The J - 1/T plot for V=2.0 kV gives an activation energy E_{act} of 0.56 eV which can be interpreted as this discrete energy level. For voltage above V_{th} , J is proportional to V^n with $n > 6$ implying that the large current may be associated with the field-induced electrons and the release of trapped carriers due to the re-absorption of electroluminescence. E_{act} for $V > V_{th}$ tends to decrease with increasing V, and such a change in E_{act} may be attributed to the effect of the re-absorption of electroluminescence.

(7) The brightness is temperature-dependent and the electroluminescence disappears at a certain temperature depending on the applied voltage as shown in Fig. 4.4.

(8) V_{th} is affected by the on-and-off time. For example, V_{th} for the first onset is 1.4 kV. If now the voltage source is switched off and then immediately switched on again, V_{th} is reduced to 1.0 kV. But if the switch-off time is longer than 30 minutes, V_{th} would go back to 1.4 kV.

We believe that the supply of minority electrons for the formation of singlet excitons is from the tunneling process through the so called "blocking contact" at high fields [74] rather than from the impact ionization avalanches [176] for two reasons. Firstly, we have found experimentally that V_{th} for samples with Ag electrodes is different from those

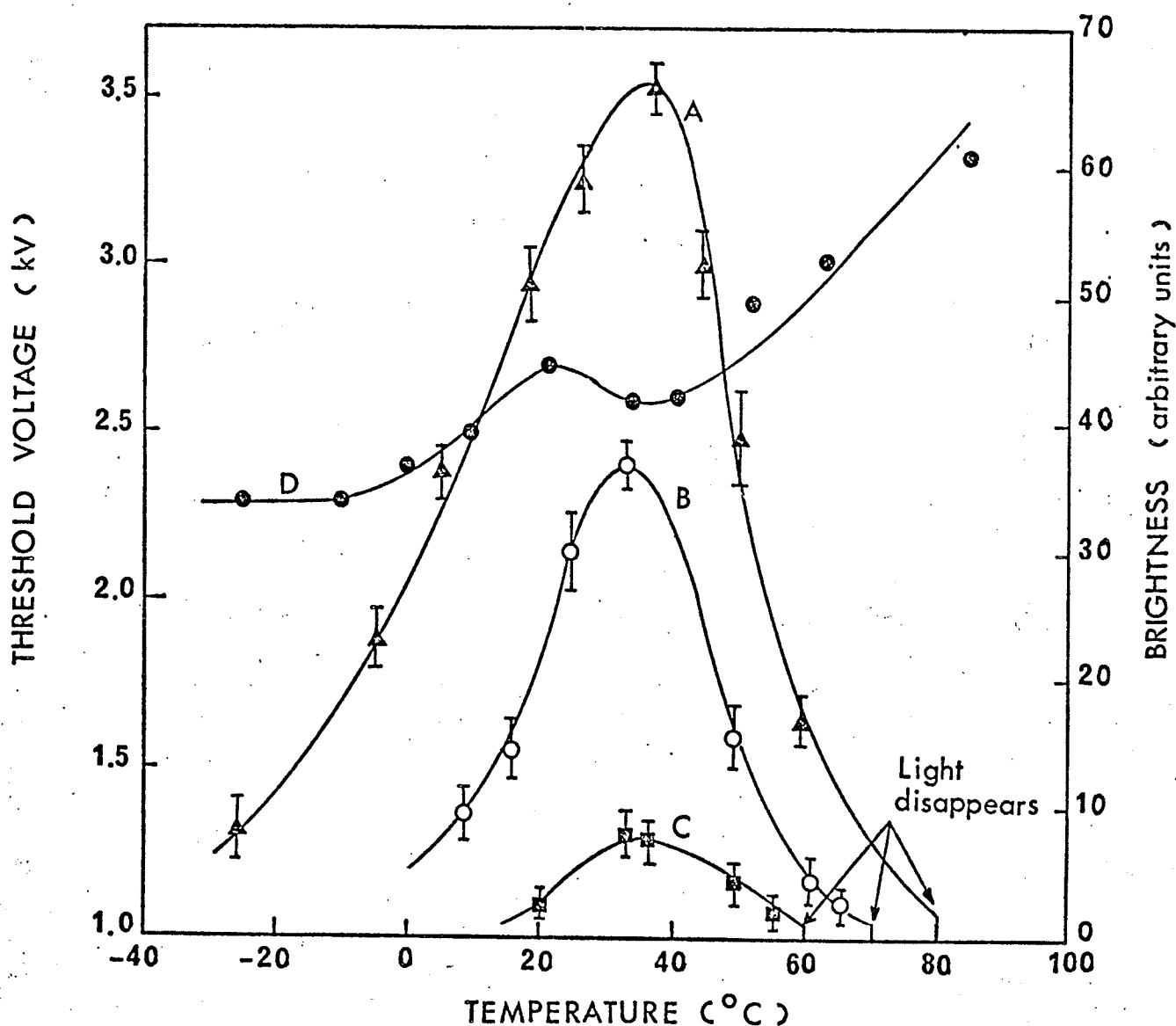


Fig. 4.4: Electroluminescent brightness (A, B and C curves) and d.c. threshold voltage for the onset of electroluminescence (D curve) as functions of temperature.

A---Sample No.: 9; Sample thickness: 0.81 mm; Electrode diameter: 1.6 mm; Applied d.c. voltage: 3.0 kV.

B---Sample No.: 4; Sample thickness: 0.6 mm; Electrode diameter: 1.4 mm; Applied d.c. voltage: 2.0 kV.

C---Same sample as B but with applied d.c. voltage of 1.6 kV.

D---Sample No.: 31; Sample thickness: 0.90 mm; Electrode diameter: 1.6 mm.

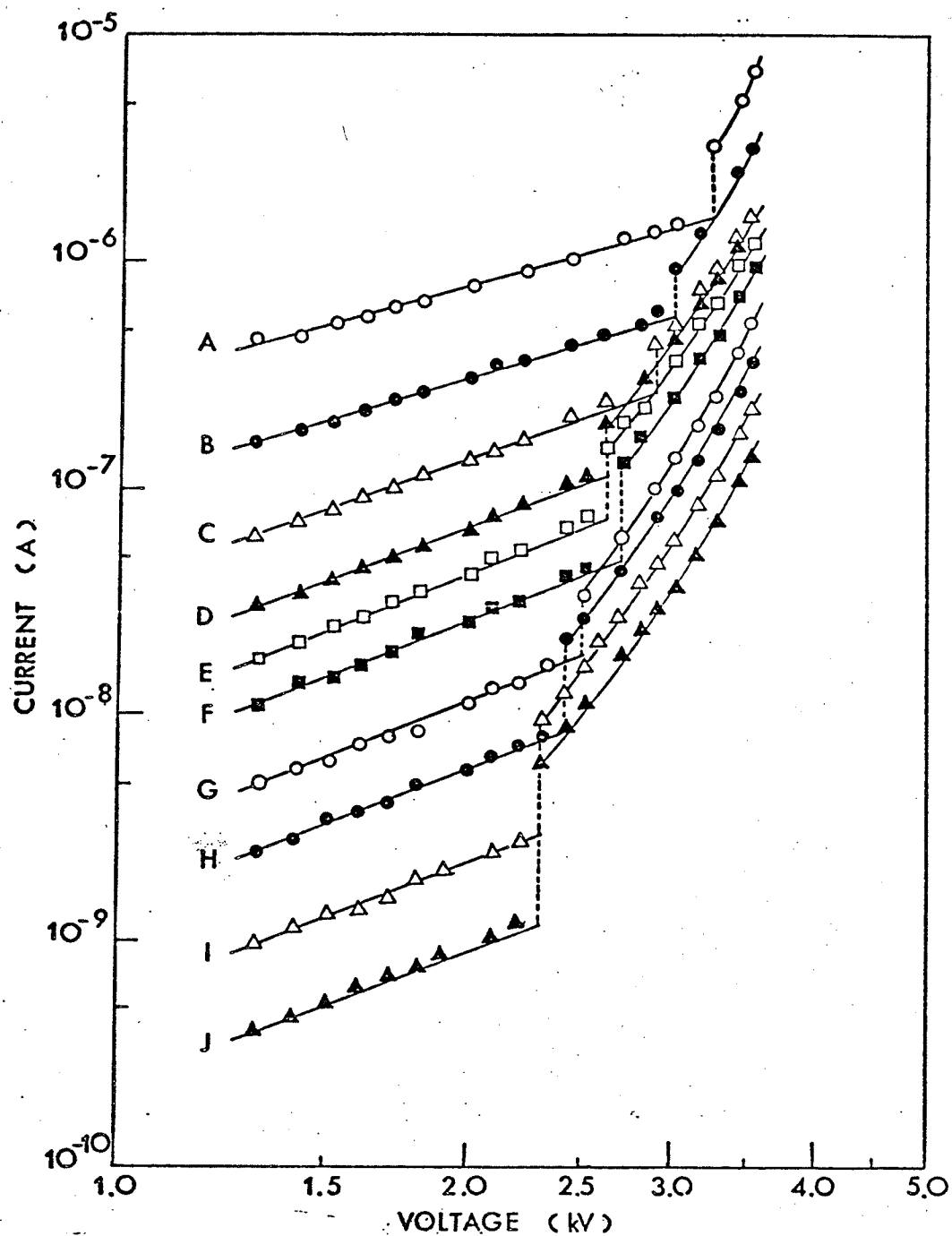


Fig. 4.5: The d.c. current-voltage characteristics.

Sample No.: 31; Sample thickness: 0.9 mm; Electrode diameter: 1.6 mm.

Temperature: A, 87°C; B, 63°C; C, 51°C; D, 41°C; E, 34.5°C; F, 20°C; G, 10°C; H, 0°C; I, -10°C; J, -20°C.

for the same specimen thickness with In or Al electrodes. Secondly, it is unlikely that electrons, even ^{if} available, can gain energy of the order of 4 eV from the field at V_{th} to ionize anthracene molecules. (Thus, the so-called single injection electrodes would become double injection electrodes near the threshold voltage for the onset of electroluminescence.) The temperature dependence results can be explained in terms of the following three processes: (a) exciton-trapped exciton interactions [52,133], (b) carrier-exciton interaction [39,53,160,161], and (c) exciton-surface state interactions [65,97,115]. In general, the effect of process (c) is very small [110]. The detailed discussion has been given in Section 4.2.

4.4 CONCLUDING REMARK

The general expressions for the filamentary double injection current-voltage characteristics in a molecular crystal with traps confined in a single discrete energy level and distributed exponentially within the forbidden energy gap have been derived using a unified mathematical approach. On the basis of this model the brightness of electroluminescence as a function of applied electric field, current density and temperature has also been derived, and the computed results are in good agreement with the experimental results for undoped anthracene and anthracene doped with tetracene. The current-voltage characteristics can be used as a tool to determine the trap distribution and hence the purity of a crystal, and the electroluminescent brightness distribution to study the current filaments.

CHAPTER V

PHOTOVOLTAIC EFFECT IN ORGANIC SEMICONDUCTORS

Since the photovoltaic effect has neither been systematically studied experimentally nor rigorously analyzed theoretically for organic semiconductors, we shall present a general theoretical formulation for the photovoltaic effect in organic semiconductors in this chapter, taking into account the effects of traps and local charge non-neutrality. Analytical expressions will be derived for the photovoltage for the following cases: (1) local charge neutrality with traps and (2) local charge non-neutrality without traps. These models will be used to explain quantitatively some presently available experimental results in organic semiconductors.

5.1 THEORY OF THE PHOTOVOLTAIC EFFECT

In the theoretical analysis we make the following assumptions:

- (1) The mobilities of photo-generated excess electrons and holes are not affected by the presence of traps nor are they affected by the light intensity or the concentration of excess electrons Δn and excess holes Δp .
- (2) The excess electrons and holes recombine in the bulk and at the surfaces of the crystal, and their lifetimes are constant.
- (3) The treatment is one-dimensional with the plane at $x = 0$ as the front surface electrode (or as the illuminated surface) and that at $x = d$ as the back surface electrode, the electrode area being one unit and the specimen thickness being d .

- (4) The photovoltage is produced under the open-circuit condition, and then under this condition the sum of the electron current flow J_n and the hole current flow J_p is zero.
- (5) The light intensity is small such that the excess carrier densities Δn (for electrons) and Δp (for holes) are much smaller than the equilibrium carrier density n_0 (for electrons before illumination) and p_0 (for holes before illumination), respectively. Thus, small signal theory can be applied.

We shall deal with the photovoltaic effect under steady state conditions. The behaviour of the excess electrons and holes generated by photons in a semiconductor is governed by the current flow equations

$$J_n = q\mu_n n_f F + q D_n \frac{d\Delta n_f}{dx} \quad (5.1)$$

$$J_p = q\mu_p p_f F - q D_p \frac{d\Delta p_f}{dx} \quad (5.2)$$

$$J = J_n + J_p = 0 \quad (5.3)$$

the continuity equations;

$$-(1/q)(dJ_n/dx) = g_b(x) - \Delta n/\tau_n \quad (5.4)$$

$$(1/q)(dJ_p/dx) = g_b(x) - \Delta p/\tau_p \quad (5.5)$$

and the Poisson's equation

$$dF/dx = (q/\epsilon) [\Delta p - \Delta n] \quad (5.6)$$

in which

$$\Delta n = n - n_0 = \Delta n_t + \Delta n_f \quad (5.7)$$

$$\Delta p = p - p_0 = \Delta p_t + \Delta p_f \quad (5.8)$$

$$\Delta n_t = n_t - n_{to} \quad (5.9)$$

$$\Delta p_t = p_t - p_{to} \quad (5.10)$$

$$\Delta n_f = n_f - n_{fo} \quad (5.11)$$

$$\Delta p_f = p_f - p_{fo} \quad (5.12)$$

where n and p are, respectively, the total electron and hole densities n_t and p_t are, respectively, the trapped electron and trapped hole densities; n_{to} and p_{to} are, respectively, the trapped electron and trapped hole densities in thermal equilibrium without light illumination; n_f and p_f are, respectively, the total free electron and hole densities; n_{fo} and p_{fo} are, respectively, the free electron and hole densities in thermal equilibrium without light illumination; μ_n and μ_p are, respectively, the electron and hole mobilities, D_n and D_p are, respectively, the electron and hole diffusion constants; τ_n and τ_p are, respectively, the lifetimes of excess electrons and holes inside the crystal; $g_b(x)$ is the electron-hole pair generation rate; ϵ is the dielectric constant of the semiconductor; q is the electronic charge; and F is the electric field (or potential gradient) produced by the carrier concentration gradients inside the crystal.

To study the photovoltaic effect, we shall consider first a general analysis by taking into account the effects of traps and non-neutrality of local charge. Considering the traps are confined in single discrete energy levels, the total trapped electron and trapped hole densities are given by equations (3.47) and (3.49). For convenience, we rewrite them in the following:

$$n_t = H_n g_n \exp [(E_{Fn} - E_{tn})/kT] \quad (5.13)$$

$$p_t = H_p g_p^{-1} \exp [(E_{tp} - E_{Fp})/kT] \quad (5.14)$$

where H_n and H_p are trap densities, g_n and g_p are degeneracy factors of trap states, E_{tn} and E_{tp} are trapping energy levels, and E_{Fn} and E_{Fp} are quasi-Fermi levels, for electrons and holes, respectively; k is the Boltzmann constant; and T is the absolute temperature. By writing

$$n = n_f + n_t = K_n n_f \quad (5.15)$$

$$p = p_f + p_t = K_p p_f \quad (5.16)$$

$$\Delta n = \Delta n_f + \Delta n_t = K_n \Delta n_f \quad (5.17)$$

$$\Delta p = \Delta p_f + \Delta p_t = K_p \Delta p_f \quad (5.18)$$

the lifetime of excess electrons and holes can be, respectively, defined as

$$\tau_n = K_n \tau_{nf} \quad (5.19)$$

$$\tau_p = K_p \tau_{pf} \quad (5.20)$$

where

$$K_n = 1 + \frac{g_n H_n}{N_c} \exp [(E_c - E_{tn})/kT] \quad (5.21)$$

$$K_p = 1 + \frac{H_p}{g_p N_v} \exp [(E_{tp} - E_v)/kT] \quad (5.22)$$

$$\tau_{nf} = \frac{\mu_p (n_{fo} + p_{fo})}{\mu_n n_{fo} + \mu_p p_{fo}} \tau_o \quad (5.23)$$

$$\tau_{pf} = \frac{\mu_n (n_{fo} + p_{fo})}{\mu_n n_{fo} + \mu_p p_{fo}} \tau_o \quad (5.24)$$

in which N_c and N_v are, respectively, the effective densities of states

in the conduction and the valence bands; E_c and E_v are, respectively, the energy levels at conduction band and valence band edges; and τ_o is the equilibrium electron-hole pair life time.

Using the relation $kT/q = D_n/\mu_n = D_p/\mu_p$ and assumption-(5), and from equations (5.1) - (5.3), we obtain

$$\begin{aligned} J_p &= - \left(\frac{q D_n \mu_p}{\mu_n n_{fo} + \mu_p p_{fo}} \right) \left(n_{fo} \frac{d\Delta n_f}{dx} + p_{fo} \frac{d\Delta p_f}{dx} \right) \\ &= - q \left(\frac{kT}{q} \right) \left(\frac{\mu_n \mu_p}{\mu_n n_{fo} + \mu_p p_{fo}} \right) (n_{fo} + p_{fo}) \left[\frac{d}{dx} \left(\frac{n_{fo} \Delta p_f + p_{fo} \Delta n_f}{n_{fo} + p_{fo}} \right) \right] \\ &= - q D \frac{d\xi}{dx} \end{aligned} \quad (5.25)$$

in which

$$D = \frac{kT}{q} \left(\frac{\mu_n \mu_p}{\mu_n n_{fo} + \mu_p p_{fo}} \right) (n_{fo} + p_{fo}) \quad (5.26)$$

$$\xi = \frac{n_{fo} \Delta p_f + p_{fo} \Delta n_f}{n_{fo} + p_{fo}} \quad (5.27)$$

Substituting equations (5.3) and (5.25) in equations (5.4) and (5.5), we obtain

$$D \frac{d^2 \xi}{dx^2} - \frac{\xi}{\tau_o} + g_b(x) = 0 \quad (5.28)$$

From equations (5.1) - (5.3) we have

$$\begin{aligned} F &= - \frac{kT}{q} \left(\frac{1}{\mu_n n_{fo} + \mu_p p_{fo}} \right) \left(\mu_n \frac{d\Delta n_f}{dx} - \mu_p \frac{d\Delta p_f}{dx} \right) \\ &= - \frac{kT}{q} \frac{d}{dx} \left[\frac{\mu_n \Delta n_f - \mu_p \Delta p_f}{\mu_n n_{fo} + \mu_p p_{fo}} \right] \\ &= - \frac{d\psi}{dx} \end{aligned} \quad (5.29)$$

in which

$$\psi = \frac{kT}{q} \left[\frac{\mu_n \Delta n_f - \mu_p \Delta p_f}{\mu_n n_{fo} + \mu_p p_{fo}} \right] \quad (5.30)$$

From equations (5.6), (5.27), (5.29) and (5.30), we obtain

$$\frac{d^2 \psi}{dx^2} - m_1^2 \psi + m_2^2 \xi = 0 \quad (5.31)$$

in which

$$m_1^2 = \frac{q^2}{\epsilon kT} (n_{fo} + p_{fo}) \quad (5.32)$$

$$m_2^2 = \frac{q}{\epsilon} \frac{(\mu_n - \mu_p)(n_{fo} + p_{fo})}{\mu_n n_{fo} + \mu_p p_{fo}} \quad (5.33)$$

Thus, the photovoltage generated by the light illumination can be calculated by the following equation

$$\begin{aligned} V_b &= - \int_0^d F dx \\ &= \psi(d) - \psi(0) \\ &= \frac{kT}{q} \left[\frac{(\mu_n \Delta n_f - \mu_p \Delta p_f)_{x=d} - (\mu_n \Delta n_f - \mu_p \Delta p_f)_{x=0}}{\mu_n n_{fo} + \mu_p p_{fo}} \right] \end{aligned} \quad (5.34)$$

Equation (5.34) implies that once we can determine Δn_f and Δp_t at $x=0$ and $x=d$, we can calculate V_b . However, to obtain these, we have to solve equations (5.28) and (5.31). But it is not possible to solve these equations analytically without making further assumptions. Many previous investigators [44,48,95,150] have assumed that no traps are present and the local charge neutrality prevails in the semiconductor. This assumption is crude because there are always traps in the semiconductor and because of the different mobilities of the two types of carriers (electrons and holes) the local charge would not be neutral. Although

it is possible to solve equations (5.28) and (5.31) by a numerical method to remove the shortcomings of this assumption, we shall not attempt to do so at present. Rather, we would like to obtain analytical solutions by making the assumptions that the local charge neutrality prevails in the crystal in order to study the effect of traps and that there is no traps in the semiconductor in order to study the effect of non-neutrality of local charge. These two cases are now presented as follows:

5.1.1 Local charge neutrality with traps

Because of local charge neutrality, $\Delta n = \Delta p$, we obtain from equations (5.17) and (5.18)

$$\Delta n_f = (K_p/K_n) \Delta p_f \quad (5.35)$$

and from equation (5.27)

$$\xi = \frac{(n_{fo} + K_p p_{fo}/K_n) \Delta p_f}{n_{fo} + p_{fo}} \quad (5.36)$$

Defining the effective diffusion length as

$$L = \sqrt{D \tau_o} \quad (5.37)$$

and using [79,97]

$$g_b(x) = g_{bo} \exp(-\epsilon_a x) \quad (5.38)$$

where

$$g_{bo} = Q\zeta \left[\frac{\epsilon_a \lambda_s}{1 + \epsilon_a \lambda_s} \left(\frac{1}{1 + x_s/\lambda_s} \right) \right], \quad (5.39)$$

Q is the quantum yield of carrier generation, ζ is the illuminated light intensity, ϵ_a is the absorption coefficient, λ_s and x_s are, respectively, the diffusion length of singlet excitons, and the surface path

length of singlet excitons; equation (5.28) becomes

$$\frac{d^2 \Delta p_f}{dx^2} - \frac{\Delta p_f}{L^2} + \frac{n_{fo} + p_{fo}}{(n_{fo} + K_p p_{fo}/K_n)} g_{bo} \exp(-\epsilon_a x) = 0 \quad (5.40)$$

The general solution of equation (5.40) is

$$\Delta p_f = a_1 e^{x/L} + a_2 e^{-x/L} + a_3 e^{-\epsilon_a x} \quad (5.41)$$

To determine the constants, a_1 , a_2 and a_3 we use the following boundary conditions

$$\begin{aligned} D \frac{d\xi}{dx} \Big|_{x=0} &= s_1 \xi(0) \\ D \frac{d\Delta p_f}{dx} \Big|_{x=0} &= s_1 \Delta p_f(0) \end{aligned} \quad (5.42)$$

$$\begin{aligned} -D \frac{d\xi}{dx} \Big|_{x=d} &= s_2 \xi(d) \\ -D \frac{d\Delta p_f}{dx} \Big|_{x=d} &= s_2 \Delta p_f(d) \end{aligned} \quad (5.43)$$

where s_1 and s_2 are the surface recombination velocities at the front and the back surfaces, respectively. Substituting equation (5.41) into equation (5.42) and (5.43) and solving them, we obtain

$$a_1 = \frac{a_3 [(s_1 - \epsilon_a D)(s_2 - D/L) e^{-d/L} - (s_1 + D/L)(s_2 - \epsilon_a D) e^{-\epsilon_a d}]}{2[s_1 s_2 + (D/L)^2] \sinh(d/L) + 2(s_1 + s_2)(D/L) \cosh(d/L)} \quad (5.44)$$

$$a_2 = - \frac{a_3 [(s_1 + \epsilon_a D)(s_2 + D/L) e^{d/L} - (s_1 - D/L)(s_2 - \epsilon_a D) e^{-\epsilon_a d}]}{2[s_1 s_2 + (D/L)^2] \sinh(d/L) + 2(s_1 + s_2)(D/L) \cosh(d/L)} \quad (5.45)$$

and

$$a_3 = \frac{g_{bo} L^2}{D(1 - \epsilon_a^2 L^2)} \cdot \frac{K_n (n_{fo} + p_{fo})}{(K_n n_{fo} + K_p p_{fo})} \quad (5.46)$$

Using equations (5.44), (5.45) and (5.46), we can calculate the photo-voltage generated by light illumination from the following equation

$$\begin{aligned}
 V_b &= \frac{kT}{\sigma} \frac{\mu_n K_p - \mu_p K_n}{K_n} [\Delta p(d) - \Delta p(0)] \\
 &= \frac{kT}{\sigma} \frac{\mu_n K_p - \mu_p K_n}{K_n} [a_1(e^{d/L} - 1) + a_2(e^{-d/L} - 1) + a_3(e^{-\epsilon_a d} - 1)]
 \end{aligned}
 \tag{5.47}$$

5.1.2 Local charge non-neutrality without traps

Because there are no traps, $K_n = K_p = 1$. The general solutions of equations (5.28) can be written as

$$\xi = b_1 e^{x/L} + b_2 e^{-x/L} + b_3 e^{-\epsilon_a x}
 \tag{5.48}$$

Using the same boundary conditions given in equations (5.42) and (5.43) we can determine the constants b_1 , b_2 and b_3 and they are

$$b_1 = \frac{b_3 [(s_1 + \epsilon_a D)(s_2 - D/L) e^{-d/L} - (s_1 + D/L)(s_2 - \epsilon_a D) e^{-\epsilon_a d}]}{2[s_1 s_2 + (D/L)^2] \sinh(d/L) + 2(s_1 + s_2)(D/L) \cosh(d/L)}
 \tag{5.49}$$

$$b_2 = - \frac{b_3 [(s_1 + \epsilon_a D)(s_2 + D/L) e^{d/L} - (s_1 - D/L)(s_2 - \epsilon_a D) e^{-\epsilon_a d}]}{2[s_1 s_2 + (D/L)^2] \sinh(d/L) + 2(s_1 + s_2)(D/L) \cosh(d/L)}
 \tag{5.50}$$

and

$$b_3 = \frac{g_{bo} L^2}{D(1 - \epsilon_a L^2)}
 \tag{5.51}$$

The general solution of equation (5.31) can be written as

$$\psi = c_1 e^{m_1 x} + c_2 e^{-m_1 x} + c_3 e^{x/L} + c_4 e^{-x/L} + c_5 e^{-\epsilon_a x}
 \tag{5.52}$$

Using the boundary conditions

$$\left. \frac{d\psi}{dx} \right|_{x=0} = 0 \quad (5.53)$$

$$\left. \frac{d\psi}{dx} \right|_{x=d} = 0 \quad (5.54)$$

and equations (5.31), (5.48) and (5.52), we can determine the constants c_1 , c_2 , c_3 , c_4 and c_5 ; and they are

$$c_1 = \frac{(c_3 - c_4 - c_5 \epsilon_a L) e^{-m_1 d} - (c_3 e^{d/L} - c_4 e^{-d/L} - c_5 \epsilon_a L e^{-\epsilon_a d})}{2 m_1 L \sinh(m_1 d)} \quad (5.55)$$

$$c_2 = \frac{(c_3 - c_4 - c_5 \epsilon_a L) e^{m_1 d} - (c_3 e^{d/L} - c_4 e^{-d/L} - c_5 \epsilon_a L e^{-\epsilon_a d})}{2 m_1 L \sinh(m_1 d)} \quad (5.56)$$

$$c_3 = \frac{m_2^2 b_1}{(m_1^2 - 1/L^2)} \quad (5.57)$$

$$c_4 = \frac{m_2^2 b_2}{(m_1^2 - 1/L^2)} \quad (5.58)$$

and

$$c_5 = \frac{m_2^2 b_3}{(m_1^2 - \epsilon_a^2)} \quad (5.59)$$

Using equations (5.49) - (5.51) and (5.55) - (5.59), we can calculate the photovoltage generated by the light illumination from the following equation

$$\begin{aligned} V_b &= \psi(d) - \psi(0) \\ &= c_1 (e^{m_1 d} - 1) + c_2 (e^{-m_1 d} - 1) \\ &\quad + c_3 (e^{d/L} - 1) + c_4 (e^{-d/L} - 1) \\ &\quad + c_5 (e^{-\epsilon_a d} - 1) \end{aligned} \quad (5.60)$$

5.2 COMPUTED RESULTS AND DISCUSSIONS

In Section 5.1 we have presented the expressions for calculating the component of photovoltage due to the charge separation in the bulk of the semiconductor. The total photovoltage across the whole semiconductor specimen consists of V_b , the potential created in the bulk of the semiconductor; ϕ_{s1} , the potential created at the front surface; and ϕ_{s2} , the potential created at the back surface. Thus we can write

$$V_{ph} = V_b + \phi_{s1} + \phi_{s2} \quad (5.61)$$

In the following we shall discuss these components separately.

5.2.1 The photovoltage created in the bulk of the crystal

Equations (5.47) and (5.60) can be reduced to much simpler forms by considering the limits of some physical parameters. In this section we shall present our computed results based on equations (5.47) and (5.60) for two cases: (i) strong absorption and (ii) weak absorption.

(i) Strong absorption:

For this case, ϵ_a can be considered to be much larger than $1/d$ and $1/L$. Under this condition, equation (5.47) for the case of local neutrality with traps becomes

$$V_{bI} = \frac{kT}{\sigma} \left(\frac{\mu_n K_p - \mu_p K_n}{K_n} \right) a_3 \left[\left(\frac{a_1}{a_3} \right) (e^{d/L} - 1) + \left(\frac{a_2}{a_3} \right) (e^{-d/L} - 1) - 1 \right] \quad (5.62)$$

in which

$$\begin{aligned}
a_1 &= \frac{a_3[(s_1 + \epsilon_a D)(s_2 - D/L)e^{-d/L}]}{2[s_1 s_2 + (D/L)^2] \sinh(d/L) + 2(s_1 + s_2)(D/L) \cosh(d/L)} \\
a_2 &= \frac{-a_3[(s_1 + \epsilon_a D)(s_2 + D/L)e^{d/L}]}{2[s_1 s_2 + (D/L)^2] \sinh(d/L) + 2(s_1 + s_2)(D/L) \cosh(d/L)} \\
a_3 &= \frac{g_{bo} L^2}{D(1 - \epsilon_a^2 L^2)} \cdot \frac{K_n(n_{fo} + p_{fo})}{(K_n n_{fo} + K_p p_{fo})}
\end{aligned} \tag{5.63}$$

If $d \gg L$, equation (5.62) can be further reduced to

$$V_{bI} = V_{bsI} \frac{s_1 L/D + 1}{\epsilon_a L - 1} \left(\frac{a_1}{a_3} \right) (e^{d/L} - 1) + \left(\frac{a_2}{a_3} \right) (e^{-d/L} - 1) - 1 \tag{5.64}$$

where V_{bsI} is the saturated photovoltage for $d \gg L$, and it is given by

$$V_{bsI} = \left(\frac{kT}{\sigma} \right) \left(\frac{\mu_n K_p - \mu_p K_n}{K_n} \right) \left[\frac{\epsilon_a - L/D}{s_1 + L/D} \right] \cdot a_3 \tag{5.65}$$

Similarly, under the conditions, $\epsilon_a \gg 1/d$ and $\epsilon_a \gg 1/L$, equation (5.60)

for the case of local charge non-neutrality without traps becomes

$$V'_{bI} = c_1(e^{m_1 d} - 1) + c_2(e^{-m_1 d} - 1) + c_3(e^{d/L} - 1) + c_4(e^{-d/L} - 1) - c_5 \tag{5.66}$$

in which

$$c_1 = \frac{(c_3 - c_4 - c_5 \epsilon_a L) e^{-m_1 d} - (c_3 e^{d/L} - c_4 e^{-d/L})}{2 m_1 L \sinh(m_1 d)}$$

$$c_2 = \frac{(c_3 - c_4 - c_5 \epsilon_a L) e^{m_1 d} - (c_3 e^{d/L} - c_4 e^{-d/L})}{2 m_1 L \sinh(m_1 d)}$$

$$c_3 = \frac{m_2^2 b_1}{(m_1^2 - 1/L^2)}$$

$$c_4 = \frac{m_2^2 b_2}{(m_1^2 - 1/L^2)}$$

$$c_5 = \frac{m_2 b_3}{(m_1^2 - \epsilon_a^2)}$$

(5.67)

$$b_1 = \frac{b_3 [(s_1 + \epsilon_a D)(s_2 - D/L) e^{-d/L}]}{2[s_1 s_2 + (D/L)^2] \sinh(d/L) + 2(s_1 + s_2)(D/L) \cosh(d/L)}$$

$$b_2 = \frac{-b_3 [(s_1 - \epsilon_a D)(s_2 + D/L) e^{d/L}]}{2[s_1 s_2 + (D/L)^2] \sinh(d/L) + 2(s_1 + s_2)(D/L) \cosh(d/L)}$$

$$b_3 = \frac{g_{bo} L^2}{D(1 - \epsilon_a^2 L^2)}$$

For $d \gg L$, equation (5.66) can be further reduced to

$$V'_{bI} = V'_{bsI} \left[\frac{c_1 (e^{m_1 d} - 1) + c_2 (e^{-m_1 d} - 1) + c_3 (e^{d/L} - 1) + c_4 (e^{-d/L} - 1) - c_5}{c_1 (e^{m_1 d} - 1) + c_2 (e^{-m_1 d} - 1) - c_4 - c_5} \right] \quad (5.68)$$

where V'_{bsI} is the saturated photovoltage for $d \gg L$ and it is given by

$$V'_{bsI} = c_1 (e^{m_1 d} - 1) + c_2 (e^{-m_1 d} - 1) - c_4 - c_5 \quad (5.69)$$

in which

$$c_1 = \frac{-(c_4 + c_5 \epsilon_a L) e^{-m_1 d}}{2 m_1 L \sinh(m_1 d)}$$

$$c_2 = \frac{-(c_4 + c_5 \epsilon_a L) e^{m_1 d}}{2 m_1 L \sinh(m_1 d)}$$

$$c_3 = 0$$

$$c_4 = \frac{m_2^2 b_2}{(m_1 - 1/L^2)}$$

$$c_5 = \frac{m_2 b_3}{(m_1^2 - \epsilon_a^2)} \quad (5.70)$$

$$b_1 = 0$$

$$b_2 = \frac{b_3(s_1 + \epsilon_a D)}{(s_1 + D/L)}$$

$$b_3 = \frac{g_{bo} L^2}{D(1 - \epsilon_a^2 L^2)}$$

(ii) Weak absorption:

For this case ϵ_a can be considered to be much smaller than $1/d$ and $1/L$. Under this condition, equation (5.47) for the case of local charge neutrality with traps becomes

$$V_{bII} = \frac{kT}{\sigma} \left[\frac{\mu_n K_p - \mu_p K_n}{K_n} \right] a_3 \left[\left[\frac{a_1}{a_3} \right] (e^{d/L} - 1) + \left[\frac{a_2}{a_3} \right] (e^{-d/L} - 1) - \epsilon_a d \right] \quad (5.71)$$

in which

$$a_1 = \frac{a_3 [(s_1 + \epsilon_a D)(s_2 - D/L) e^{-d/L} - (s_1 + D/L)(s_2 - \epsilon_a D)]}{2[s_1 s_2 + (D/L)^2] \sinh(d/L) + 2(s_1 + s_2)(D/L) \cosh(d/L)}$$

$$a_2 = -\frac{a_3 [(s_1 + \epsilon_a D)(s_2 + D/L) e^{d/L} - (s_1 - D/L)(s_2 - \epsilon_a D)]}{2[s_1 s_2 + (D/L)^2] \sinh(d/L) + 2(s_1 + s_2)(D/L) \cosh(d/L)} \quad (5.72)$$

$$a_3 = \frac{g_{bo} L^2}{D} \cdot \frac{K_n (n_{fo} + p_{fo})}{K_n n_{fo} + K_p p_{fo}}$$

Furthermore, if $d \gg L$, equation (5.71) can be further reduced to

$$V_{bII} = \frac{kT}{\sigma} \left(\frac{\mu_n K_p - \mu_p K_n}{K_n} \right) (a_3) \left[\left(\frac{a_1}{a_3} \right) (e^{d/L} - 1) - \left(\frac{a_2}{a_3} \right) - \epsilon_a d \right] \quad (5.73)$$

in which

$$\begin{aligned} a_1 &= - \frac{a_3(s_2 - \epsilon_a D)}{(s_2 + D/L)e^{d/L}} \\ a_2 &= - \frac{a_3(s_1 + \epsilon_a D)}{(s_1 + D/L)} \\ a_3 &= \frac{g_{bo} L^2}{D} \cdot \frac{K_n(n_{fo} + p_{fo})}{K_n n_{fo} + K_p p_{fo}} \end{aligned} \quad (5.74)$$

Substituting equation (5.74) into equation (5.73) we obtain

$$\begin{aligned} V_{bII} &= \left(\frac{kT}{\sigma} \right) \left(\frac{\mu_n K_p - \mu_p K_n}{K_n} \right) \left\{ \frac{(D/L) \{ [(s_1 + s_2) + 2(D/L)] \epsilon_a L + (s_1 - s_2) \}}{(s_1 + D/L)(s_2 + D/L)} - \epsilon_a d \right\} \\ &\approx \left(\frac{kT}{\sigma} \right) \left(\frac{\mu_n K_p - \mu_p K_n}{K_n} \right) (D/L) \left\{ \frac{(s_1 - s_2) - (L/D) \epsilon_a d}{(s_1 + D/L)(s_2 + D/L)} \right\} \end{aligned} \quad (5.75)$$

It is interesting to note here that the conditions for the reverse of the photovoltage polarity can be determined from equation (5.75). By putting $V_{bII} = 0$, we obtain

$$\mu_n K_p = \mu_p K_n \quad (5.76)$$

$$\epsilon_a = \frac{D(s_1 - s_2)}{dL(s_1 + D/L)(s_2 + D/L)} \quad (5.77)$$

This means that when either of these two conditions is satisfied, the photovoltage starts to reverse its polarity.

Similarly, under the condition, $\epsilon_a \ll 1/d$, $\epsilon_a \ll 1/L$, equation

(5.60) for the case of local charge non-neutrality without traps becomes

$$V'_{bII} = c_1(e^{m_1 d} - 1) + c_2(e^{-m_1 d} - 1) + c_3(e^{d/L} - 1) + c_4(e^{-d/L} - 1) - \epsilon_a d c_5 \quad (5.78)$$

in which

$$\begin{aligned} c_1 &= \frac{(c_3 - c_4 - c_5 \epsilon_a L) e^{-m_1 d} - (c_3 e^{d/L} - c_4 e^{-d/L} - c_5 \epsilon_a L)}{2m_1 L \sinh(m_1 d)} \\ c_2 &= \frac{(c_3 - c_4 - c_5 \epsilon_a L) e^{m_1 d} - (c_3 e^{d/L} - c_4 e^{-d/L} - c_5 \epsilon_a L)}{2m_1 L \sinh(m_1 d)} \\ c_3 &= \frac{m_2^2 b_1}{(m_1^2 - 1/L^2)} \\ c_4 &= \frac{m_2^2 b_2}{(m_1^2 - 1/L^2)} \\ c_5 &= \frac{m_2^2 b_3}{(m_1^2 - \epsilon_a^2)} \\ b_1 &= \frac{b_3 [(s_1 + \epsilon_a D)(s_2 - D/L) e^{-d/L} - (s_1 + D/L)(s_2 - \epsilon_a D)]}{2[s_1 s_2 + (D/L)^2] \sinh(d/L) + 2(s_1 + s_2)(D/L) \cosh(d/L)} \\ b_2 &= \frac{-b_3 [(s_1 + \epsilon_a D)(s_2 + D/L) e^{d/L} - (s_1 - D/L)(s_2 - \epsilon_a D)]}{2[s_1 s_2 + 1 D/L)^2] \sinh(d/L) + 2(s_1 + s_2)(D/L) \cosh(d/L)} \\ b_3 &= \frac{g_{bo} L^2}{D} \end{aligned} \quad (5.79)$$

and if $d \gg L$, these equations reduce to much simpler form, then equation (5.78) becomes

$$V'_{bII} \cong c_1(e^{m_1 d} - 1) + c_2(e^{-m_1 d} - 1) + c_3 e^{d/L} - c_4 - \epsilon_a d c_5 \quad (5.80)$$

in which

$$\begin{aligned}
 c_1 &= \frac{(c_3 - c_4) e^{-m_1 d} - c_3 e^{d/L}}{2m_1 L \sinh(m_1 d)} \\
 c_2 &= \frac{(c_3 - c_4) e^{m_1 d} - c_3 e^{d/L}}{2m_1 L \sinh(m_1 d)} \\
 c_3 &= \frac{m_2^2 b_1}{(m_1^2 - 1/L^2)} \\
 c_4 &= \frac{m_2^2 b_2}{(m_1^2 - 1/L^2)} \\
 c_5 &= \frac{m_2^2 b_3}{(m_1^2 - \epsilon_a^2)} \\
 b_1 &= -\frac{b_3(s_2 - \epsilon_a D)}{(s_2 + D/L) e^{d/L}} \\
 b_2 &= -\frac{b_3(s_1 + \epsilon_a D)}{(s_1 + D/L)} \\
 b_3 &= \frac{g_{bo} L^2}{D}
 \end{aligned} \tag{5.81}$$

Again, from equations (5.80) and (5.81) the conditions for the reverse of the photovoltage polarity are

$$m_2^2 = 0 \tag{5.82}$$

and

$$\epsilon_a = \frac{D[(s_1 - s_2)(m_1 L) \sinh(m_1 d) + 2s_1[1 - \cosh(m_1 d)]]}{dL[(s_1 + (D/L))(s_2 + D/L)(m_1^2 - 1/L^2) m_1 L \sinh(m_1 d)]} \tag{5.83}$$

The condition given by equation (5.82) should be ruled out since in most crystals $\mu_n \neq \mu_p$. Thus, the condition given by equation (5.83) is the only condition in which the photovoltage would start to reverse its polarity.

5.2.2 The photovoltage created at the front and back surface

The photo-excess electrons and holes densities within the surface region are given [88] by

$$\Delta n_s = n_s - n_{fo} = n_{fo} (e^{q\phi_s/kT} - 1) \quad (5.84)$$

$$\Delta p_s = p_s - p_{fo} = p_{fo} (e^{-q\phi_s/kT} - 1) \quad (5.85)$$

where n_s and p_s are, respectively, the surface free electrons and holes densities under non-equilibrium conditions. Within the surface space charge region, the electric field is given by [88]

$$F_s = \pm \frac{2kT}{qL_D} G \left(\frac{q\phi_s}{kT} \frac{n_{fo}}{p_{fo}} \right) \quad (5.86)$$

where

$$L_D = \sqrt{2kT / q^2 p_{fo}} \quad (5.87)$$

$$G \left(\frac{q\phi_s}{kT} \frac{n_{fo}}{p_{fo}} \right) \equiv \left[\left(e^{-q\phi_s/kT} + \frac{q\phi_s}{kT} - 1 \right) + \frac{n_{fo}}{p_{fo}} \left(e^{q\phi_s/kT} - \frac{q\phi_s}{kT} - 1 \right) \right]^{\frac{1}{2}} \quad (5.88)$$

and ϕ_s is the potential across the surface space charge region. For p-type semiconductor, when $\phi_s < 0$, there is an accumulation of holes near the surface and the band bends upward; when $\phi_s = 0$, the band becomes flat band; when $\phi_B > \phi_s > 0$, where ϕ_B is the potential different between

the Fermi-level and the midgap of the semiconductor, there is a depletion of holes; and when $\phi_S > \phi_B$, there is an inversion region due to electron enhancement and thus the band bends downward. Although we can calculate the surface potential at the front surface ϕ_{S_1} and at the back surface ϕ_{S_2} from equation (5.86) it would be more convenient to obtain ϕ_{S_1} or ϕ_{S_2} , by using equations (5.61), (5.47) or (5.60) based on the following relations

$$\phi_{S_1} + \phi_{S_2} = V_{ph} - V_b$$

or

$$\phi_{S_1} = V_{ph} - V_b \quad (\text{if } \phi_{S_2} \text{ is assumed to be zero}) . \quad (5.89)$$

5.2.3 Computed results

To show the effects of traps and local-charge non-neutrality on the bulk photovoltage characteristics, we take naphthalene, anthracene and tetracene crystals as examples; and to show the effect of surface states on the total photovoltage characteristics, we take anthracene crystal as an example. Generally, in these materials the hole mobility is larger than the electron mobility [69,80,100], and holes are generally the majority carriers. If we assume that an organic semiconductor has no traps and local charge neutrality prevails inside the crystal, then the photovoltage is given by

$$V_{bo} = \frac{kT}{\sigma} (\mu_n - \mu_p) a_{30} \left[\left(\frac{a_1}{a_{30}} \right) (e^{d/L} - 1) + \left(\frac{a_2}{a_{30}} \right) (e^{-d/L} - 1) + (e^{-\epsilon a^d} - 1) \right] \quad (5.90)$$

where a_1 and a_2 are given in equations (3.44) and (5.45), and a_{30}

corresponds to a_3 without traps and it is given by

$$a_{30} = \frac{g_{bo} L^2}{D(1 - \epsilon_a^2 L^2)} \quad (5.91)$$

The presence of traps or local charge non-neutrality in the crystal alters equation (5.90) as has been discussed in Section 5.1. In the following we shall present some computed results to show the effects of traps, non-neutrality and surface states using the physical parameters for organic semiconductors given below

$$\mu_p / \mu_n = 2$$

$$\epsilon_a d = 40$$

$$s_1 d / D = 10^{-2}$$

$$s_1 = s_2$$

(i) Bulk photovoltages

On the assumption that the bulk photovoltage is predominant and the surface photovoltage is negligible, we shall discuss the following two cases.

(a) Local charge neutrality with traps

Strong absorptions

For this case, the expression for the photovoltage characteristics [equation (5.47)] is similar to equation (5.90) except that $(\mu_n - \mu_p) a_{30}$ is replaced with $(\mu_n^k - \mu_p^k) a_3 / K_n$. Figure 5.1 shows the variation of bulk photovoltage V_{bI} with the thickness of the sample under strong

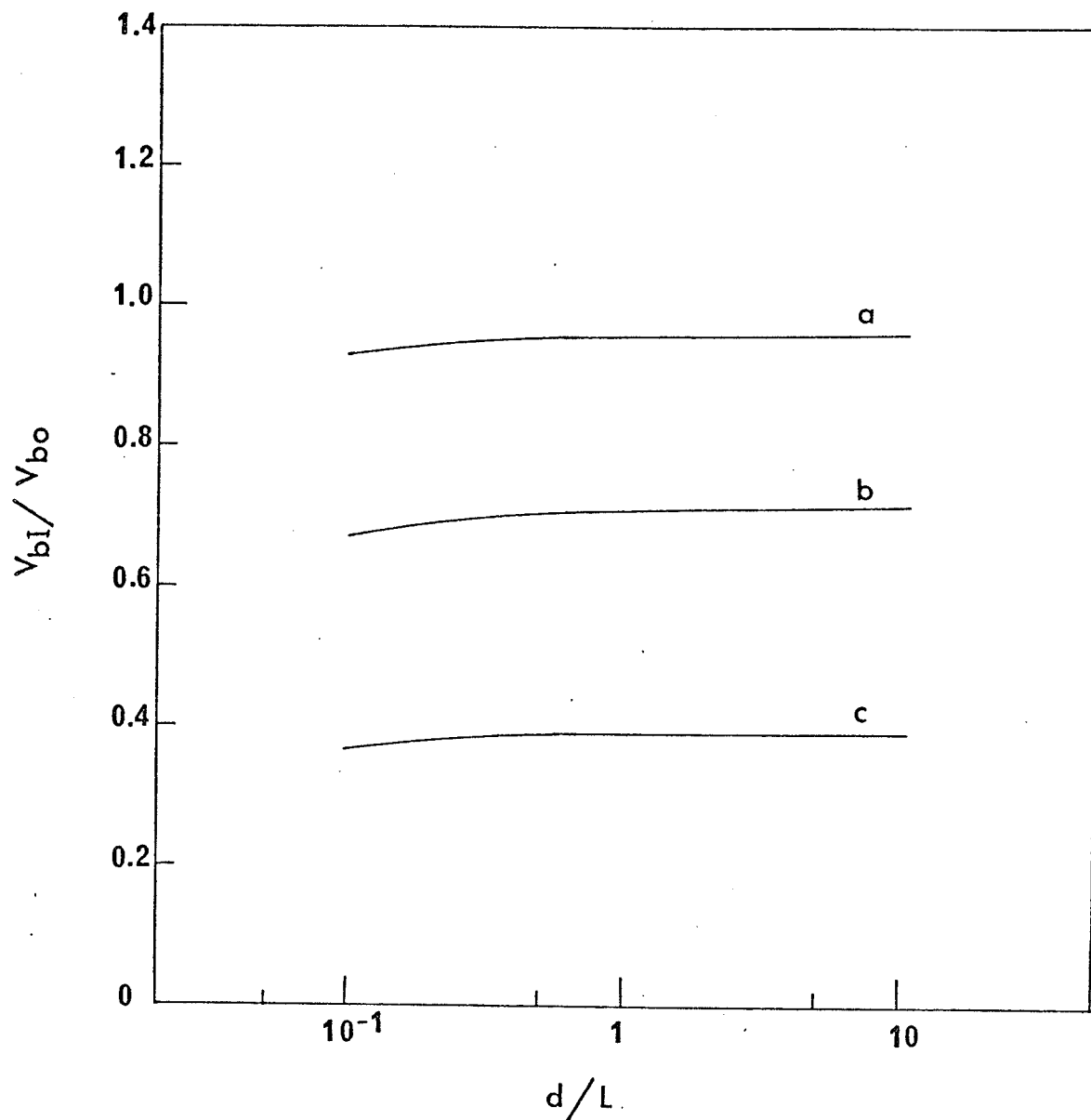


Fig. 5.1: The variation of V_{bI}/V_{bo} with d/L for the case of local-charge neutrality with traps under strong absorption conditions. a: $k_n/k_p = 1$; b: $k_n/k_p = 1.2$; c: $k_n/k_p = 1.5$.

absorption conditions ($\epsilon_a \gg 1/d$) for various concentrations of traps based on equation (5.64). V_{bI} tends to approach asymptotically a constant value of V_{bSI} given by equation (5.65). It can be seen that the presence of traps reduces the photovoltage. So far no experimental results on sample thickness dependence or carrier diffusion length on photovoltage are available so we cannot compare our theory with experiments. But Vertisimakha et al [157] have reported that for anthracene V_{bi}/V_{bo} is about 0.24 at d/L of about 4 (by assuming L to be 5×10^{-5} cm). Their results lie below the curve for $k_n/k_p = 1.2$ indicating the effects of traps.

Weak absorptions

Figure 5.2 shows the variation of the bulk photovoltage, V_{bII} with the thickness of the sample under weak absorptions ($\epsilon_a \ll 1/d$) for various concentrations of traps based on equation (5.71). It can be seen that for given values of S_1 and S_2 , V_{bII} decreases with increasing value of (d/L) ; for a given value of (d/L) , V_{bII} decreases with increasing value of (k_n/k_p) indicating the strong effect of traps. The bulk photovoltage under weak absorption conditions would be predominant in thin specimens. This agrees well with the experimental results of Lyons et al [87] for tetracene films. It should be noted that when $(k_n/k_p) = (\mu_p/\mu_n)$, the sign of V_{bII} may be reversed. The reverse sign in V_{bII} may be taken as an indication of photo-detrapping of minority-carriers from traps (electron-traps inside the crystals). Such a phenomenon has been observed experimentally in anthracene by Vladimirov [15].

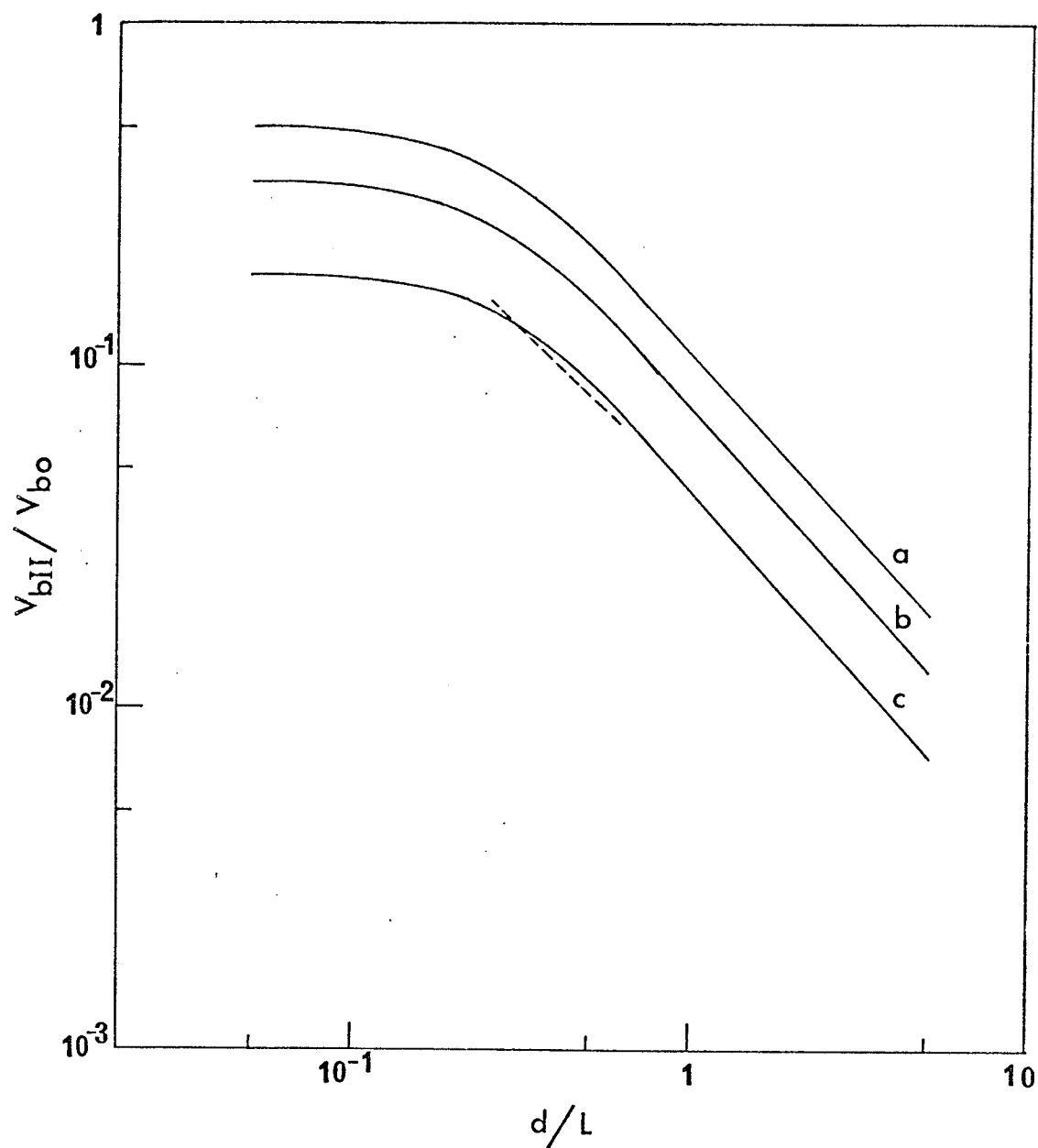


Fig. 5.2: The variation of V_{bII}/V_{bo} with d/L for the case of local-charge neutrality with traps under weak absorption condition. S

Solid lines are based on the theory - a: $k_n/k_p = 1$; b: $k_n/k_p = 1.2$; and c: $k_n/k_p = 1.5$; and, dashed line is the experimental results after Lyons & Newmann.

(b) Local charge non-neutrality without trapsStrong absorptions

For this case, the expression for the photovoltage characteristics [equation (5.66)] is similar to equation (3.90) except that $kT(\mu_n - \mu_p)a_{30}/\sigma$, a_1/a_{30} and a_2/a_{30} are replaced with $m_2^2/[m_1 L \sinh(m_1 d)]$ $[1/(m_2^2 - 1/L^2)]$ $\{(1+e^{d/L})[1-\cosh(m_1 d)] - (1-e^{d/L})m_1 L \sinh(m_1 d)\}(a_1/a_{30})$ and $[1/(m_2^2 - 1/L^2)]$ $\{(1+e^{-d/L})[1-\cosh(m_1 d)] + (1-e^{-d/L})m_1 L \sinh(m_1 d)\}(a_1/a_{30})$, respectively. By assuming that $m_1^2 \gg 1/L^2$, $m_1^2 \gg \epsilon_a^2$, $(m_1 L) \sinh(m_1 d) = 1$ and $(1-\cosh m_1 d) = 0$, equation (5.60) can be reduced to equation (5.90) for the case of local-charge neutrality without traps. Figure 5.3 shows the variation of bulk photovoltage, V'_{bI} with the thickness of the specimen for various degree of local charge non-neutrality based on equation (5.65) for strong absorption conditions ($\epsilon_a \gg 1/d$). The higher the degree of local charge non-neutrality the larger the photovoltage would be generated. Tavares [149] has reported that in naphthalene the value of V'_{bI}/V_{bo} is about 1 when the sample is illuminated with light wavelength of 7500 Å, and this value jumps up to about 3 when the sample has been previously illuminated with light of short wavelength (4100 Å or 5000 Å) indicating the space charge effect which is associated with local charge non-neutrality.

Weak absorptions

Figure 5.4 shows the variation of bulk photovoltages, V'_{bII} with the thickness of the sample for various degree of local charge non-neutrality under weak absorptions ($\epsilon_a \ll 1/d$) based on equation (5.78). For given values of S_1 and S_2 , V'_{bII} decreases with increasing value of (d/L) ; and for a given value of (d/L) , V'_{bII} increases with increasing value of A_x and A_y in which

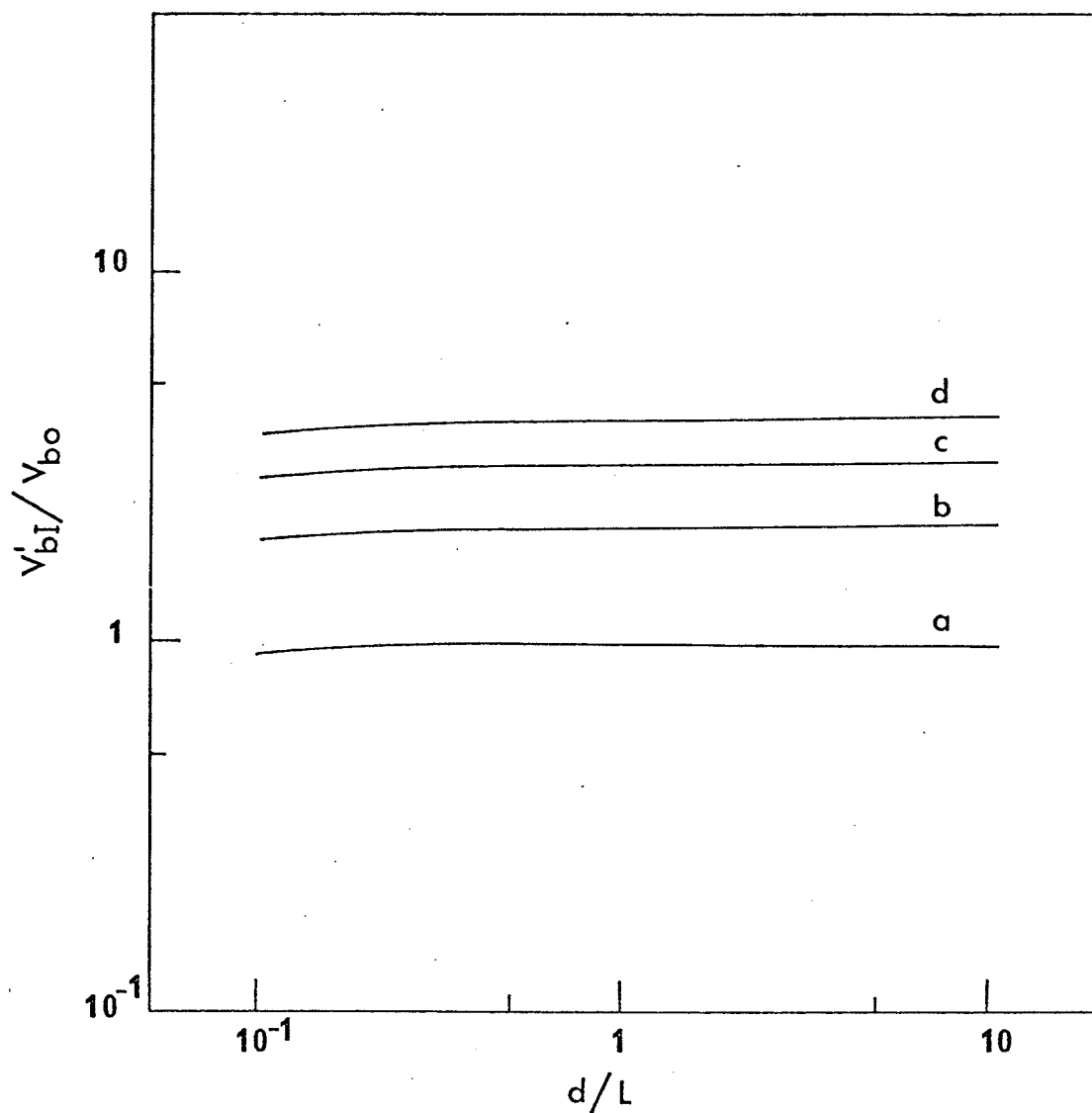


Fig. 5.3: The variation of V_{bI}'/V_{bo} with d/L for the case of local-charge non-neutrality without traps under strong absorption conditions.

a: $A_x = 1, A_y = 0$; b: $A_x = 1, A_y = 2$; c: $A_x = 2, A_y = 3$
and d: $A_x = 3, A_y = 4$.

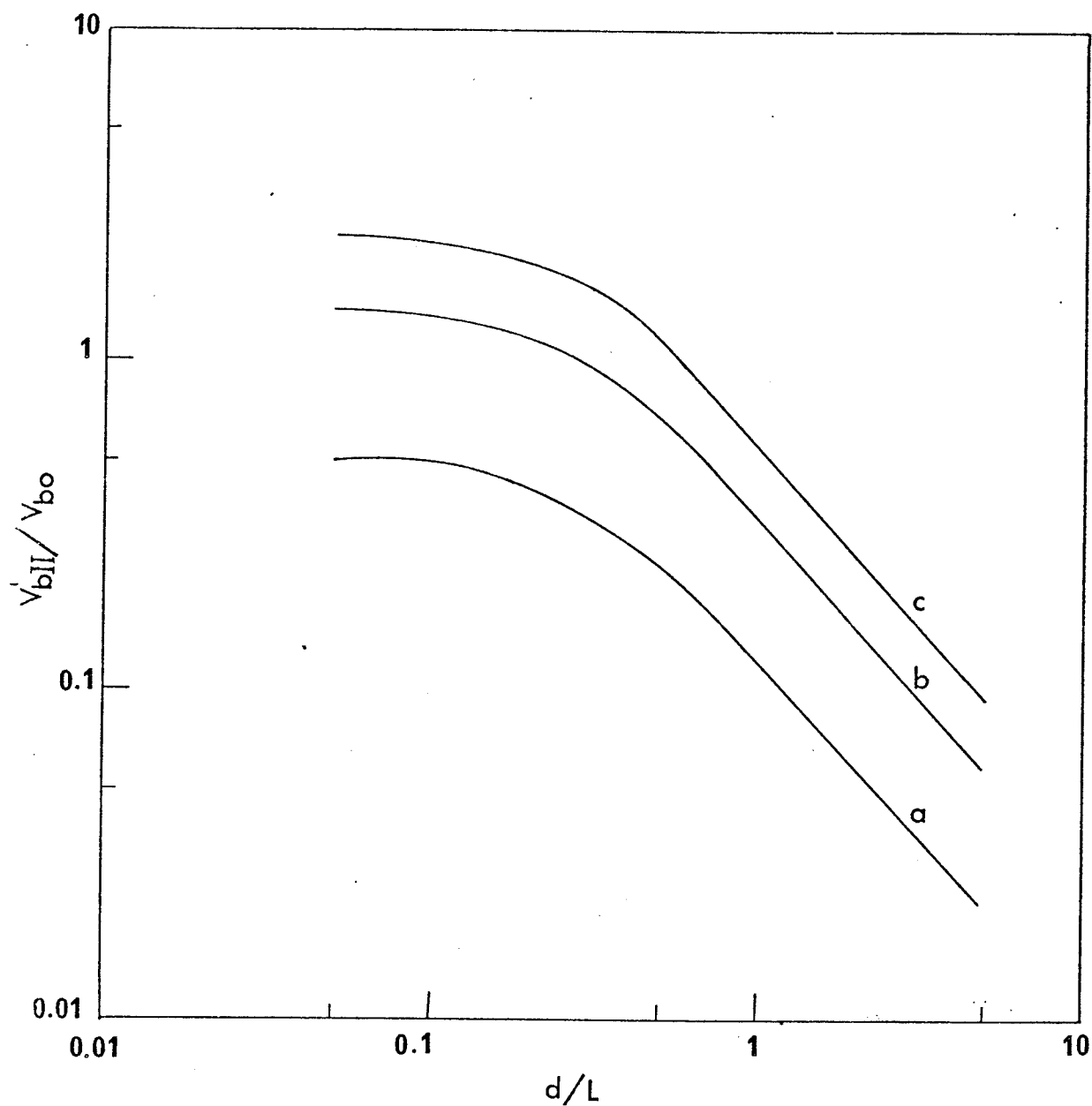


Fig. 5.4: The variation of V'_{bII}/V_{bo} with d/L for the case of local-charge non-neutrality without traps under weak absorption conditions.

a: $A_x = 1$, $A_y = 0$; b: $A_x = 2$, $A_y = 3$; and c: $A_x = 4$, $A_y = 5$.

$$Ax = 1 - \cosh(m_1 d)$$

$$Ay = m_1 L \sinh(m_1 d) \quad (5.92)$$

It is interesting to note that the conditions for the change of the sign of the photovoltage depend also on the degree of local-charge non-neutrality according to equation (5.83); and that the effect of local-charge non-neutrality is due to unequal distribution of the double-space-charge of opposite signs in the bulk of the crystal. However, so far this important space-charge effect has not yet been reported in the literature.

(ii) Surface photovoltage

It is possible that under certain conditions the surface photovoltage may be as equally important as the bulk photovoltage, or even pre-dominant. The magnitude and sign of ϕ_{S_1} (or ϕ_{S_2}) depend strongly on the surface states of the crystal. External factors such as gas molecule adsorption or additional illumination, etc. may alter the surface states and hence the value of ϕ_{S_1} (or ϕ_{S_2}). The generation of surface photovoltage may be due to the boundary bending of the energy band near the surface. According to equation (5.89) we can predict that the presence of surface states would tend to decrease the photovoltage. Nakada [102] and Vladimirov [159] have reported that the adsorption of oxygen on the surface crystal reduces the magnitude of the total photovoltage.

5.3 CONCLUDING REMARKS

The general analytic expressions for the bulk photovoltage in a solid with traps and non-neutrality of local charges have been derived using a unified mathematical approach. It is found that the presence of

traps tends to reduce the magnitude of the photovoltages and to affect the conditions for the change of the sign of the photovoltages, and that the non-neutrality of local charges tends to enhance the photovoltages and also to affect the conditions for the change of the sign of the photovoltages. It should be noted that we choose the two cases: (1) local charge neutrality with traps and (2) local charge non-neutrality without traps, to show the effects of traps and local-charge non-neutrality using some approximations mainly for mathematical simplicity. Although the computed results are in reasonable agreement with experimental results, for vigorous treatment the photovoltage has to be calculated from equation (5.34) under the conditions of local charge non-neutrality and with traps.

It should also be noted that the analysis described in this chapter may, in principle, be used as a tool to determine the surface recombination velocity and the diffusion length of carriers.

CHAPTER VI

CONCLUSIONS

On the basis of the present investigations, we can now draw the following conclusions:

- (1) The general expressions for the single injection and the double injection current-voltage characteristics in a solid with traps distributed uniformly and non-uniformly within the forbidden energy gap and in space have been derived.
- (2) The general expressions for the filamentary double injection current-voltage characteristics in a solid with traps confined in a single discrete energy level and distributed exponentially within the forbidden energy gap have been derived; and on the basis of the filamentary double injection theory the brightness of electroluminescence as a function of applied electric field, current density and temperature has also been derived, and the computed results are in good agreement with the experimental results for undoped anthracene and anthracene doped with tetracene.
- (3) The so-called single injection in anthracene becomes double injection at high fields.
- (4) The general formulation of bulk photovoltage taking into account the effects of traps and local charge non-neutrality has been presented. The presence of traps tends to reduce the magnitude of the photovoltage and to affect the conditions for the change

of the sign of the photovoltage, and the effect of non-neutrality of local charges tends to enhance the photovoltage and also to affect the conditions for the change of the sign of the photovoltage.

A P P E N D I X

By setting

$$D = \frac{q\mu N_V g \exp(-E_g/kT)}{J} \quad (A1)$$

equation (3.22) can be written as

$$\int_0^{F(t)} \frac{dF}{\ln \frac{1}{DF}} = - \frac{qH_c kT}{\epsilon} \int_0^t [\theta_c + S(x)] dx \quad (A2)$$

The value of DF is of the order of $\exp[-(E_g - E_f)/kT]$ which is much smaller than unity. Thus by setting $u = \ln \frac{1}{DF}$ and making use of the relation

$$\int_u^\infty \frac{e^{-u}}{u} du \approx e^{-u} \left(\frac{1}{u} - \frac{1}{u^2} + \frac{2!}{u^3} - \frac{3!}{u^4} + \dots \right)$$

we obtain

$$\int_0^{F(t)} \frac{dF}{\ln \frac{1}{DF}} \approx \frac{F(t)}{\ln \frac{1}{DF(t)}} \quad (A3)$$

Substitution of equation (A3) into equation (A2) and then integration give

$$\begin{aligned} \int_0^d \frac{F(t) dt}{\ln \frac{1}{DF(t)}} &= - \frac{qH_c kT}{\epsilon} \frac{1}{2} \left\{ 2 \int_0^d \int_0^t [\theta_c + S(x)] dx dt \right\} \\ &= - \frac{qH_c kT}{2\epsilon} d_{eff}^2 \end{aligned} \quad (A4)$$

d_{eff} can be physically interpreted in such a way that a specimen of true

thickness d having a non-uniform spatial distribution of traps is equivalent to the same specimen having a uniform spatial distribution of traps but with d changed to d_{eff} . Based on this interpretation, we have

$$\begin{aligned}
 V &= - \int_0^d F dx = - \int_0^{d_{\text{eff}}} F^* dx \\
 &= - \int_0^{F_d^*} F^* \frac{\partial x}{\partial F^*} dF^* = - \int_0^{F_d^*} \frac{\epsilon}{qH_c kT} \frac{F^* dF^*}{\ln\left(\frac{1}{DF^*}\right)} \\
 &= - \frac{\epsilon}{2qH_c kT} \frac{(F_d^*)^2}{\ln\left(\frac{1}{DF_d^*}\right)} \quad (A5)
 \end{aligned}$$

where F^* and F_d^* which correspond to the effective thickness d_{eff} are the effective fields at any point and at $x = d$, respectively. From equations (A2) and (A3) we have

$$\frac{F_d^*}{\ln\left(\frac{1}{DF_d^*}\right)} = - \frac{qH_c kT}{\epsilon} d_{\text{eff}} \quad (A6)$$

From equations (A5) and (A6) we obtain

$$F_d^* = \frac{2V}{d_{\text{eff}}} \quad (A7)$$

From equations (A4) and (A6) we obtain

$$\int_0^d \frac{F(t) dt}{\ln\left(\frac{1}{DF(t)}\right)} = - \frac{\epsilon}{2qH_c kT} \left(\frac{F_d^*}{\ln\left(\frac{1}{DF_d^*}\right)} \right)^2 \quad (A8)$$

Substitution of equations (A7) and (A8) into equation (A4) gives equation (3.24).

REFERENCES

1. Adolph, J. and Williams, D.F., "Temperature dependence of singlet-triplet intersystem crossing in anthracene crystals," J. Chem. Phys. 46, 4248-51 (1967).
2. Aris, F.C., Lewis, T.J., Thomas, J.M., Williams, J.D. and Williams, D.F., "Influence of deformation on the mobility and lifetimes of charge-carriers in anthracene crystals," Solid-State Commun. 12, 913-917 (1973).
3. Arnold, S., Witten, W.B. and Damask, A.D., "Triplet exciton trapping by dislocations in anthracene," J. Chem. Phys. 53, 2878-2884 (1970).
4. Avakian, P., Ern, V., Merrifield, R.E. and Suna, A., "Spectroscopic approach to triplet exciton dynamics in anthracene," Phys. Rev. 165, 974-80 (1968).
5. Avakian, P. and Merrifield, R.E., "Triplet excitons in anthracene crystals - a review," Mol. Cryst. 5, 37-77 (1968).
6. Baessler, H. and Vaubel, G., "Surface states of anthracene crystals," Phys. Rev. Lett. 21, 615-7 (1968).
7. Baessler, H., Hermann, G., Riehl, N. and Vaubel, G., "Space-charge-limited currents in tetracene single-crystals," J. Phys. Chem. Solid. 30, 1579-1585 (1969).
8. Barnett, A.M. and Milnes, A.G., "Filamentary injection in semi-insulating silicon," J. Appl. Phys. 37, 4215-4223 (1966).
9. Barnett, A.M., "Current Filament Formation," in Semi-conductors and Semi-metals, Williamson, R.K. and Beer, A.C. Eds., Academic Press, New York, Vol. 6, 141-200 (1970).
10. Baron, R. and Mayor, J.W., "Double Injection in Semi-conductors," in Semi-conductors and Semi-metals, Vol. 6, 201-313 (1970).
11. Batt, R.H., Braun, C.L. and Hornig, J.F., "Electric-field and temperature dependence of photoconductivity," J. Chem. Phys. 49, 1967-1968 (1968).
12. Becker, G., Riehl, N. and Baessler, H., "Injection-determined dark-current in anthracene single crystals," Phys. Lett. 20, 221-222 (1966).
13. Berderskii, V.A. and Lavrushko, A.G., "Reabsorption of light and photoconductivity of anthracene crystals," Soviet-Phys.-Solid State 13, 1072-1076 (1971).

14. Berderskii, V.A. and Lavrushko, A.G.: "Investigations of pulsed photocurrents in anthracene crystals," Soviet Phys. - Solid State 13, 1280-1283 (1971).
15. Bergh, A.A. and Dean, J.P.: "Light-emitting diodes," Proc. IEEE 60, 156-223 (1972).
16. Bergman, A., Bergman, D. and Jortner, J.: "Singlet exciton collisions in crystalline anthracene," Israel J. Chem. 10, 471-483 (1972).
17. Birks, J.B.: Photophysics of Aromatic Molecules, Wiley - Interscience, New York, (1970).
18. Brodzeli, M.I., Elignlashvili, I.A., Kertsman, E.L., Nakashidze, G.A.: "Injection electroluminescence of anthracene," Soviet Phys. - Semicond. 4, 811-12 (1970).
19. Castro, G. and Hornig, J.F.: "Multiple charge-carrier generation processes in anthracene," J. Chem. Phys. 42, 1459 (1965).
20. Castro, G.: "On warrier excitons in anthracene," J. Chem. Phys. 46, 4997-99 (1967).
21. Caywood, J.M.: "Photoemission from metal contacts into anthracene crystals: A critical review," Mol. Cryst. Liquid Cryst. 12, 1-26 (1970).
22. Chaiken, R.F. and Kearns, D.R.: "Intrinsic photoconduction in anthracene crystals," J. Chem. Phys. 45, 3966-3976 (1966).
23. Chance, R.R. and Braun, C.L.: "Intrinsic photoconduction in anthracene single crystals: Electric field dependence of hole and electron quantum yields," J. Chem. Phys. 59, 2269-2272 (1973).
24. Choi, S.I. and Rice, S.A.: "Exciton-excitons and photoconductivity in crystalline anthracene," J. Chem. Phys. 38, 366-393 (1963).
25. Choi, S.I., Jortner, J., Rice, S.A. and Silbey, R.: "Charge-transfer exciton states in aromatic molecular crystals," J. Chem. Phys. 41, 3294-3306 (1964).
26. Choi, S.I.: "Collision annihilation of singlet excitons in molecular crystals," Phys. Rev. Lett. 19, 358-60 (1967).
27. Cook, B.E. and LeComber, P.G.: "The optical properties of anthracene crystals in the vacuum ultraviolet," J. Phys. Chem. Solids. 32, 1321-1329 (1971).

28. Craig, D.P. and Walmsley, S.H.: Excitons in Molecular Crystals, W.A. Benjamin, Inc., New York, (1968).
29. Davydov, A.S.: Theory of Molecular Excitons, McGraw Hill Book Company, Inc., New York, (1962).
30. Davydov, A.S. and Sheka, E.F.: "Structure of exciton bands in crystalline anthracene," Phys. State. Sol. 11, 877-890 (1965).
31. Dember, H.: "Photoelectromotive force in cuprous oxide crystals," Z. Physik 32, 554, 856 (1931); 33, 207 (1932).
32. Dresner, J.: "Double injection electroluminescence in anthracene," RCA Rev. 30, 322-334 (1969).
33. Dresner, J. and Goodman, A.M.: "Anthracene electroluminescent cells with tunnel-injection cathodes," Proc. IEEE Lett. 58, 1868-1869 (1970).
34. Dresner, J.: "Volume generation and hall mobility of holes in anthracene," J. Chem. Phys. 52, 6343-6347 (1970).
35. Druger, S.D.: "Photoionization and photogeneration of carriers in anthracene," Chem. Phys. Lett. 17, 603-607 (1972).
36. Durocher, D.F. and Williams, D.F.: "Temperature dependence of triplet diffusion in anthracene," J. Chem. Phys. 51, 1675-1676 (1969).
37. Eremenko, V.V. and Medvedev, V.S.: "Dependence of the photoconductivity and the intensity of luminescence of anthracene crystals on the excitation wave length," Soviet Phys. - Solid State 2, 1426-1428 (1960).
38. Ern, V. and Merrifield, R.E.: "Magnetic field effect on triplet exciton quenching in organic crystals," Phys. Rev. Lett. 21, 609-611 (1968).
39. Ern, V., Bouchriha, H., Fourny, J. and Delacote, G.: "Triplet exciton - trapped hole interaction in anthracene crystals," Solid State Commun. 9, 1201-1203 (1971).
40. Fielding, P.E. and Jaragin, R.C.: "Excimer and defect structure for anthracene and some derivatives in crystals, thin films and other rigid matrices," J. Chem. Phys. 47, 247-252 (1967).
41. Frankevich, E.L., Sokolik, I.A. and Lukin, L.V.: "Triplet exciton charge carrier interaction in anthracene," Phys. State Sol. (b) 54, 61-65 (1972).

42. Fünfschilling, J. and Zschokke-Gränacher, I.: "Triplet-triplet exciton annihilation in tetracene-doped anthracene crystals," *Helvetica Physica Acta.* 43, 768-770 (1970).
43. Gärtner, W.: "Spectral distribution of the photomagnetolectric effect in semiconductors: theory," *Phys. Rev.* 105, 823-829 (1957).
44. Geacintov, N., Pope, M. and Kallmann, H.: "Photogeneration of charge carriers in tetracene," *J. Chem. Phys.* 45, 2639-2649 (1966).
45. Geacintov, N. and Pope, M.: "Photogeneration of charge carriers in anthracene," *J. Chem. Phys.* 45, 3884-3885 (1966).
46. Geacintov, N. and Pope, M.: "Low-lying valence band states and intrinsic photoconductivity in crystalline anthracene and tetracene," *J. Chem. Phys.* 50, 814-822 (1969).
47. Gooch, C.H.: Injection Electroluminescent Devices, John Wiley and Sons, New York, (1973).
48. Gutmann, F. and Lyons, L.E.: Organic Semiconductors, John Wiley and Sons, New York, 836 pp. (1967).
49. Hamann, C.: "On the trap distribution in thin film of copper phthalocyanine," *Phys. Stat. Sol.* 26, 311-318 (1968).
50. Hasegawa, K. and Yoshimura, S.: "Photocarrier generation in anthracene due to exciton interaction of two photo excited singlets," *Phys. Rev. Lett.* 14, 689-690 (1965).
51. Helfrich, W. and Schneider, W.G.: "Recombination radiation in anthracene crystals," *Phys. Rev. Lett.* 14, 229-231 (1965).
52. Helfrich, W. and Lipsett, F.R.: "Fluorescence and defect fluorescence of anthracene at 4.2°K," *J. Chem. Phys.* 43, 4368-4376 (1965).
53. Helfrich, W.: "Destruction of triplet excitons in anthracene by injected electrons," *Phys. Rev. Lett.* 16, 401-403 (1966).
54. Helfrich, W. and Schneider, W.G.: "Transients of volume-controlled current and of recombination radiation in anthracene," *J. Chem. Phys.* 44, 2902-2909 (1966).
55. Helfrich, W.: "Space-charge-limited and volume-controlled currents in organic solids," in Physics and Chemistry of the Organic Solid State, Fox, D. Labes, M. and Weissberger, A. Eds., Vol. 3, 1-65 (1967).
56. Hernandez, J.P.: "Photo-ionization of crystalline anthracene," *Phys. Rev.* 169, 746-749 (1968).

57. Hoesterey, D.C. and Letson, G.M.: "The trapping of photocarriers in anthracene by anthraquinone, anthrone and naphthracene," J. Phys. Chem. Solids 24, 1609-1615 (1963).
58. Hwang, W. and Kao, K.C.: "A unified approach to the theory of current injection in solids with traps uniformly and non-uniformly distributed in space and energy, and size effects in anthracene films," Solid-St. Electron. 15, 523-9 (1972).
59. Hwang, W. and Kao, K.C.: "A unified approach to the theory of double injection in solids with traps uniformly and non-uniformly distributed in the energy band gap," Solid-St. Electron. 16, 407-415 (1973).
60. Hwang, W. and Kao, K.C.: "Electroluminescence in anthracene crystals caused by field induced minority carriers at moderate temperatures," J. Chem. Phys. 58, 3521-22 (1973).
61. Hwang, W. and Kao, K.C.: "On the theory of filamentary double injection and electroluminescence in molecular crystals," (scheduled for publication in Journal of Chemical Physics, 1974).
62. Johnston, G.R. and Lyons, L.E.: "Photocarrier generation mechanism in anthracene crystals under ultra-high vacuum," Aust. J. Chem. 23, 1571-1579 (1970).
63. Kallmann, H. and Pope, M.: "Photovoltaic effect in organic crystal," J. Chem. Phys. 30, 585-586 (1959).
64. Kallmann, H., Kramer, B., Shain, J. and Spruch, G.M.: "Photovoltaic effects in CdS crystals," Phys. Rev. 117, 1482-1486 (1960).
65. Kallmann, H., Vaubel, G. and Baessler, H.: "Interaction of excitons in organic materials with an absorbing surface," Phys. Stat. Sol. (b) 44, 813-820 (1971).
66. Kawabe, M., Masuda, K. and Namba, S.: "Electroluminescence of green light region in doped anthracene," Japan J. Appl. Phys. 10, 527-528 (1971).
67. Kearns, D.R.: "Generation of charge carriers in organic molecular crystals through multiple exciton interactions," J. Chem. Phys. 39, 2697-2703 (1963).
68. Kemeny, G. and Rosenberg, B.: "Small polonons in organic and biological semiconductors," J. Chem. Phys. 53, 3549-3551 (1970).
69. Kepler, R.G.: "Charge carrier production and mobility in anthracene crystals," Phys. Rev. 119, 1226-1229 (1960).
70. Kepler, R.G. and Merrifield, R.E.: "Exciton-exciton interaction and photoconductivity in anthracene," J. Chem. Phys. 40, 1173-1174 (1964).

71. Kepler, R.G.: "Electron and hole generation in anthracene crystals," Pure and Appl. Chem. 27, 515-526 (1972).
72. Killesreiter, H. and Baessler, H.: "Dissociation of Frenkel excitons at the interface between a molecular crystal and metal," Phys. Stat. Sol. 51, 657-668 (1972).
73. Knox, R.S.: Theory of Excitons, Academic Press, New York, (1963).
74. Kikuchi, M.: "Observation of negative resistance and oscillation phenomena in the forward direction of point contact semiconductor diodes," Japan J. App. Phys. 2, 31-46 (1963).
75. Lampert, M.A.: "Simplified theory of space-charge-limited currents in an insulator with traps," Phys. Rev. 103, 1648-1656 (1956).
76. Lampert, M.A. and Schilling, R.B.: "Current injection in solids: The regional approximation method," in Semiconductor and Semi-metals Vol. 6, 1-96 (1970).
77. Lampert, M.A. and Mark, P.: Current Injection in Solids, Academic Press, New York, (1970).
78. Landsberg, P.T.: "Non-radiative transitions in semiconductors," Phys. Stat. Sol. 41, 457-489 (1970).
79. Lavrushko, A.G. and Benderskii, V.A.: "Efficiency of the various charge-carrier generation processes in anthracene crystals," Soviet Phys.-Solid State 13, 1223-25 (1971).
80. LeBlanc, O.H.: "Conductivity," in Physics and Chemistry of the Organic Solid State, Fox, D., Labes, M.M., Weissberg, A., Eds., Interscience, New York Vol. 3, 133-198 (1967).
81. Levinson, J. and Weisz, S.Z.; Cabas, A. and Rolon, A.: "Determination of the triplet exciton-trapped electron interaction rate constant in anthracene crystals," J. Chem. Phys. 52, 2794-2795 (1970).
82. Lindmayer, J, Reynolds, J. and Wrigley, C.: "One carrier space-charge limited current in solids," J. Appl. Phys. 34, 809-812 (1963).
83. Lohmann, F. and Mehl, W.: "Dark injection and radiative recombination of electrons and holes in naphthalene crystals," J. Chem. Phys. 50, 500-506 (1969).
84. Lupien, Y. and Williams, D.F.: "Preparation of high-purity anthracene: Zone refine and the triplet lifetime," Mol. Cryst. 5, 1-7 (1968).

85. Lupien, Y., Williams, J.O. and Williams, D.F.: "Effects of crystal growth environment on defect concentrations in anthracene crystals," *Mol. Cryst. Liquid Cryst.* 18, 129-141 (1972).
86. Lyons, L.E.: "Photoconductance in tetracene-type crystals: Theory of spectral dependence," *J. Chem. Phys.* 23, 220 (1955).
87. Lyons, L.E. and Newman, O.M.G.: "Photovoltages in tetracene films," *Aust. J. Chem.* 24, 13-23 (1971).
88. Many, A., Goldstein, Y. and Grover, N.B.: Semiconductor Surfaces, North-Holland, Amsterdam, (1965).
89. Mark, P. and Helfrich, W.: "Space-charge-limited currents in organic crystals," *J. Appl. Phys.* 33, 205-215 (1962).
90. McMahon, D.H. and Kestigram, M.: "Triplet-triplet annihilation in anthracene at low excitation intensities - wavelength and temperature dependence," *J. Chem. Phys.* 46, 137-142 (1967).
91. Mehl, W. and Bucher, W.: "Electroluminescence of anthracene crystals existed by electrochemical double injection," *Z. Physik Chem. (Frankfurt)* 47, 76-88 (1965). (In German)
92. Mehl, W. and Funk, B.: "Dark injection of electrons and holes and radiative recombination in anthracene with metallic contacts," *Phys. Lett.* 25A, 364-365 (1967).
93. Mey, W. and Hermann, M.A.: "Drift mobilities of holes and electrons in naphthalene single crystals," *Phys. Rev.* B7, 1652-56 (1973).
94. Morris, R. and Silver, M.: "Direct electron-hole recombination in anthracene," *J. Chem. Phys.* 50, 2969-2973 (1969).
95. Moss, T.S., Pincherle, L. and Woodward, A.M.: "Photoelectromagnetic and photodiffusion effects in germanium," *Proc. Phys. Soc. (Lond.)* 66B, 743-752 (1953).
96. Moss, T.S.: Optical Properties of Semiconductors, Academic Press, New York, (1959).
97. Mudler, B.J.: "Diffusion and surface reactions of singlet excitons in anthracene," *Philips Res. Rep. Suppl.* N4, 128 pp. (1968).
98. Muller, R.S.: "A unified approach to the theory of space-charge-limited currents in an insulator with traps," *Solid St. Electron.* 6, 25-32 (1963).

99. Mott, N.F. and Gurney, R.W.: Electronic Processes in Ionic Crystals, Oxford University Press, (1940).
100. Munn, R.W. and Siebrand, W.: "Theory of charge carrier transport in aromatic hydrocarbon crystals," J. Chem. Phys. 52, 6391-6406 (1970).
101. Munn, R.W. and Siebrand, W.: "Transport of quasilocalized excitons in molecular crystals," J. Chem. Phys. 52, 47-63 (1970).
102. Nakada, I. and Kojima, T.: "On the surface photo-voltaic effect anthracene," J. Phys. Soc. Japan 19, 695-701 (1964).
103. Nicolet, M.A.: "Unipolar space charge-limited current in solids with nonuniform spacial distribution of shallow traps," J. App. Phys. 36, 4224-4235 (1966).
104. Northrop, D.C. and Simpson, O.: "Electrical properties of aromatic hydrocarbons, I. Electrical conductivity," Proc. Roy. Soc. (London) 234, 124-135 (1956).
105. Northrop, D.C. and Simpson, O.: "Electronic properties of aromatic hydrocarbons, (IV) Photo-electric effects," Proc. Roy. Soc. (London) A244, 377-389 (1958).
106. Parmenter, R.H. and Ruppel, W.: "Two-carrier space-charge-limited current in a trap-free insulator," J. App. Phys. 30, 1548-1558 (1959).
107. Paritskii, I.G. and Rozental, A.I.: "Influence of the charge exchange in impurity centers on the space-charge-limited current," Soviet Phys. - Semicond. 1, 210-215 (1967).
108. Pope, M. and Kallmann, H.: "Photoconductivity and semiconductivity in organic crystals," Discus. Faraday Soc. 51, 7-16 (1971).
109. Pope, M., Kallmann, H.P. and Magnante, P.: "Electroluminescence in organic crystals," J. Chem. Phys. 35, 2042-2043 (1963).
110. Pope, M., Burgos, J. and Wotherspoon, N.: "Singlet exciton-trapped carrier interaction in anthracene," Chem. Phys. Lett. 12, 140-143 (1971).
111. Pope, M. and Selshy, R.: "Excitonic Sounding: A proposed method for measuring a charge density gradient in anthracene," Chem. Phys. Lett. 14, 226-230 (1972).
112. Pott, G.T. and Williams, D.F.: "Electron photoemission from anthracene crystals," J. Chem. Phys. 51, 203-210 (1969).

113. Pott, G.T. and Williams, D.F.: "Low temperature electron injection and space-charge-limited transients in anthracene crystals," J. Chem. Phys. 51, 1901-1906 (1969).
114. Reucroft, P.J. and Mullins, F.D.: "Physical basis for exponential carrier trap distributions in molecular solids," J. Chem. Phys. 58, 2918-2921 (1973).
115. Rice, S.A. and Jortner, J.: "Comments on the theory of exciton states of molecular crystals," in Physics and Chemistry of the Organic Solid State, Vol. 3, 199-497 (1967).
116. Robertson, R., Fox, J.J. and Mantin, A.M.: "Photo-conductivity of diamonds," Nature 129, 579 (1932).
117. Rose, A.: "Space-charge-limited currents in solids," Phys. Rev. 97, 1538-1544 (1955).
118. Rosenstock, H.B.: "Luminescent emission from an organic solid with traps," Phys. Rev. 187, 1166-1168 (1969).
119. Sano, M, Pope, M. and Kallmann, H.: "Electroluminescence and band gap in anthracene," J. Chem. Phys. 43, 2920-2921 (1965).
120. Schadt, M. and Williams, D.F.: "Low-temperature hole injection and hole trap distribution in anthracene," J. Chem. Phys. 50, 4364-4368 (1969).
121. Schmidt, K. and Wedel, K.: "Negative photo-effect by double injection into anthracene single crystals," Phys. Stat. Sol. 34, 167-168 (1969).
122. Schmidt, K. and Wedel, K.: "Negative resistance by double injection into anthracene crystals," Phys. Stat. Sol. 35, k89-96 (1969).
123. Schott, M. and Berrehar, J.: "Detrapping of holes by singlet excitons or photons in crystalline anthracene," Mol. Cryst. and Liquid Cryst. 20, 13-25 (1973).
124. Schwob, H.P., Fünfschilling, J. and Zschokke-Gränacher, I.: "Recombination radiation and fluorescence in doped anthracene crystals," Mol. Cryst. and Liquid Cryst. 10, 39-45 (1970).
125. Schwob, H.P. and Zschokke-Gränacher, I.: "Doppelinjektion und elektrolumineszenz in dotierten anthracenkristallen," Mol. Cryst. and Liquid Cryst. 13, 115-136 (1971).
126. Schwob, H.P. and Williams, D.F.: "Charge transfer exciton fission in anthracene crystals," Chem. Phys. Lett. 13, 581-584 (1972).

127. Schwob, H.P. and Williams, D.F.: "Charge transfer exciton fission in anthracene crystals," J. Chem. Phys. 58, 1542-1547 (1973).
128. Sharma, R.D.: "Exciton-exciton collision in anthracene crystal," J. Chem. Phys. 46, 3475-3478 (1967).
129. Sharma, R.D.: "Intrinsic photoconduction in anthracene," J. Chem. Phys. 46, 2841-2843 (1967).
130. Siebrand, W.: "Trapping of triplet excitons and the temperature dependence of delayed fluorescence in anthracene crystals," J. Chem. Phys. 42, 3951-3954 (1965).
131. Siebrand, W.: "Temperature dependence of radiationless transitions," J. Chem. Phys. 50, 1040-1041 (1969).
132. Siebrand, W.: "On the relation between radiative and non-radiative transitions in molecules," Chem. Phys. Lett. 9, 157-159 (1971).
133. Singh, S. and Lipsett, F.R.: "Effect of purity and temperature on the fluorescence of anthracene excited by red light," J. Chem. Phys. 41, 1163-1164 (1964).
134. Singh, S., Jones, W.J., Siebrand, W., Stoicheff, B.P. and Schneider, W.G.: "Laser generation of excitons and fluorescence in anthracene," J. Chem. Phys. 42, 330-342 (1965).
135. Sinharay, N. and Meltzer, B.: "Characteristics of insulator diodes determined by space-charge and diffusion," Solid St. Electron. 7, 125-136 (1964).
136. Silver, M., Olness, D., Swicord, M. and Jarnagin, R.C.: "Photo-generation of free carriers in organic crystals via exciton-exciton interaction," Phys. Rev. Lett. 10, 12-14 (1963).
137. Silver, M., Weisz, S.L., Kim, J.S. and Jarnagin, R.C.: "Relative contribution of singlet-singlet and singlet-triplet interactions to the photogeneration of carriers in anthracene," J. Chem. Phys. 39, 3163-3164 (1963).
138. Silver, M. and Sharma, R.: "Carrier generation and recombination in anthracene," J. Chem. Phys. 46, 692-696 (1967).
139. Silver, M.: "Conduction processes in organic crystals, conduction in low-mobility materials," Proc. 2nd International Conferences, 347-356 (1971).
140. Smith, G.C.: "Triplet exciton phosphorescence in crystalline anthracene," Phys. Rev. 166, 839-847 (1968).

141. Strome, F.C., Jr.: "Direct, 2-photon photocarrier generation in anthracene," Phys. Rev. Lett. 20, 3-5 (1968).
142. Suna, A.: "Kinematics of exciton-exciton annihilation in molecular crystals," Phys. Rev. B1, 1716-1739 (1970).
143. Sussman, A.: "Space-charge-limited currents in copper phthalocyanine thin films," J. Appl. Phys. 38, 2738-2748 (1967).
144. Sworakowski, J. and Mager, J.: "Space-charge-limited currents in single crystals of anthracene doped with perylene," Acta Phys. Polon. 36, 483-486 (1969).
145. Sworakowski, J. and Pigon, K.: "Trap distribution and space-charge-limited currents in organic crystals, anthracene," J. Phys. Chem. Solids 30, 491-496 (1969).
146. Sworakowski, J.: "Space-charge-limited currents in solids with nonuniform spatial trap distribution," J. Appl. Phys. 41, 292-295 (1970).
147. Szymanski, A. and Labes, M.M.: "Charge carrier mobility in tetracene," J. Chem. Phys. 50, 1898-99 (1969).
148. Szymanski, A.: "Space-charge-limited currents in polycrystalline p-quaterphenyl layers," Mol. Cryst. 3, 339-355 (1968).
149. Tavares, A.D.: "Photovoltaic effects in crystals of organic semiconductors as a function of wavelength," J. Chem. Phys. 53, 2520-2524 (1970).
150. Tauc, J.: "Generation of an emf in semiconductors with non-equilibrium current carrier concentrations," Rev. Modern Phys. 29, 308-324 (1959).
151. Thomas, J.M., Williams, J.O. and Cox, G.A.: "Lattice imperfections in organic solids, III: A study, using the conductivity glow-curve of trapping centres in crystalline anthracene," Trans. Faraday Soc. 64, 2496-2504 (1968).
152. Thomas, J.M., Williams, J.O. and Turton, L.M.: "Lattice imperfection in organic solids, IV: A study - using space-charge-limited currents of trapping centres in crystalline anthracene," Trans. Faraday Soc. 64, 2505-2513 (1968).
153. Touraine, A., Vautier, C. and Charles, D.: "Caracteristiques courant-tension en regime de charge d'espace en presence d'une distribution uniforme de pieges - II: Application aux resultats experimentaux des couches minces de selenium amorphe," Thin Solid Films 9, 229-239 (1972).

154. Trlifj, M.: "Nonradiative destruction of triplet excitons by excess electrons in organic crystals," Czech. J. Phys. B23, 558-566 (1973).
155. Vaubel, G., Baessler, H. and Mobius, D.: "Reaction of singlet excitons at an anthracene metal interface: Energy transfer," Chem. Phys. Lett. 10, 334-336 (1971).
156. Vertsimakha, Ya I., Kurik, M.V. and Piryatinskii, Yu P.: "Temperature dependence of the photo-conductivity spectrum of anthracene," Soviet Phys. - Solid State 14, 1241-1244 (1972).
157. Vertsimakha, Ya I., Kurik, M.V. and Piryatinskii, Yu P.: "Photo-voltaic effect of anthracene crystals," Soviet Phys. - Solid State 14, 2035-2039 (1973).
158. Vityuk, N.V. and Mikho, V.V.: "Electroluminescence of anthracene excited by Π -shaped voltage pulses," Soviet Phys. - Semicon. 6, 1497-1499 (1973).
159. Vladimirov, V.V., Kurik, M.V. and Piryatinskii, Yu P.: "Sign inversion of the photo-emf in anthracene," Soviet Phys. - Doklady 13, 789-790 (1969).
160. Wakayawa, N. and Williams, D.F.: "Singlet exciton-charge-carrier interaction in anthracene," Chem. Phys. Lett. 9, 45-47 (1971).
161. Wakayama, N. and Williams, D.F.: "Carrier-exciton interactions in crystalline anthracene," J. Chem. Phys. 57, 1770-1779 (1972).
162. Weisz, S.Z., Richardson, P., Cobas, A. and Jarnagin, R.C.: "Triplet sampled radiation damage," Mol. Cryst. 3, 168 (1967).
163. Williams, D.F. and Schneider, W.G.: "Phosphorescence emission from anthracene single crystals," J. Chem. Phys. 45, 4756-4757 (1966).
164. Williams, D.F., Adolph, J. and Schneider, W.A.: "Diffusion of triplet exciton in anthracene crystals," J. Chem. Phys. 45, 575-577 (1966).
165. Williams, D.F. and Adolph, J.: "Diffusion length of triplet excitons in anthracene crystals," J. Chem. Phys. 46, 4252-4254 (1967).
166. Williams, D.F.: "Phosphorescence spectrum of anthracene crystal," J. Chem. Phys. 47, 344-345 (1967).

167. Williams, D.F. and Schadt, M.: "A simple organic electroluminescent diode," *Proc. IEEE* 58, 476 (1970).
168. Williams, D.F. and Schadt, M.: "DC and pulsed electroluminescence in anthracene and doped anthracene crystals," *J. Chem. Phys.* 53, 3480-3487 (1970).
169. Williams, D.F. and Schadt, M.: "Temperature dependence of D.C. and pulsed electroluminescence in anthracene crystals," *Proceedings of the International Conference on Photoconductivity*, edited by E.M. Pell, Pergamon, Oxford, 303-309 (1971).
170. Williams, W.G., Spong, P.L. and Gibbons, D.J.: "Double injection electroluminescence in anthracene and carrier injection properties of carbon fibres," *J. Phys. Chem. Solids* 33, 1879-1884 (1972).
171. Wolf, H.C.: "The electronic spectra of aromatic molecular crystals," *Solid State Phys.* 9, 1-81 (1959).
172. Wolf, H.C.: "Energy transfer in organic molecular crystals: A survey of experiments," in *Advances in Atomic and Molecular Physics*, Vol. 3, 119-142, Academic Press, New York (1967).
173. Wolf, H.C. and Benz, K.W.: "Energy trapping processes in aromatic crystals," *Pure and Appl. Chem.* 27, 439-455 (1971).
174. Wright, G.T.: "Mechanisms of space-charge-limited current in solids," *Solid St. Electron.* 2, 165-189 (1961).
175. Zschokke-Gränacher, I., Schwob, H.P. and Baldinger, E.: "Recombination radiation in anthracene doped with tetracene," *Solid-State Commun.* 5, 825-828 (1967).
176. Zvyagintsev, A.M.: "Preflashover electroluminescence of anthracene," *Zh. Prikl. Spektrosk.* 13, 165-167 (1970).